

MULTIFUNCTIONAL AND HYBRID
NANOCOMPOSITES FROM MICRO/NANO
FIBRILLATED CELLULOSE

Pruthvi Kumar Bangalore Sridhara

Per citar o enllaçar aquest document:
Para citar o enlazar este documento:
Use this url to cite or link to this publication:
<http://hdl.handle.net/10803/673936>



<http://creativecommons.org/licenses/by-nc/4.0/deed.ca>

Aquesta obra està subjecta a una llicència Creative Commons Reconeixement-NoComercial

Esta obra está bajo una licencia Creative Commons Reconocimiento-NoComercial

This work is licensed under a Creative Commons Attribution-NonCommercial licence



DOCTORAL THESIS

**Multifunctional and Hybrid Nanocomposites from
Micro/Nano Fibrillated Cellulose**

Pruthvi Kumar Bangalore Sridhara

2021



DOCTORAL THESIS

**Multifunctional and Hybrid Nanocomposites from
Micro/Nano Fibrillated Cellulose**

Pruthvi Kumar Bangalore Sridhara

2021

DOCTORAL PROGRAMME IN TECHNOLOGY

Supervised by: Dr. Fabiola Vilaseca Morera

**Presented to obtain the degree of PhD at the
University of Girona**



Dr. Fabiola Vilaseca Morera, Head of Advanced Biomaterials and Nanotechnology [BIMATEC] Group, Professor at the Department of Chemical Engineering Agriculture, and Food Technology of the University of Girona.

I DECLARE:

That the thesis titled “Multifunctional and Hybrid Nanocomposites from Micro/Nano Fibrillated Cellulose”, presented by Pruthvi Kumar Bangalore Sridhara to obtain a doctoral degree, has been completed under my supervision.

For all intents and purposes, I hereby sign this document.

Signature,

Dr. Fabiola Vilaseca Morera

Girona, 02 July 2021



I, Dr. Peter Olsén, as co-author of the following article:

“Strong Polyamide-6 Nanocomposites with Cellulose Nanofibers Mediated by Green Solvent Mixtures”, published in “Nanomaterials” journal,

Accepts that Mr. Pruthvi Kumar Bangalore Sridhara presents the cited article as the principal/main author and as part of his doctoral thesis and that said articles cannot, therefore, form part of any other doctoral thesis.

And for all intents and purposes, hereby signs this document.

Signature,

Peter Olsén,

Stockholm, 06 September 2021



I, Mr. Ferran Massó Riera, as non-doctoral co-author of the following article:

“Strong Polyamide-6 Nanocomposites with Cellulose Nanofibers Mediated by Green Solvent Mixtures”, published in “Nanomaterials” journal,

Accepts that Mr. Pruthvi Kumar Bangalore Sridhara presents the cited article as the principal/main author and as part of his doctoral thesis and that said articles cannot, therefore, form part of any other doctoral thesis.

And for all intents and purposes, hereby signs this document.

Signature,

Ferran Massó Riera,

Girona, 06 September 2021

Thesis presented as a “Compendium of Publications”.

ACKNOWLEDGEMENTS

This work has been a reflection of a collective effort put in by a number of people and I wish to thank them all.

I would like to begin by expressing my sincere gratitude to Professor Fabiola Vilaseca for giving me this opportunity to pursue research with freedom and for enabling a thriving atmosphere to fulfil it. I want to thank her for the patient supervision and inspirational discussions that have guided the direction of this work. Her research oriented insights and scientific feedbacks have been of utmost importance source of motivation. Her non-scientific worldly wisdom is also deeply appreciated.

I have had the opportunity to be part of productive collaborations during my PhD. I would like to extend my gratitude to all my co-authors. I would like to convey my gratitude to Professor Lars Berglund, of the Wallenberg Wood Science Center (WWSC) for his useful insights during the research collaboration. Dr. Pere Mutje Pujol, of the Laboratory of Paper and Polymeric Materials (LEPAMAP) is earnestly appreciated for aiding in the use of laboratory equipment during my PhD. I would like to acknowledge the grants from (i) KTH, Sweden (KAW2018.0451), (ii) UdG grant (IFUdG 2017), and (iii) The Spanish Ministry of Science, Innovation and Universities (RTI 2018-102070-B-C22) for funding this research.

I had the pleasure of meeting many colleagues at the UdG and KTH. I am thankful for their friendships which has made me feel comfortable and played an important role in day-to-day moments. Jaume, Anna and Manel are thanked for helping me to settle and ease my transition in Girona. My colleagues; Helena, Marc, Quim, Ferran, Peter, Joan-Pere, Daniel Reyes, Albert, Israel and Ramon are thanked for their patient support and casual discussions which has made work more enjoyable. Anbu, Lea, Mireia, Jesus, Pepe, Jorge, Kazza, Umang, Surya, Subash and Keertan are acknowledged for their friendships and for making this journey pleasant. Back in India and the rest of the world, I want to thank my dear friends; Abhishek, Anusha, Ganesh, Darshan, and Vijay who have always been cheerful and kept my spirits high. All the interactions with my colleagues and friends have helped me gain a wider perspective of life.

Most importantly, I am forever grateful to my parents; Sridhara and Puttathayamma, for numerous sacrifices to provide us with the best and who have always put our comforts above their own. Their hard work, blessing, love and support have been significantly influential in putting me where I am. I want to thank Suhas for being the perfect sibling. My warmth and love reaches out to my extended family. In the end, I would like to thank my wife; Rachana, for being the constant support and motivator. Her love, patience, her decision to sacrifice her job to move with me to Girona and her caring nature has been a blessing in disguise in my life. I would also like to thank Rachana's parents; Ramakanth and Kathyayini, for their extended love and support towards us.

LIST OF PUBLISHED ARTICLES

This thesis is a compendium of the following three appended articles:

Article I. Sridhara, P.K. and Vilaseca, F., 2020. Assessment of fiber orientation on the mechanical properties of PA6/cellulose composite. *Applied Sciences*, 10(16), p.5565. DOI: 10.3390/app10165565

Journal Impact Factor: 2.679 (2020), Journal Rank: JCR – Q2 (38/91 in Engineering, Multidisciplinary)

Article II. Sridhara, P.K. and Vilaseca, F., 2021. High Performance PA 6/Cellulose Nanocomposites in the Interest of Industrial Scale Melt Processing. *Polymers*, 13(9), p.1495. DOI: 10.3390/polym13091495

Journal Impact Factor: 4.329 (2020), Journal Rank: JCR – Q1 (18/88 in Polymer Science)

Article III. Sridhara, P.K., Masso, F., Olsén, P. and Vilaseca, F., 2021. Strong Polyamide-6 Nanocomposites with Cellulose Nanofibers Mediated by Green Solvent Mixtures. *Nanomaterials*, 11(8), p.2127. DOI: 10.3390/nano11082127

Journal Impact Factor: 5.076 (2020), Journal Rank: JCR – Q1 (31/160 in Physics, Applied)

The authors contributions to the appended articles are as follows:

Article I. Participated in planning, designed and performed most of the experimental work, and wrote the manuscript.

Article II. Major part of planning, designed and performed all the experimental work, and wrote the manuscript.

Article III. Participated in planning, designed most and performed part of the experimental work, and wrote the manuscript.

CONFERENCE PARTICIPATIONS

- I. Pruthvi K. Sridhara, Fabiola Vilaseca, June 2018. High performance (nano)cellulose – polyamides. *Presentation - TAPPI International Conference on Nanotechnology for Renewable Materials, Madison, Wisconsin, USA.*
- II. Pruthvi K Sridhara, Ferran Masso, Ferran Sera, Fabiola Vilaseca, June 2019. High Cellulose Nanofibril content polyamide-6 nanocomposites. *Presentation – Wallenberg Wood Science Center Workshop Program, Stockholm, Sweden.*
- III. Pruthvi K. Sridhara, Ferran Masso, Fabiola Vilaseca, October 2019. Polyamide-6 / Nanocellulose Nanocomposites produced by Solvent Casting. *Presentation - 6th EPNOE International Polysaccharide Conference, Aveiro, Portugal.*
- IV. Pruthvi K. Sridhara, Fabiola Vilaseca, June 2021. Industrial Scalability of Polyamide 6 / CNF Nanocomposites. *Presentation – V Conference of Pre-Doctoral Researchers of the University of Girona, Spain.*

LIST OF ABBREVIATIONS

A	ATR	Attenuated total reflection
	ASTM	American Society for Testing and Materials
B	BC	Bacterial cellulose
C	CNF	Cellulose nanofibers or nanofibrils
	CNC	Cellulose nanocrystals
D	DSP	Digital speckle pattern
	DMA	Dynamic mechanical analysis
	DSC	Differential scanning calorimeter
	DTGA	Derivative of TGA
	D	Diffusion coefficient
E	E	Young's modulus or elastic modulus
	E_F	Flexural modulus
	E_{NC}	Nanocomposite elastic modulus
	E_L	Longitudinal modulus
	E_T	Transverse modulus
F	F	Force
	FTIR	Fourier-transform infrared spectroscopy
G	g	Acceleration due to gravity

K	k	A constant of the melt fluid
L	L x B x T	Length x width x thickness
M	MFI	Melt flow index
	M	Mass
	MCC	Micro crystalline cellulose
N	n	Pseudoplasticity index
P	PA6	Polyamide 6 or nylon-6
	PA66	Polyamide 6,6
	PLA	Poly lactic acid
	PA10	Polyamide 10
	PA11	Polyamide 11
	PA12	Polyamide 12
	PA 6/10	Polyamide 6,10
	PA 6/12	Polyamide 6,12
	PA46	Polyamide 46
Q	Q	Volume flow rate
R	RoM	Rule of mixture
	RH	Relative humidity
	rpm	Revolutions per minute
	r	Die radius

	R	Piston radius
T	TEMPO	2,2,6,6-tetramethylpiperidiny1-1-oxyl
	T_g	Glass transition temperature
	T_c	Crystallization temperature
	T_m	Melting temperature
	t	Time
	TGA	Thermogravimetric analysis
S	SEM	Scanning electron microscopy
U	UV	Ultraviolet
V	V_{CNF}	Volume fraction of CNF
W	W	Weight fraction
	wt%	Weight fraction percentage
Symbols	σ_y	Yield strength
	σ_F	Flexural resistance
	σ_{NC}	Nanocomposite yield strength
	σ_{PA6}	Yield strength of PA6
	ρ	Density
	χ_C	Degree of crystallinity
	μ	Viscosity
	ΔH	Melting enthalpy
	γ	Shear rate

γ_T	True shear rate
τ	Shear stress
π	Pi value = 3.14

CONTENTS

LIST OF FIGURES

LIST OF TABLES

ABSTRACT

RESUMEN

RESUM

Chapter 1	Introduction.....	1
1.1	Nanocelluloses	2
1.1.1	Nanocellulose from wood.....	2
1.1.2	Bacterial cellulose.....	4
1.2	Extraction/Isolation of CNF	4
1.3	CNF as Nano-Reinforcement.....	5
1.3.1	CNF Network Structure	6
1.4	CNF Nanocomposites	8
1.4.1	Reinforcement Mechanism	9
1.4.2	Polyamide 6/Nylon 6 (PA6)	10
1.4.3	Composite Interface	11
1.4.4	Composite Processing.....	12
1.5	State of the Art on ‘PA6 and Cellulose’ Composites.....	15
Chapter 2	Objectives.....	17
Chapter 3	Methods and Experimental.....	19
3.1	Materials.....	19
3.2	Materials Preparation	19
3.3	Characterization	22
Chapter 4	Results and Discussion.....	31
4.1	Pulp-Fiber Composites.....	31
4.1.1	Effect of Fiber Orientation on the Mechanical Properties	31
4.1.2	Hygro-Mechanical Properties	34
4.2	Nanocomposites via Solvent Casting.....	36
4.2.1	Processing Approach	36
4.2.2	Dispersion, High Specific Surface Area and CNF Network.....	37
4.2.3	Cellulose Pulp Fibers vs. CNF as Reinforcement.....	44

4.3	Nanocomposites for Industrial Scale Melt Processing.....	45
4.3.1	Processing Approach	46
4.3.2	Hygro-Mechanical Stability and Interfacial Effects	47
4.3.3	Capillary Rheological Properties	50
Chapter 5	Summary of Results	53
Conclusion....	57
Future Outlook.....	59
References.....	60
Appendix A Appended Articles.....	A-1
A.1	Article I	A-1
A.2	Article II.....	A-2
A.3	Article III.....	A-3

LIST OF FIGURES

Figure 1.1 Schematic showing the hierarchical structure of wood to nanocellulose. This figure is adapted from reference ¹¹	3
Figure 1.2 (i) Schematic of the CNF nanopaper filtration process. The figure is adapted from reference ³⁴ . (ii) Highly transparent CNF nanopaper obtained from filtration process (densely packed CNF nanopaper of thickness ~15 μm). SEM images of CNF nanopaper (iii) showing CNFs physically entangled network and (iv) cross-section showing layered structure of CNF networks.	7
Figure 1.3 Stress-strain curve for low porosity CNF nanopaper. This curve was obtained from CNF nanopaper prepared in this study with a mean thickness of ~15 μm	8
Figure 1.4 (i) Estimated global bio-polyamide market outlook by regions. This figure was adapted from Global Bio-Polyamide Market- Forecast and Analysis (2020-2027) Report by Maximize Market Research Pvt. Ltd., and (ii) Forecast of global PA6 and PA66 market in terms of applications. This figure was adapted by Global Polyamide Market Size, Share & Trends Analysis by Grand View Research.	10
Figure 1.5 Schematic of GELIMAT [®] Mixer. (i) Basic Gelimat mixing material movement in the Gelimat mixing chamber at different mixing blade top speeds increasing from top to bottom. (ii) Types of Gelimat mixers based on feeding mechanism: (a) Top hopper feed for start/stop drive and (b) Axial side feed screw for continuous drive. These figures were adapted from the DUSATEC [™] Inc.'s brochure on GELIMAT Technology: Ultrahigh-Speed Thermo-Kinetic Mixing, Compounding & Fluxing. (iii) An axial feed screw Gelimat equipment.	14
Figure 4.1 (i) Square samples of dimensions (L x B x T) 70 x 70 x 1.5 mm, and square samples from which (ii) 0°, (iii) 90°, and (iv) 45° oriented test specimens were laser cut. (v) Square mould used for injection moulding and (vi) Flow simulation showing the orientation of the pulp fibers within the square mould. Figure adapted from Article I.	32
Figure 4.2 Cross-sectional images of 25 wt% pulp fiber composites at various magnification levels indicating good wetting between fibers and matrix. Figure adapted from Article I.	34
Figure 4.3 Cross-sectional SEM images of PA6/CNF nanocomposites films: (ii & iii) CNF nanopaper, (v & vi) 20 wt%, and (viii & ix) 50 wt% formulations. This images are adapted from Article III. Casted CNF nanocomposite films: (i) neat CNF nanopaper film, (iv) 20 wt%, and (vii) 50 wt% formulations.	37
Figure 4.4 Storage modulus as a function of temperature for PA6/CNF nanocomposites (10, 30 and 50 wt% formulations). Figure from Article III.	38
Figure 4.5 Characteristic stress-strain curves from uniaxial tensile tests for PA6/CNF nanocomposites with relative humidity 50%. Figure adapted from Article III.	40

Figure 4.6 Experimental and theoretically predicted values for (i) tensile strength and (ii) elastic moduli for PA6-CNF nanocomposites. Figure from Article III.	42
Figure 4.7 Schematic of the complete manufacturing process for the PA6/CNF nanocomposites. This figure is taken from Article II.	47
Figure 4.8 Water absorption percent as a function of CNF content versus time for PA6/CNF nanocomposites at room temperature. This figure is adopted from Article II.	50
Figure 4.9 Rheogram representing viscosity and true shear rate at 230 °C for the PA6/CNF nanocomposites. This figure is taken from Article II.	51

LIST OF TABLES

Table 1. Summary of tensile properties of pulp fiber composites showing the variation of yield strength with respect to fiber orientation with the matrix for dry samples. Table adapted from Article I.	33
Table 2. Summary of the mechanical properties for the PA6-pulp fiber composites after 48-hour conditioning of samples at 23° and relative humidity 50%. Table adapted from Article I.	35
Table 3. Summary of the tensile mechanical properties for the PA6/CNF nanocomposites at relative humidity 50%. Table from Article III.	40
Table 4. Thermal parameters and degree of crystallinity for the PA6 polymer in the plain matrix and in the PA6-CNF nanocomposites. Table from Article III.	44
Table 5. Summary of the uniaxial tests for PA6/CNF nanocomposites at dry sample conditions and at relative humidity (RH 50%). For standard deviations of values, refer to Article II. This table was adopted from Article II.	48

ABSTRACT

As a renewable alternative to petroleum-based materials, wood or plant-based materials offer a greater prospect in the transition towards sustainable replacements. Native to wood, cellulose nanofibers (CNF) form the major load bearing component and possess tremendous potential as a reinforcement material in polymeric matrices. This study focuses on nanocellulose-based composites and aims to prepare and characterize bio-(nano)composites with high cellulose weight/volume fraction. The influence of nanoscale reinforcement or nanostructure on the macroscopic properties of the nanocomposites are investigated. Distinct prominence is given to the effect of nanocellulose dispersion and nanocellulose/polymer interface on the physical characteristics of biocomposites.

In an initial study, effects of cellulose pulp fibers (micro scale dimensions) were investigated in pulp-fiber/polyamide 6 (PA6) composites system obtained by melt compounding and injection moulding. Strong influence on the pulp fiber reinforcement on the polymer matrix were observed with well dispersed pulp-fibers resulting in enhanced mechanical properties. Further, the effect of pulp fiber orientation within the composites was assessed and the composites with longitudinal fiber alignment recorded the highest mechanical properties.

Regarding the investigation of PA6 and cellulose nanofibers, two different approaches were used to process the nanocomposites. Firstly, solvent casting-based approach, where CNF derived from enzymatic pretreatment were used to produce high content of CNF biocomposites by adopting a green solvent mixture to disperse the CNF and then impregnated by the dissolved polymer. Nanocomposite formulations up to 50 wt% of CNF were prepared and characterized. Unique characteristics due to the nanostructure of composites are discussed corresponding to CNF dispersion, CNF network, and CNF/matrix interface. In addition, a comparison between the reinforcement effect of pulp-fiber and CNF are discussed to emphasize the importance of nano-scale reinforcement and their contribution in enhancing the physical properties of thermoplastic-matrix composites. Subsequently, melt processing approach with a high speed thermo-kinetic mixer was used to prepare PA6/CNF nanocomposites with up to 25 wt% formulations. This study focused on the industrial scalability and provided a methodology to produce high cellulose content CNF-nanocomposites at a commercial spectrum. Mechanical

properties were characterized at different relative humidity and the investigation revealed good hygro-mechanical properties. All in all, the current nanocomposites exhibited excellent dispersion without major agglomerations and the mechanical properties were significantly enhanced with the addition of CNF in both the approaches.

Nanocomposites from polyamide-6 and high content of cellulose nanofibers were successfully prepared in this work, with remarkable improvement in the mechanical performance compared to the neat matrix, for both Young's modulus and tensile strength. This in itself is an outstanding achievement, as compared to the literature up today. Moreover, the used methodology stands for industrial scalability and feasible processes towards the use of renewable and more sustainable products.

RESUMEN

Como alternativa renovable a los materiales producidos a partir de petróleo, la madera o los materiales producidos a partir de plantas ofrecen una mayor posibilidad en la transición hacia reemplazos sostenibles. Las nanofibras de celulosa procedentes de la madera forman la mayor carga en el comportamiento del componente y poseen un tremendo potencial como material de refuerzo en matrices poliméricas. Este estudio se enfoca en materiales compuestos en base a nanocelulosa, en concreto en la preparación y caracterización de bio-(nano)-compuestos con alto contenido de celulosa en fracción masa/volumen. Se investigará la influencia del refuerzo nanométrico o nanoestructura en las propiedades macroscópicas de los nanocompuestos. La dispersión de las nanofibras de celulosa y su interfase con el polímero, van a jugar un papel importante en las propiedades físicas de los biocompuestos.

La primera parte del trabajo, los efectos de la pulpa de fibras de celulosa (dimensiones micrométricas) fueron investigadas en sistemas de materiales compuestos de pulpa/poliamida 6 (PA6) obtenidos por termo-fluencia y inyección. Una gran influencia del refuerzo de pulpa de fibras en la matriz polimérica fue observada con buena dispersión de pulpa de fibras resultando en una mejora de las propiedades mecánicas. Más adelante, el efecto de la orientación de la pulpa de fibras en el compuesto fue evaluado y los materiales compuestos con las fibras alineadas longitudinalmente obtuvieron las mayores propiedades mecánicas.

Dos tipos distintos procedimientos fueron usados para procesar los nanocompuestos de PA6 y nanofibras de celulosa (CNF). En primer lugar, a partir del método solvent-casting, donde las CNF derivadas de un pretratamiento enzimático fueron usadas para producir biocompuestos con alto contenido de CNF, formando una mezcla ecológica para dispersar la CNF e impregnarlas por el polímero disuelto. Las formulaciones llegaron hasta un 50 wt% de CNF y fueron preparadas y caracterizadas. Las características únicas dadas por la nanoestructura del material compuesto son discutidas en relación a la dispersión de la CNF, la red de CNF, y la interfase CNF/matriz. Además, una comparación entre el efecto del refuerzo de pulpa de fibras y CNF es discutido para enfatizar en la importancia de los refuerzos nanométricos y sus contribuciones en mejorar las propiedades físicas de los materiales compuestos de matriz termoplástica. Posteriormente, un método de procesado por termo-fluencia con un mezclador termo-cinético de alta velocidad fue usado para preparar

materiales nanocompuestos de PA6/CNF con formulaciones de hasta un 25 wt%. Este estudio está basado en el escalado industrial i en proveer una metodología para producir nanocompuestos de CNF con un elevado contenido de celulosa a nivel comercial. Las propiedades mecánicas fueron caracterizadas a diferentes humedades relativas y la investigación reveló buenas propiedades higromecánicas. Los materiales nanocompuestos exhibieron excelente dispersión sin aglomeraciones mayores y las propiedades mecánicas fueron significativamente mejoradas con la adición de CNF en ambos métodos.

RESUM

Els materials procedents de plantes i arbres representen una alternativa renovable als materials procedents del petroli, en la transició cap a la producció de materials més sostenibles. Les nanofibres de cel·lulosa (CNF) procedents de la fusta són el principal component de càrrega i tenen un gran potencial com a material de reforç de matrius polimèriques. El present estudi es focalitza en la preparació i caracterització de bio-nano-compòsits amb un alt contingut en nanofibres de cel·lulosa (CNF). En concret, s'investiga la influència de la nanoestructura o del nano-reforç en les propietats macroscòpiques del nanocompòsit. L'efecte del grau de dispersió i de la interface nanocel·lulosa/polímer són factors claus sobre les propietats físiques dels nanocompòsits.

En la primera part del treball, s'ha investigat l'efecte de fibres de cel·lulosa (de dimensions micro) com a reforç en materials compòsits de poliamida-6 (PA6)/cel·lulosa, obtinguts per un procés de barreja (*melt-compounding*) i posterior moldeig per injecció. S'ha observat una marcada influència de la pasta de cel·lulosa a l'hora d'actuar com a reforç de la matriu polimèrica, presentant una bona dispersió de les fibres, i consegüentment es van obtenir molt bones propietats mecàniques. També s'ha investigat la influència del grau d'orientació de les fibres dins dels compòsits, obtenint-se millors propietats quan les fibres estaven alineades longitudinalment en la direcció de l'assaig mecànic,

Pel que fa al reforç de la matriu de PA6 amb nanofibres de cel·lulosa, s'han estudiat dos tipus diferents procediments per a processar els nanocompòsits de PA6/CNF. Per un costat es va fer servir el mètode solvent-càsting. En aquest cas, les CNF derivades d'un pretractament enzimàtic, es van dispersar i impregnar amb el polímer dissolt en una barreja de solvents "verds". Es van produir biocompòsits amb un alt contingut de CNF, de fins al 50% en pes. Les elevades propietats dels materials es van justificar en base a la bona dispersió de les CNF, la mateixa xarxa de CNF en sí, i la interfase CNF/matriu. A més, una comparació entre l'efecte del reforç de polpa de fibres i reforç de CNF va emfatitzar la importància dels reforços nanomètrics i la seva contribució en la millora de les propietats físiques dels compòsits de matriu termoplàstica. Per altra banda es va fer utilitzar un procés de barreja tèrmica amb un mesclador termo-cinètic d'alta velocitat per a preparar els nanocompòsits de PA6/CNF amb formulacions de fins a un 25 wt%. Aquest estudi se centra en l'escalat industrial i en proveir

una metodologia per a produir nanocompòsits de CNF amb un elevat contingut de cel·lulosa a nivell comercial. Les propietats mecàniques es van avaluar a diferents valors humitats relatives i es van obtenir molt bones propietats higromecàniques. En tots els casos, els materials nanocompòsits presentaven una bona dispersió sense grans aglomeracions i les propietats mecàniques van millorar significativament amb l'addició de CNF en tots dos mètodes.

Chapter 1 Introduction

From the beginning of the last century, the demands of the growing population and rapid advancements in technology have led to the increased dependency of the world on materials derived from fossil fuels.¹ In the recent decades, significant attention has been focused on greener material sources that can offer environmental safety and a sustainable way of life.² As an alternative source, wood and wood-based materials have shown promising potential due to their copious abundance and renewable origin.³ Moreover, wood-based products are key in diversification of the forest industry, especially in the view of declining market for some of the traditional wood-based products such as newspaper prints.⁴ Ingenious utilization of wood-based materials not only gives a major boost to the forest industry, but also open up innovative and carbon neutral solutions for various material applications. In this context, the major load bearing component in trees; cellulose, especially nanocellulose becomes of prominence due to their specific strength and stiffness.

Nanocellulose is part of the wood cell wall and is the major component of most natural fibers. From a materials perspective, nanocellulose fibrils are characterized by high strength (~3 GPa) and crystalline modulus of (~135 GPa) in the longitudinal direction.⁵ The high specific strength, combined with the low density of ~1.5 g/cm³ makes nanocellulose attractive for biocomposite applications. In the recent past, numerous energy efficient ways, developed to derive nanocellulose for wood have provided a notable momentum in the research of nanocellulose-based materials. This has generated a huge amount of interest in the field of nanoreinforcements for polymer matrix composites.⁶⁻⁸ An important use of nanoreinforcement in composites is that, materials can be designed to exhibit overall best property of the combined one or more separate components. This multi-functionality applies not only to mechanical properties, but also to optical, barrier and electrical properties. Recent progress in the field of nanocellulosic composites has shown the potential of nanocellulose as reinforcement in the

production of advanced and high-performance nanocomposites,⁹ which has encouraged major forest product industries to invest in nanocellulose pilot plants.

1.1 Nanocelluloses

1.1.1 Nanocellulose from wood

Wood as a source for cellulose has many advantages; most significantly, it is abundant. The annual production of cellulose in nature is about 1 trillion tons. In addition, an existing infrastructure has already been in place for harvesting, processing and handling.¹⁰ Wood tissue is a hierarchical designed structure that has evolved to perform two main function; (a) provide mechanical support and (b) transport water and nutrients through the tree. Variation in this natural process commands the aspect ratio, crystallinity, and morphology of the resulting microfibril[§]. The constituents in this hierarchical structure are arranged at different length scales so as to obtain mechanical integrity in a porous structure as shown in **Figure 1.1**¹¹. Cellulose biosynthesis involves, self-assembly of cellulose chains to form a ‘minisheet’ of ordered cellulose chains followed by the self-assembly of these cellulose minisheets and finally, assembly of cellulose fibrils into microfibrils. In brief, the cell wall is comprised of primary (P), secondary (S2, S2 and S3) and tertiary layers. The composition and orientation of components depends mainly on the source and varies across the cell walls. Predominantly, the S2 layer contains bundles of parallel oriented nanofibrils whereas, S1 layer contains randomly oriented nanofibrils. Cellulose nanofibrils with 3-5 nm in diameter and up to 1 μm in length are present as hemicellulose coated aggregates having 10-20 nm diameter in the cell wall.¹² In general, cellulose is extracted by purifying wood with most of the lignin and hemicellulose. Other than wood, cellulose can be extracted from plant fibers such as cotton¹³, flax¹⁴, sisal¹⁵, wheat straw¹⁶, etc. and animals such as tunicates¹⁷, bacteria¹⁸, and algae¹⁹.

Among plant-based nanocellulose, there are two main categories: (a) Cellulose nanocrystals (CNC) and (b) Cellulose nanofibers (CNF). CNCs (sometimes, called as cellulose

[§]Microfibril is the commonly used botany term. Cellulose nanofibril is used in this thesis to emphasis nanoscale dimension with the abbreviation CNF.

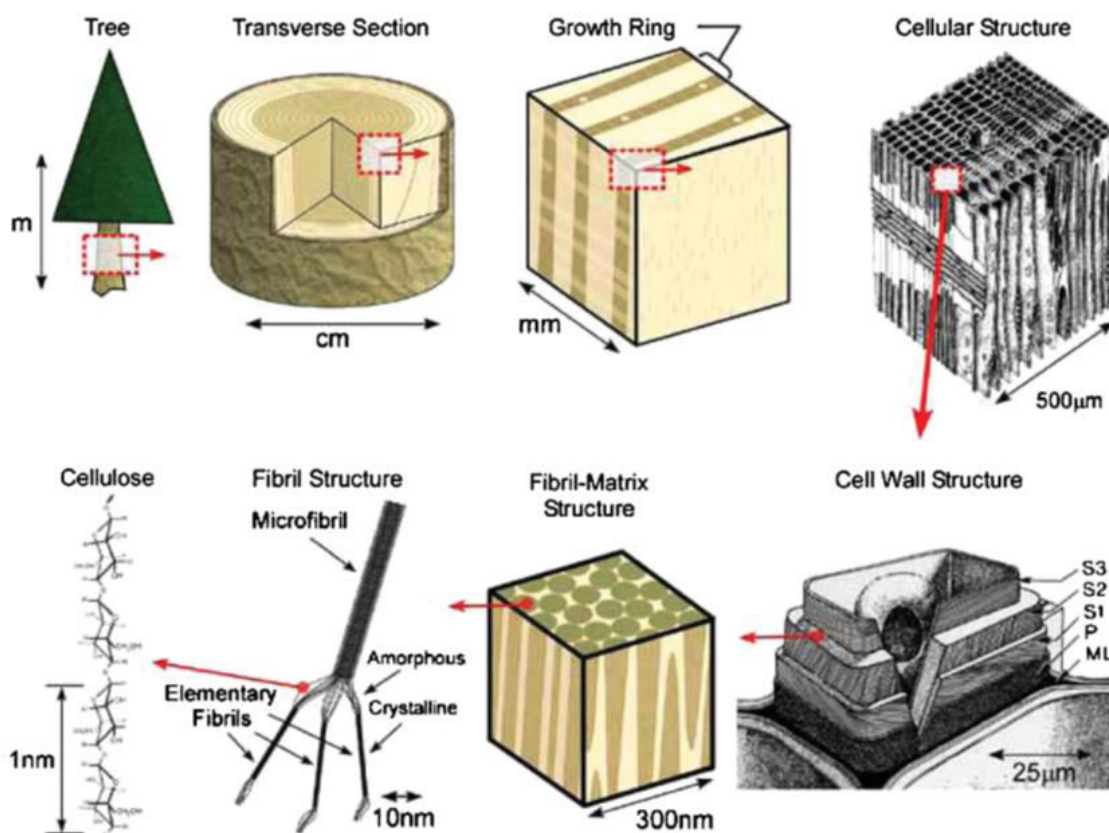


Figure 1.1 Schematic showing the hierarchical structure of wood to nanocellulose. This figure is adapted from reference ¹¹.

nanowhiskers) are obtained from sulphuric acid hydrolysis of cellulose pulp fibers. CNC derived from wood in form of colloidal suspension are characterized by 3-5 nm width and 50 to 500 nm in length. Various methods used to prepare and characterize CNCs have been previously summarized by Jonoobi *et al.*²⁰

CNF are finer particles, relatively longer than CNCs, and have a higher aspect ratio. CNF can be obtained from refined wood or plant pulp by subjecting them mild pre-treatment methods (enzymatic or chemical) followed by high pressure homogenization. The earliest attempts to produce CNF from pulp were made in the early 1980s, where high mechanical energy was used to disintegrate and obtain fibrils with a broader size distribution.²¹ CNF are characterized by a cross-sectional width/diameter of 3-20 nm and length of 500-2000 nm. The precise dimensions of these nanocellulosic particles depend on the material source and are controlled by the pre-treatment techniques to obtain such materials.

1.1.2 Bacterial cellulose

Alternative to forest and plant-based resources which from the principal source of cellulose currently, bacterial cellulose (BC) has been considered as a good candidate for renewable cellulosic-based materials.²² BC was initially discovered by Brown *et al.* in the late 1800s.²³ BC is secreted by bacteria at the interface between air and a liquid media which allows the sustenance of bacterial cells by forming an interwoven network of nanofibers which also act as a self-defence mechanism from UV light and prevents dehydration of nutrients.²⁴ A single bacterial cell can polymerize up to 200,000 glucose molecules per second.²⁵ The production and morphological properties of BC depends on the species of bacteria which excrete the cellulose (bio-synthesis) and the culture media with optimum parameters which propagates growth of bacteria and BC.²⁶

In brief, BC form 3D percolated network, are transparent, porous and agglomerate upon drying similarly to nanocelluloses derived from wood. The functionality to produce 3D structures greatly enlarge the scope of BC in nanocomposites applications. Composites and layered laminates structures can be produced by combining the functional 3D network of BC and with polymers, graphene derivatives, ceramics and metal-alloys to synergistically fabricate mechanically and thermally stable materials.²⁷ Recent research highlights that various additive materials impart electronic, optical, magnetic, catalytic and bioactive properties to BC composites.²⁸

1.2 Extraction/Isolation of CNF

The extraction of cellulose can be achieved in two steps. Firstly, pre-treatment methods to assist the disintegration process of the raw material (generally pulp) to obtain individual cellulose fibrils. Secondly, further fibrillation methods, which are employed depending on the material source and the desired final morphology of nanocellulose. Processes for such alterations generally involve these methods separately or combined. Various pre-treatment methods have been developed to obtain CNF. Chemical pre-treatment can induce surface charges and facilitate disintegration due to the induced electrostatic repulsion. For example,

TEMPO mediated oxidation allow the formation of negative charged carboxyl groups from the primary hydroxyls on the surface of the fibril.^{29,30} Through TEMPO mediated oxidation, CNF with a surface charge density of 1500 $\mu\text{eq/g}$ can be obtained.²⁹ Cellulose molar mass is reduced substantially during the pre-treatment and fibrils of the order 3-5 nm in diameter and 0.5 μm in length can be obtained, when TEMPO oxidized to a high charge.³¹ Nevertheless, other chemical pre-treatment methods such as cationic functionalization^{32,33} and carboxymethylation³⁴ have been used to disintegrate CNF.

In addition, enzymatic pre-treatment confides on the action of enzymes and disintegration is further expedited by the presence of hemicelluloses.³⁵ Enzymatic pre-treatment does not alter the surface morphology and retains the native chemical structure of cellulose. After enzymatic pre-treatment, small amount of charged hemicelluloses ($\sim 40\text{-}100$ $\mu\text{eq/g}$) are sustained and these help in CNF colloidal dispersion.³⁶ Longer fibrils up to a few μm with a broader diameter distribution (3-10 nm) may be obtained by enzymatic pre-treatment.³⁷ In this current work, enzymatic CNF is used because of the comparatively unmodified structure, high molar mass and ease of processing. CNF have large number of hydroxyl on the surface owing to the chemical structure of cellulose and crystal arrangements.³⁸ The presence of hydroxyls provides a functional surface and is vital as a reinforcement in deciding the macroscopic properties of CNF-based composites. Moreover, CNF can physically entangle and form percolated networks due to strong hydrogen bonds and other secondary interactions. In case of high CNF content formulations, the efficient penetration of the CNF network by the matrix material is key to obtain high-performance biocomposites.

1.3 CNF as Nano-Reinforcement

From the early 1990s onwards, nanocellulosic elements have attracted a great deal of interest as reinforcement in bionanocomposites.³⁹ Biobased reinforcement materials produced from naturally occurring substances still lack certain characteristics when compared to synthetic fibers. However, the use of biobased nanoscale reinforcements allows to suppress such drawbacks. The reinforcing potential cellulose in nanoscale dimension integrates the benefits of biobased materials and nanotechnology in a synergistic demeanour. Attributable to the

nanometer sizes, CNF-based polymer composites exhibit remarkably enhanced properties when compared to neat polymers and/or their traditional polymer blends. Often, these properties are more than that of predicted properties through micro-mechanical models. Nano-size reinforcements provide higher surface area to form strong interfacial interactions with the polymer, thereby, dictating the effective reinforcement.⁴⁰ The limitations associated with hierarchical structure can be eliminated with cellulose at nanoscale and new cellulose-based nano-building blocks becomes available for the next generation of bionanocomposites. Combined with renewability, high aspect ratio, high strength to weight distribution, low density ($\sim 1.5 \text{ g/cm}^3$), low thermal expansion and surface functionalization properties due the presence of surface hydroxyl groups, make CNF an ideal biobased nanoreinforcement.

1.3.1 CNF Network Structure

CNFs form physically entangled networks when filtered from a dilute colloidal suspension.⁴¹ The obtained dried thin structure is referred to as CNF nanopaper and the schematic showing the preparation of CNF nanopaper is shown in **Figure 1.2** (i). The CNF nanopaper is characterized by strongly interacting and randomly oriented 2D network of CNFs, which are arranged in layers within the nanopaper (**Figure 1.2** (iii, iv)). The porosity/density of network structures can be suitably controlled by a combination of casting and/or drying methods. Porous aerogels with high specific surface area or densely packed nanopaper films can be obtained as a result of such methods.^{42,43} Distinctive and collective properties such as low thermal expansion⁴⁴, oxygen and gas barrier⁴⁵, high transparency⁴⁶ (**Figure 1.2**(ii)), and functional substrates⁴⁷ can be obtained from such CNF network structures.

Furthermore, CNF network structures have high mechanical strength of $\sim 200 \text{ MPa}$, Young's modulus of $\sim 12 \text{ GPa}$ and deformation strain at break of $\sim 7\%$. In case of random in-plane orientation, the mechanical properties strongly depend on the network porosity,

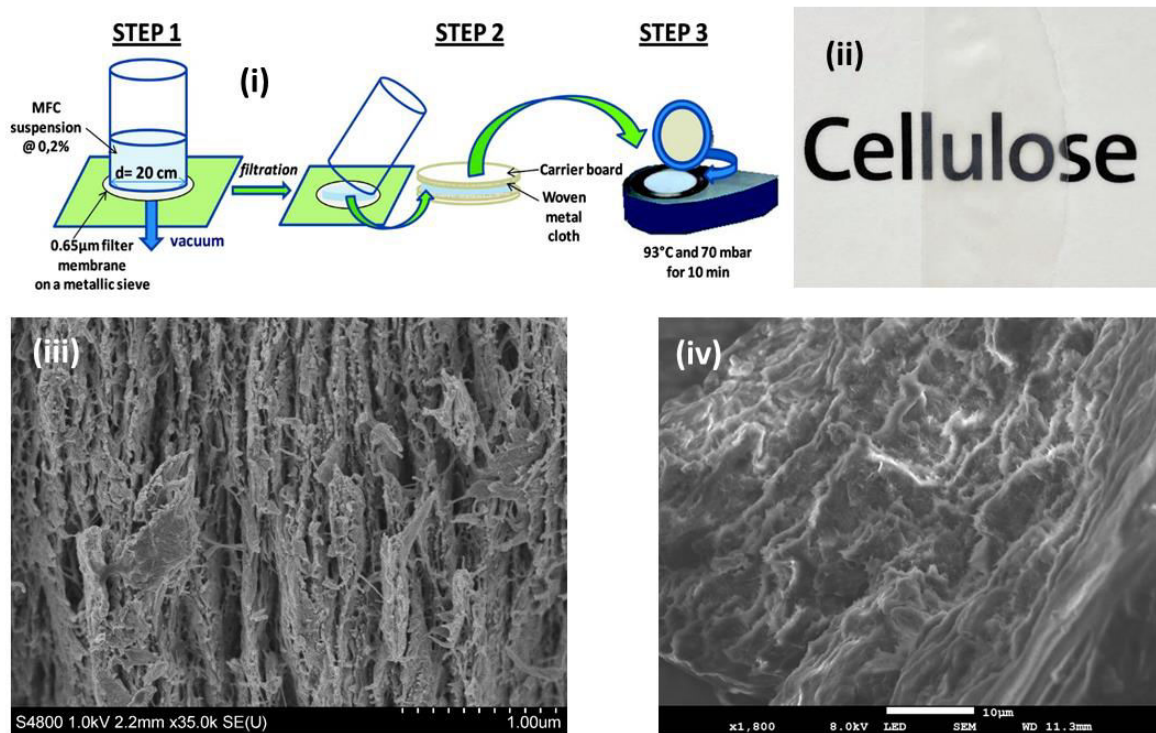


Figure 1.2 (i) Schematic of the CNF nanopaper filtration process. The figure is adapted from reference ³⁴. (ii) Highly transparent CNF nanopaper obtained from filtration process (densely packed CNF nanopaper of thickness $\sim 15 \mu\text{m}$). SEM images of CNF nanopaper (iii) showing CNFs physically entangled network and (iv) cross-section showing layered structure of CNF networks.

respective CNFs and surrounding humidity.⁴⁸ A typical stress-strain plot (**Figure 1.3**) of the CNF nanopaper reveals linear elastic behaviour until $\sim 1\%$ strain, followed by yielding and considerable strain hardening. The plastic strain hardening in CNF nanopaper originates from the network structure and is attributed to the structural rearrangements associated with fibril sliding and orientation, resulting in high ductility and ultimate strength of CNF nanopapers.⁴⁹ Strain hardening during plastic deformation can be turned to an advantage to orient nanofibrils along the test direction, thereby, amplifying the modulus and stiffness of nanopaper. CNF hydrogel can be subjected to slow uniaxial stretching up to pre-fracture strain and dried quickly to fix the fibril orientation in the nanopaper structure.⁵⁰ This characteristic can be taken advantage of when manufacturing nanocomposites during injection moulding, where the hydrodynamic force of the polymer melt flow can be used to orient the fibers within the composite. CNF nanopaper with oriented fibrils structure exhibit a modulus of $>50 \text{ GPa}$ and tensile strength of $>500 \text{ MPa}$.⁵¹

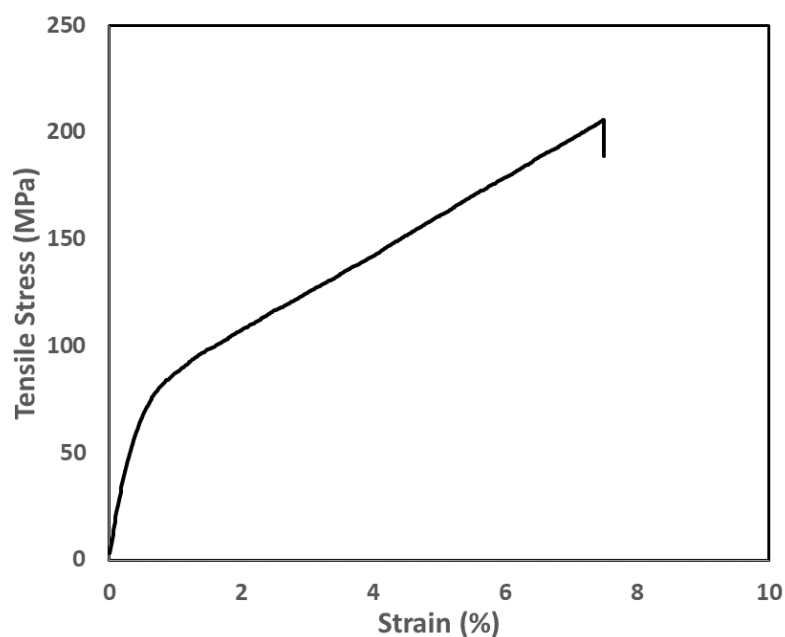


Figure 1.3 Stress-strain curve for low porosity CNF nanopaper. This curve was obtained from CNF nanopaper prepared in this study with a mean thickness of $\sim 15 \mu\text{m}$.

1.4 CNF Nanocomposites

In addition to high mechanical property, the low density and bio-derived aspect of CNF makes them attractive for bionanocomposites application. Nanocelluloses (CNC and CNF) provide high interfacial area to increase the interactions with the matrix phase and thus, improving the properties of the nanocomposite with relatively low concentrations of incorporated nanocellulose. Due to nanoscale reinforcement, the fracture-initiating defects are also expected to be in smaller size, thereby, delaying the failure of the nanocomposites.¹⁰ Initially, the reinforcing potential of nanocellulose (CNC from tunicate) in polymer composites was brought to the foreground by Favier *et al.*, where CNC nanocomposites were prepared with SBA latex as matrix.⁵² The strong reinforcement effect was accredited to hydrogen bonded network of CNCs in the composite.⁵³ Since nanocellulose could be easily dispersed in water, earlier developments in nanocellulose composites were based on water soluble polymers. Later on, CNC nanocomposites were prepared by dispersing them in organic solvents which unfolded the scope for water-insoluble polymers as matrix choices.⁵⁴ Another interesting outlook is that, the surface characteristic of CNFs and CNCs can be modified by surface modification methods

to improve dispersion and interfacial properties, especially to prepare composites with hydrophobic matrices.⁵⁵⁻⁵⁷ Further, wide range of matrix materials including thermoplastics and thermosets have been extensively investigated for CNC and CNF-based nanocomposites.^{58,59} Oksman *et al.* highlighted that conventional melt processing technique can be used to prepare nanocellulose reinforced engineering thermoplastic (with PLA) composites with improved mechanical properties.⁶⁰ However, lower thermal degradation temperature (~230 °C) is a limitation for melt processing methods. Nevertheless, comprehensive reviews focusing on nanocellulose composites and its corresponding processing techniques have been published until date.^{9,40,61-63}

1.4.1 Reinforcement Mechanism

Incorporating CNF in polymer matrices aids in enhancing the energy dissipation in the resulting composites without compromising on strength and toughness. The large surface to volume ratio of CNF, rooted from their nanometer dimensions, presents a great opportunity to dissipate energy through interfacial interactions.⁶⁴ Despite CNF showcasing excellent reinforcing potential in composites, the ability is principally dependent on the specific mechanics at the fibril-matrix interface. Load transfer between fibrils and matrix in an efficient energy dissipation way along the interface generally results in enhanced strength and toughness of composites. The classic shear lag model for traditional fiber-reinforced composites proposed by Cox⁶⁵ suggests that, the effective energy dissipation of discontinuous fiber reinforced matrix is mainly instigated by elastic mismatch between the fibril and matrix.⁶⁶ For higher concentration of CNF, the percolating phases increase and eventually reach percolation threshold, which is defined as the initial formation of a connected network.⁶⁷ In cellulose nanocomposites, the interaction is at a molecular level. The properties of matrix, CNF, and CNF composition along with optimum dispersion majorly influence the interactions between CNF and matrix. In general, for high CNF weight fraction nanocomposites, the strong reinforcing effect of CNF may be attributed to the formation of percolating network structure above the percolation threshold as result of hydrogen bonding between CNFs.^{68,69} The percolation approach predicts an approximate lower bound and nanocomposites' evaluation is

based on exceeding this lower bound. In the recent decades, computer aided simulations have been effective in modelling the percolation phenomenon in cellulose nanocomposites.⁶¹

1.4.2 Polyamide 6/Nylon 6 (PA6)

Polyamide 6 (PA6) is an engineering plastic that is positioned between the cheaper commodity plastics and the high-performance polymers, both in price, performance and process-ability. It is especially attractive because PA6 can also be produced by using bio-based raw materials or renewable raw materials.⁷⁰ Such bio-polyamides also includes PA10, PA11, PA12, PA46, PA6/12, PA6/10. Among these segments, the largest producer segment is bio-polyamide 6 in the global market owing to its effective cost and high-performance ratio (**Figure**

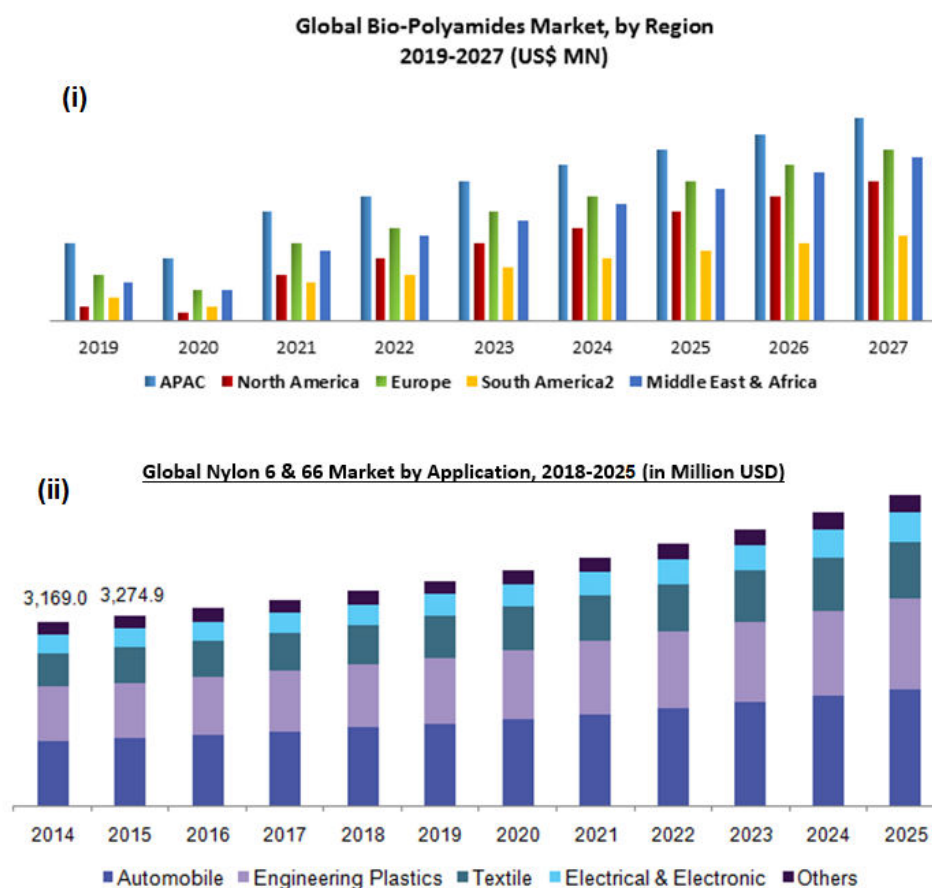


Figure 1.4 (i) Estimated global bio-polyamide market outlook by regions. This figure was adapted from Global Bio-Polyamide Market- Forecast and Analysis (2020-2027) Report by Maximize Market Research Pvt. Ltd., and (ii) Forecast of global PA6 and PA66 market in terms of applications. This figure was adapted by Global Polyamide Market Size, Share & Trends Analysis by Grand View Research.

1.4(i). CNF or in general natural fibers when incorporated with bio-polyamides opens up possibilities for nanocomposites which are 100% biodegradable. The global the market size of PA6 is estimated to grow tremendously as a result of environmental concerns and the demand for greener materials (**Figure 1.4(ii)**). However, the main disadvantage of these bio-sourced materials is that they are currently more expensive compared to traditional polyamides/nylon.

PA6 is a more attractive as an engineering polymer as it is competing with thermoset plastics and metals for ‘under the hood’ automotive applications due to their resistance to high temperature, oils and corrosive chemicals, relative strength to weight ratio and recyclability.⁷¹ A major potential application of cellulose (CNF and CNC) reinforced composites is the automotive industry as there is the need for light-weight, durable, inexpensive and potentially recyclable parts. When compared with conventional glass fillers, CNF are strong, lightweight, eco-friendly and most importantly impart stiffness enhancement along with better sound dampening.⁷² The application of these biocomposites in automobile interior components is forecast to increase drastically by each year due to environmental concerns.⁷³ PA6 as a matrix for CNF has the potential to create nanocomposites with superior mechanical and flexural strength, better dimensional stability, lower expansion, and better thermo-mechanical properties. Various researchers have successfully investigated the preparation and characterization of PA6 and cellulose composites and/or nanocomposites by adopting different methodologies.^{74–79} However, PA6/CNF nanocomposites is a relatively new research area, especially for nanocomposites with high formulation of CNF and this study provides useful insights on the development of PA6/CNF nanocomposites, aimed at contributing towards bio-based materials/composites and greener ways to produce them.

1.4.3 Composite Interface

The fibril – matrix interface is one of the primary factors defining the failure properties of the nanocomposites. As enumerated earlier, stress transfer occurs through the fiber matrix interface. The use of natural fibers (pulp fibers with ~30-50 μm diameter) usually provides improved modulus with a wide range of matrices, but the ductility is substantially reduced making the composite brittle. As a result, strength improvements often require a coupling agent.⁸⁰ Micron scale brittle composites are characterized by de-bonding at the fiber-matrix

interface leading to crack formation and propagation, resulting in specimen failure.^{40,81} In order to improve composite strength, it is desirable to obtain stronger interfacial adhesion at the fiber-matrix interface. CNF have high surface charge density due to the hydroxyl groups, making them sensitive to moisture and given the smaller dimensions, specific surface area is higher when compare to microfibers.

With PA6 being a hydrophilic matrix, good level of CNF dispersion can be achieved. In addition, at a molecular level the amide groups of PA6 form strong interfacial adhesion with the hydroxyl groups on the surface of the CNF.⁸² Due to the hydrophilic nature of both PA6 and CNF, the resulting nanocomposites become sensitive to moisture. Absorbed moisture content reduces the glass transition temperature (T_g) which in turn decreases the amorphous modulus and also the yield stress.⁸³ Nevertheless, efficient energy dissipation due to good interfacial adhesion, and fibril dispersion and distribution are two critical aspects for achieving the effective reinforcement in strength of the composite.⁸⁴ In high CNF content nanocomposites, the network forming ability of CNF has several functional advantages when the matrix is properly impregnated. The efficient impregnation of PA6 is challenge, as thermoplastic polymers have not been widely studied to impregnate nanocellulose structure.⁸⁵ This study demonstrates that PA6 can be successfully impregnated within the percolated CNF network by adapting suitable processing methodologies.

1.4.4 Composite Processing

Two processing techniques that have been utilized in this study are: (i) Melt processing using the GELIMAT[®] and (ii) Solvent casting technique. Other processing methods commonly used to produce CNF (or micro/nanocellulose) based composites are melt processing using extrusion and brabender, electrospinning, and solid-phase compounding. Such methods are discussed in detail elsewhere.^{62,86,87}

Solvent casting has been, by far the go to strategy for preparing nanocellulose-based composites. Typically, solvent casting involves mixing the components in a suitable (aqueous or organic) and pouring in mould, followed by drying/evaporation. In general, the rate of evaporation is critical to prevent agglomerations.⁸⁸ The mechanical properties are improved

drastically with this technique when compared to neat polymer/matrix. Initially, Qua *et al.* prepared nanocellulose – PA6 composites by solvent casting and the tensile strength was improved almost two folds with just 5 wt% formulation.⁸⁹ The strength is usually high with smaller weight fractions of CNF and for larger weight fractions, it usually decreases due to the CNF agglomerations. The impregnation of polymer matrices in this method capitalizes on the cross-linking proceeds in the presence of hydroxyl rich CNF which strongly influence the composite properties.⁹⁰ Hence for low cellulose composition nanocomposites, solvent casting method is ideal

Melt compounding process is used to incorporate nanocellulose into thermoplastic and thermoset polymers by involving thermo-mechanical mixing of melt mixture. This is usually followed by injection moulding or compression moulding into specific geometric configurations depending on the application.⁹¹ Iwatake *et al.* prepared cellulose composites by pumping a concentrated solution of nanowhiskers (along with a plasticizer agent) into an extruder with a partially molten polymer matrix.⁹² However, introducing aqueous suspension of CNF (or CNF) into polymer melt has direct limitation and is commercial not feasible. Moreover, such extrusion methods cannot be implemented for PA6 matrix as the high processing temperature, time and shear stresses might compromise the thermal stability of CNF leading to reduction in mechanical properties. In addition, drying the CNF before adding them into the polymer melt also causes irreversible agglomerations in nonpolar matrices resulting in poor mechanical properties.⁹³ Hence, only few reports concerning nanocellulose reinforced composites produced by melt processing techniques have been reported.⁹⁴

Of particular interest, the thermo-kinetic mixer; GELIMAT[®] which was used to produce cellulose pulp fiber composites and CNF nanocomposites is briefly discussed. The schematic of the types of Gelimat mixers are shown in **Figure 1.5**.⁹⁵ The compounding process involves exerting high shear rates on the materials, which increase the temperature of the compounding mixture and a final homogenous compound with excellent dispersion can be obtained.⁹⁶ Compared to twin screw extruder and Brabender, composites with well dispersed and distributed fibrils can be obtained by the Gelimat.⁹⁷ The obstacles of thermal stability can be overcome and good dispersion of CNF within the PA6 matrix can be achieved by melt compounding with a high speed thermo-kinetic mixer. Materials can be compounded in

extremely less time, therefore, due to shorter heating cycle of less than 30-60 seconds, the CNF are exposed to processing temperatures for extremely shorter period. Therefore, time-temperature sensitive materials such as in CNF/PA6 composites, thermal stability is preserved. Moreover, homogenous compounds can be obtained in a single cycle, whereas, similar levels of dispersion require two or three passes in an extruder.

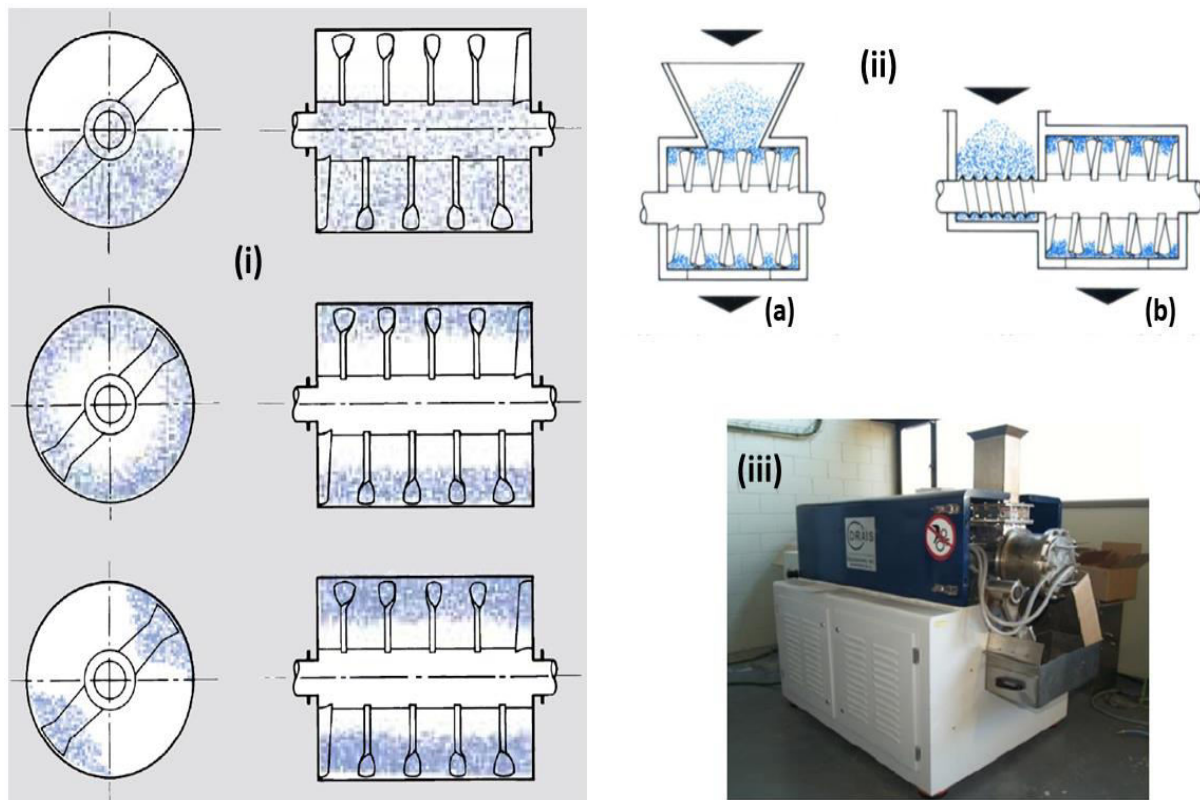


Figure 1.5 Schematic of GELIMAT[®] Mixer. (i) Basic Gelimat mixing material movement in the Gelimat mixing chamber at different mixing blade top speeds increasing from top to bottom. (ii) Types of Gelimat mixers based on feeding mechanism: (a) Top hopper feed for start/stop drive and (b) Axial side feed screw for continuous drive. These figures were adapted from the DUSATEC[™] Inc.'s brochure on GELIMAT Technology: Ultrahigh-Speed Thermo-Kinetic Mixing, Compounding & Fluxing. (iii) An axial feed screw Gelimat equipment.

1.5 State of the Art on 'PA6 and Cellulose' Composites

In this section some of the noteworthy developments on the topic of cellulose reinforced PA6 composites are mentioned. Polyamides reinforced with various bio-sourced reinforcements such as wood flour, pulp fibers, micro crystalline cellulose and nanocellulose has been discussed by Sessini *et al.*⁹⁸ Additionally, natural, plant-based fibers such as flax, hemp and cotton fibers have been and are an obvious choice to reinforce thermoplastic polymers, as fibers can be incorporated in composites without the need of any pre-treatment process. Initially in the early 1980s, Klason *et al.* prepared PA6 and bleached wood-flour by using single screw extrusion and injection moulding.⁹⁹ In the early 2000s, the use of processing aids to reduce the viscosity of the composite melt of PA6 and cellulose pulp-fibers during extrusion was employed by Jacobson *et al.*¹⁰⁰ Up to ~40 wt% formulation of wood-flour and PA6 composites with a non-disclosed processing aid (up to 7 wt%) was produced with single screw extrusion and injection moulding by Chen *et al.* showing that high natural fiber content thermoplastic composites could be produced using traditional melt processing methods.¹⁰¹ Many papers have been published on the reinforcement effect of natural fibers and also hybrid natural fibers for the PA6 matrix and have been characterized for mechanical and thermal properties.^{74,102–106} CNCs also have strong reinforcing effects and studies have also shown their positive impact on the physical properties of thermoplastic polymer composites.¹⁰⁷ Correa *et al.* coated CNCs with PA6 and then incorporated them with the PA6 matrix and the resulting composites displayed improved dispersion and mechanical properties.⁷⁸ Creep and viscoelastic materials functions of the PA6 reinforced CNC composites was investigated by Rahimi *et al.*¹⁰⁸ Effect of CNCs on crystallization, morphology and phase transition of polyamide 6 was recently analysed by Aitha *et al.*¹⁰⁹ More recently, Lee *et al.* prepared PA6 and CNF composites by utilizing a wet laid sheet forming approach and witnessed significant improvements in tensile properties.¹¹⁰ Takeshi *et al.* acetylated wood-kraft pulp to increase the heat resistance and used twin screw extruder to facilitate nanofibrillation of cellulose fibers to produce composites with improved mechanical properties.¹¹¹ Peng *et al.* obtained composite formulations up to 10 wt% CNF content with PA6 via thermal compounding using a Brabender with improvements in the tensile properties.⁷⁵ Lee *et al.* prepared 40 wt% CNF/PA6 by silane treatment and calendaring process achieving ~2.5GPa and ~12.5MPa tensile modulus and

strength, respectively.⁸² Joshi *et al.* obtained up to 50 wt% of regenerated cellulose composite membranes with PA6 using electrospinning method with tensile strength and modulus increments corresponding to ~12% and ~150% respectively.¹¹² Qua *et al.* used solution casting technique to prepare 5 wt% flax and MCC nanofibers obtained from acid hydrolysis and PA6 composites with almost twice the amount of improvement in tensile strength and minor improvement of modulus.⁸⁹ Xiang *et al.* fabricated polyamide 6/reduced graphene oxide nanocomposites by conductive cellulose skeleton structure and improved the conductivity of the composite.¹¹³ Studies related to other polyamides such as PA6.6^{114,115}, PA11¹¹⁶⁻¹¹⁹ and PA12^{120,121} have also been successfully reinforced with cellulosic materials.

Chapter 2 Objectives

This chapter consists of a brief discussion on the challenges and objectives as a whole for the doctoral thesis.

The drive for environmentally friendly materials has led to ground-breaking advancements in cellulose. This along with progress in polymer-matrix cellulose composites has allowed us to venture into property ranges that cannot be possible with individual components. Lately, cellulose nanofibrils (and nanocrystals) have gained traction as reinforcement because of their high intrinsic mechanical properties and sustainable resource. Plant and wood-based fibers (pulp fibers) have been used for a long time, however the use of nanocellulose provides greater possibilities in property enhancements and to develop newer functions. The nano-scale dimensions offer a better control over the design parameters and structural morphology. The tendency of nanocellulose to aggregate is a major challenge while processing such nanocomposites and may have pernicious effects on the physical properties. Hence, it is critical to preserve the nanostructure of cellulose in the bulk composite by means of uniform dispersion.

The principal objective of this work is to prepare nanocellulose (CNF) biocomposites with high CNF content and investigate the effects on the physical properties due to the nanostructure. One aspect of the study is to aim for high degree of dispersion of CNF in the nanocomposite and analyse the fibril/matrix interface by choosing an engineering polymer as matrix and varying the processing methods/techniques. Another aspect is to investigate the composites with different reinforcement sizes and also by varying the reinforcement concentrations. Therefore, in an initial study, cellulose composites with PA6 as matrix and cellulose pulp-fibers (in general with dimensions in few μm) as reinforcement was investigated. The reinforcement effect induced by the pulp fibers on the composite as a whole was studied with respect to the improvement of mechanical properties corresponding to the cellulose

composition. This was followed by investigating CNF nanocomposites which are prepared with two different methodologies; first, solvent casting approach and secondly, melt processing approach. A comparison between the reinforcing effect of cellulose pulp-fibers and CNF is made to emphasize the nanoscale dimension of reinforcement. Specific attributes such as dispersion, interface morphology, and effect of composite processing method/s and their respective influence on the material properties are investigated to expedite our understanding, so that materials with overall or distinctly improved properties can be designed. Overall, this investigation aims to contribute towards the fast-growing and sustainability-driven discipline of nanocellulose biocomposites.

Chapter 3 Methods and Experimental

This chapter contains a brief summary of materials preparation and characterizing techniques. More details can be found in appended Articles I to III.

3.1 Materials

Polyamide 6 (PA6) was obtained commercially from two manufacturers, both in form of pellets. Firstly, a natural coloured with low viscosity, extrusion and injection moulding grade PA6 namely Radilon[®] S 24E 100 NAT from Radici Group, Italy. This grade of PA6 is suitable for producing parts which require low material viscosity for efficient processing. Secondly, an easy flowing and finely crystalline grade namely, Ultramid[®] B3S was obtained from BASF, Germany. This PA6 is suitable to produce thin-walled technical parts.

Softwood pulp with high cellulose content (ca. 97%), kindly supplied by Domsjö Fabriker AB, Sweden, was used to prepare pulp-fiber composites and PA6/CNF nanocomposites via melt processing. CNF for nanocomposites produced using solvent casting was prepared from commercial never-dried softwood sulphite pulp (containing 87% cellulose, ~12% hemicellulose, and ~0.7% lignin) from Nordic Paper, Sweden.

3.2 Materials Preparation

Pulp fiber composites: As part of an initial study, softwood pulp fibers were used to prepare pulp fiber biocomposites with PA6. The pulp which was in form of sheets was disintegrated mechanically using a micro paper disintegrator. To prepare different compositions of pulp composites, batches of PA6 were dried for 8 h in 80°C to remove moisture content. Non-dried micro disintegrated cellulose pulp and dried PA6 were melt compounded

in the Gelimat[®] (G5 S, Draiswerke, USA). Non-dried pulp fibers were used to avoid fiber hornification.¹²² As the speed of the rotor blades increased, the mixture reached melting temperature and the compounding was completed in less than 60 seconds. The compounded mixture was collected and cooled immediately to prevent excessive thermal degradation. Subsequently after cooling, the compound was introduced into the pelletizer mill (SM100, Retsch, Germany) to obtain pulp composite pellets. This was repeated for all the planned formulation of the composites. To evaluate the effect of fiber orientation on the properties of composites, pellets were manufactured into square shaped samples using injection moulding (AR220 M, ARBURG, Germany). The injection chamber was cleaned from contaminants and impurities using a purging agent (Ultra Purge 5150, Chem-Trend, France) prior to the injection of pulp composites. Further, the square composite samples for all formulations were laser cut into three different orientations with respect to the injection flow direction; (a) perpendicular (90°), (b) parallel (0°) and (c) 45° with the sample dimensions (L x B x T) of 65 x 6 x 1.5 mm.

CNF preparation: CNF was prepared by enzymatic pre-treatment as described by Henriksson *et al.*¹²³ In brief, pulp fibers obtained as wet cake (ca. 20 wt% dry fiber content) were diluted 10 times with water to concentration of 2 wt% and pre-treated with enzymatic action (Novozym 476, Denmark). Thereafter, the enzymatic CNF suspension was passed through a homogenizer under varied pressure with channels of 400-200 μm (3 passes) and 200-100 μm (3 passes). The viscosity of the enzymatic CNF suspension increased with each pass and a viscous CNF gel was obtained at the end.

CNF template: The CNF gel was diluted further to a concentration of 0.2 wt% and dispersed in dilute water via high shear mixing (Ultra-Turrax T25, IKA, Germany). The dilute colloidal suspension was then vacuum filtered using PVDF membranes (Durapore[®], EMD Millipore) with small pore size of 0.65 μm . The filtered CNF cake had close to ~85% water, and was subjected to a vacuum drier (Rapid Köthen) in between filter papers at 90 °C. In the end, CNF nanopaper (neat CNF film) was obtained.

PA6/CNF nanocomposites via green solvent casting: At first, PA6 pellets were converted to powdered PA6 from Powder Plastics SL (Spain). From here on in, powdered PA6 is denoted as just PA6. Five different formulations of PA6/CNF nanocomposites with high

CNF content (10 wt%, 20 wt%, 30 wt%, 40 wt% and 50 wt%) were prepared using green solvent mixtures. A petri dish with an inner diameter of 8.8 cm was used for casting the neat PA6 and PA6/CNF nanocomposites. To prepare thin films of thickness close to 0.1 mm, an approximate total weight of 0.8 g of PA6/CNF solution was required. The amount of PA6 and CNF required for each composition of nanocomposites was calculated using the mass, density and volume relation. For every formulation, 20 wt% of PA6 was dissolved completely in formic acid at 30°C. The 1.5 wt% CNF gel was then dispersed within formic acid to obtain a consistency of 0.75 wt.% CNF content in the solvent system. This pre-wetting of CNF in the same solvent was done in order to further improve CNF/PA6 compatibility and their interfacial adhesion.¹²⁴ To ensure proper dispersion of CNF, the solution was mixed with the help of the Ultra-Turrax (T 25, IKA) by stirring at a high speed of 7000 rpm for about 30 seconds. This solution was then left in an Ultrasonic bath (Exibel, Clas Ohlson, Sweden) for 10 minutes to remove any possible bubble. Finally, the CNF gel dispersed in formic acid and the dissolved PA6 in formic acid were mixed with the help of a stirrer for 2 hours to ensure uniform mixing. This mixture was again left in the ultrasonic bath to remove any bubbles which might have been formed during mixing. The mixed solution was introduced on to the petri dish and placed in an oven (Mettert UM200, Germany) at 50°C for casting the PA6-CNF nanocomposite. When all the formic acid and water had evaporated, we placed the petri dish containing the composite in a desiccator at ambient temperature to prevent deformation while cooling. The composite was removed from the petri dish with the help of spatula and tweezers. Rectangular samples were cut using a hydraulic press (Stans & Press - TJT Teknik AB, Sweden) from the thin film for tensile and DMA characterizations.

PA6/CNF nanocomposites via melt processing: Initially, PA6 pellets were powdered from Powder Plastics SL (Spain). From here on in, powdered PA6 is denoted as just PA6. Three different formulations: 5 wt%, 15 wt% and 25 wt % of PA 6/CNF nanocomposites were prepared. Batches of PA6 respectively were dried for 8 h in an 80 °C oven to remove any moisture content. Each batch of dry PA 6 was thoroughly mixed with the respective amount of CNF gel to obtain the corresponding CNF wt% formulation of the nanocomposite. These mixtures were then dried in a 60 °C oven until all the gel-moisture content was removed. The dry PA6/CNF mixture was introduced into the Gelimat at a rotor speed of 300 rpm. The speed

of the rotor blades was increased and the action of the blades at such high speed allowed a mixture to reach melting temperature. The compounding was completed in less than 60 seconds and the compounded mixture was collected from the discharge gate. The obtained compounded mixture was cooled immediately using a cold bath. The compounding process was repeated to obtain the remaining two formulations of the nanocomposites. Further, the compounded composite mixtures for all the formulations were produced into composite pellets respectively using a pelletizer mill (SM100, Retsch). The nanocomposites pellets were compression moulded into films using a laboratory hydraulic hot press (Fontijne Presses, The Netherlands) at 230 °C under a pressure of 60 kN for 10 min. Metallic spacers with 0.5 mm thickness were positioned to control the thickness of the produced films. The obtained films were light brown in colour and translucent with no optical signs of CNF aggregation.

3.3 Characterization

Uniaxial tensile tests were performed on a Universal Testing Machine (Instron 1122) for the pulp composites and PA6/CNF nanocomposites produced via melt processing. Pulp-fiber composites samples of rectangular dimensions (L x B x T) 65 x 6 x 1.5 mm were tested at different fiber orientations. For PA6/CNF nanocomposites produced via melt processing, dog-bone samples according to ASTM D638 (Type V) specifications were used for tensile tests. For both the types composites, tensile tests were performed under two parameters. Firstly, dry samples, where the composite samples were dried in an 80 °C oven for 6 h prior to testing. Secondly, 48-hours conditioned samples, where the composite samples were placed in a climatic chamber at 23 °C and 50% relative humidity for 48 h according to ASTM D618 13 prior to testing. Tests were carried out at room temperature with 5 kN load cell and at a strain rate of 2 mm/min and a gauge length of 30 mm. The thickness and width of the narrow section for each melt processed PA6/CNF nanocomposites was measured using a digital micrometer (Starrett®, USA). A minimum of 5 trials were repeated to establish statistical significance.

Uniaxial tensile tests were performed for PA6/CNF nanocomposites samples produced via green solvent casting using a Universal Testing Machine (Instron 5944). Samples were conditioned at 23 °C and relative humidity 50% for a period of two days (48 h) prior to testing.

Rectangular samples of dimensions (l x b) 45 x 6 mm and thickness 15-120 μm and a gauge length of 20-25 mm were tested under a 500 N load cell at a strain rate of 10%/min. Strain was measured optically using a digital speckle pattern (DSP). All the values reported are averaged over at least 5 samples.

For all the composites, Young's modulus (E) was calculated from the slope the initial elastic region, typically between 0.1% and 0.4% strain. The maximum yield strength (σ_y) was estimated from the intersection of tangents at elastic and plastic regions. For neat PA6, the intersection of a line parallel to E, at an offset of 0.2% strain with the stress strain curve was taken as the yield stress.

Flexural tests were performed for pulp-fiber composite samples using a Universal Testing Machine (Instron 1122) for both dry and 48 h conditioned samples. Rectangular samples of were prepared by injection moulding according to ASTM D790 standard. The flexural properties were determined using a 3-point bending rig and over the area between the loading noses. Flexural strength (σ_f) was calculated from the load deflection curve that shows a point at which the load does not increase with an increase in strain, that is, a yield point. Flexural modulus (E_f) was calculated by drawing a tangent to the steepest initial straight-line portion of the load-deflection curve.

Micromechanics study to assess the contribution of CNF to composite's tensile properties was back-calculated for the PA6/CNF nanocomposites prepared via green solvent casting. A micromechanical model based on the rule of mixture (RoM) was used to estimate the tensile strength of the nanocomposites (Equation (1)).¹²⁵

$$\sigma_{NC} = \sigma_{CNF} V_{CNF} + \sigma_{PA6} (1 - V_{CNF}) \quad (1)$$

Where σ_{NC} is the tensile strength of the nanocomposite, σ_{CNF} and σ_{PA6} are the experimental strength of CNF and PA6 respectively, and V_{CNF} is the total volume fraction of CNF. The value of σ_{NC} predicts the linear relationship between σ_{NC} and the composition of CNF. An estimation of reinforcement efficiency for all the formulations of CNF content was calculated assuming the densities of 1.13 g/cm^3 for PA6 and 1.5 g/cm^3 for CNF.

The Cox-Krenchel micromechanical model was used to back-calculate the Young's modulus. This model was developed based on the classical shear lag theory and is one of the most widely used model for randomly oriented short fibre composites.⁶⁸ This model is based on the following assumptions: (a) fiber and matrix respond elastically, (b) no axial loads on the fiber ends and (c) ideal fiber matrix interface.^{65,126} The Cox-Krenchel model is defined as:

$$E_{NC} = \eta_0 V_{CNF} E_{CNF} \left(1 - \frac{\tanh(ns)}{ns} \right) + (1 - V_{CNF}) E_{PA6} \quad (2)$$

$$n = \sqrt{2E_{PA6} / \left[E_{CNF} (1 + V_{PA6}) \ln \left(\frac{1}{V_{CNF}} \right) \right]} \quad (3)$$

Where E_{NC} is the theoretical elastic modulus of the nanocomposite, E_{CNF} and E_{PA6} are experimental moduli of CNF and PA6 respectively, fiber orientation factor $\eta_0 = 3/8$ assuming an in-plane isotropic orientation of fibers in a random short fiber polymer composite, s is the fiber aspect ratio where the weight average fiber length L can be used to calculate $s = L/D$, where D is the diameter of the fiber

Additionally, Tsai-Pagano model was also used to predict the Young's modulus assuming a random in-plane fiber orientation.¹²⁷ E_{NC} is the theoretical nanocomposite modulus for random in-plane fiber orientation and is defined by:

$$E_{NC} = \left(\frac{3}{8} \right) E_L + \left(\frac{5}{8} \right) E_T \quad (4)$$

$$E_L = E_{CNF} V_{CNF} + E_{PA6} (1 - V_{CNF}) \quad (5)$$

$$E_T = \frac{E_{CNF} E_{PA6}}{E_{CNF} (1 - V_{CNF}) + E_{PA6} V_{CNF}} \quad (6)$$

For longitudinal modulus (E_L), RoM model was used (Equation (5)) and transverse modulus (E_T , Equation (6)) was calculated assuming a unidirectional composite with cylindrical fibers.

Dynamical mechanical-thermal analysis (DMA) was performed on a TA Q800 equipment for PA6/CNF nanocomposites prepared via green solvent casting. DMA was conducted in tensile mode with a preload of 1N at a frequency of 1 Hz and at a ramp of 5 °C/min starting at 30 °C and finishing at 160 °C. Rectangular samples of dimensions (L x B) 15 x 6 mm and thickness 15-120 µm were placed in an oven for 48 h at 55 °C prior to analysis. The glass transition temperature (T_g) was estimated from the tan delta peak of DMA scans.

Scanning electron microscopy (SEM) was used to analyse the morphology of fractured surfaces for all types of composites prepared. SEM images were obtained using a Zeiss DSM 960A microscope for pulp fiber composites. The samples were coated with gold using a sputter prior to analysis and were observed at an accelerated voltage of 7kV.

SEM images for both type of PA6/CNF nanocomposites were obtained using a Hitachi S-4800 microscope. Cross-section of samples fractured from tensile testing were coated with a thin layer of conductive layer prior to observation. The samples were analysed between the accelerated voltage of 7-15kV.

Thermogravimetric analysis (TGA) were performed for all the composites samples using a Mettler Toledo TGA 1 equipment. Samples were analysed in the temperature ranged from 25 to 600 °C with a 10 °C/min heating rate. The tests were carried out by placing the samples in an open platinum pan within a nitrogen environment. All the results were recorded using a thermal analysis software.

Additionally, for the PA6/CNF nanocomposites prepared via melt processing study, TGA at isothermal conditions (230 °C) for the CNF gel was performed to check for thermal stability of CNF at processing temperature conditions.

Differential scanning calorimetry (DSC) measurements were performed on a Mettler Toledo DSC 1 for PA6/CNF nanocomposites prepared via green solvent casting. For PA6/CNF nanocomposites prepared via melt processing, DSC measurements were performed on a TA DSC Q2000 equipment. For both cases, 5-8 mg of samples, after conditioning at 23 °C for two days, were placed in an aluminium pan. The samples underwent a heating cycle from 30 to 260 °C with a heating rate of 10 °C/min. All the results were reported by a corresponding thermal

analysis software. The degree of crystallinity (χ_c) was calculated corresponding to the enthalpy of the melting endotherm using Equation (8), where ΔH_{sample} is the enthalpy of the melting endotherm of the sample from the heating cycle, $\Delta H_{\text{polymer}}$ is the melting enthalpy of PA6 polymer in the sample, W_{CNF} is the weight fraction of the CNF in the sample and $\Delta H_{100\%}$ is the theoretical melting enthalpy of 100% crystalline PA6, which is equivalent to 230 J/g.^{128,129}

$$\Delta H_{\text{polymer}} = \Delta H_{\text{sample}} \cdot \left(\frac{1}{1 - \frac{W_{\text{CNF}}}{100}} \right) \quad (7)$$

$$\chi_c = \frac{\Delta H_{\text{polymer}}}{\Delta H_{100\%}} \cdot 100 \quad (8)$$

Attenuated total reflection (ATR) FT-IR was performed solvent casted PA6/CNF nanocomposites using a Perkin Elmer spectrum 100. For real time measurements, samples were impregnated with PA6 as earlier and dried at room temperature for 30 min (but not cured). Then, they were placed on the preheated ATR crystal and the spectra recorded in the range of 4000-600 cm^{-1} . The changes in the chemical structure and the binding configuration of the nanocomposites were characterized by associated peaks.

Capillary rheological properties were studied using a melt flow indexer (MFI) device (Ceast, Italy) for PA6/CNF nanocomposites prepared via melt processing. Neat PA 6 and the corresponding nanocomposite pellets were tested for MFI at 230 °C through a capillary (die) of specific diameter and length by pressure applied through dead weight M (kg) as per ASTM 1238-73. The geometrical dimensions of the MFI apparatus are: radius of the die $r = 1$ mm; radius of the heating cylinder $R = 4.75$ mm; length of the heating cylinder $L = 30$ mm (ISO 1133). The mass series used to measure MFI values are: M1–M2–M3.....M7 (kg) = 1.2–2.16–3.8–5.0–7.16–10.0–12.16. For each mass used, five MFI values were measured for statistical significance. Capillary rheological properties can be illustrated on a rheogram, which represents variation of dynamic viscosity μ (Pa s) versus shear rate γ (s^{-1}). To go from MFI (g/10 min) to viscosity, the Equations governing the flow of fluids inside a capillary (die) was used.¹³⁰

The apparent shear rate γ depends on the volume flow rate Q (m^3s^{-1}) and the radius of the die r (m).

$$\gamma = \frac{4 \cdot Q}{\pi \cdot r^3} \quad (9)$$

The volume flow rate Q can be calculated using the MFI data and the respective hot density ρ (g cm^{-3}) of the samples.

$$Q = \frac{600 \cdot \text{MFI}}{\rho \cdot t} \quad (10)$$

Hence,

$$\gamma = \frac{2400 \cdot \text{MFI}}{\pi \cdot r^3 \cdot \rho \cdot t} \quad (11)$$

The viscosity μ is defined as shear stress τ (Pa) divided by the shear rate γ . The shear stress τ depend on the pressure P exerted at die inlet, i.e., the force F exerted by the mass M placed on the MFI piston.

$$P = \frac{F}{\pi \cdot R^2} = \frac{M \cdot g}{\pi \cdot R^2} \quad (12)$$

Hence,

$$\tau = \frac{P \cdot F}{2 \cdot L} = \frac{M \cdot g \cdot r}{\pi \cdot R^2 \cdot 2 \cdot L} \quad (13)$$

The above Equations (11) and (13) are for Newtonian fluids. PA 6 and respective nanocomposite blends have non-Newtonian behaviour. Therefore, the apparent shear rates were corrected using the Rabinowitsch shear rate correction.¹³¹ A first realistic approach to the rheological behaviour was presented by the power law symbolized by Oswald law defined by Equation (14).

$$\tau_T = k \cdot \gamma_T^n \quad (14)$$

where τ_T is the true shear stress, k is a constant of the fluid and n is the flow index (pseudoplasticity index). To find out n , the curve $\text{Ln } \tau = f(\text{Ln } \dot{\gamma})$ was plotted from the calculated apparent stresses and shear rates obtained from the MFI data. With n being the slope and $\text{Ln } k$ the intercept, the necessary Rabinowitsch correction was performed for the apparent shear rate $\dot{\gamma}$ using Equation (15).

$$\dot{\gamma}_T = \frac{(3n + 1)}{4n} \cdot \dot{\gamma} \quad (15)$$

where $\dot{\gamma}_T$ is the true shear rate, from which the true effective viscosity μ was calculated. Thus, the rheogram representing the rheological behaviour of nanocomposites at 230 °C was obtained without having to use a sophisticated rheometer.

Water uptake measurements were carried out for PA6/CNF nanocomposites prepared via melt processing. The influence of CNF content on water absorption and subsequently the mechanical properties of the composites were analysed. Periodic mass measurements of samples when submerged in water over a 24-h period was conducted. The dry samples were weighed before placing them in dilute H₂O at room temperature. The samples were removed from the water and patted dry with Kimwipes[®] prior to weighing. Mass measurements were taken at 0 h, 0.5 h, 1 h, 3 h, 6 h, 12 h, 18 h and 24 h. The weight percentage change was calculated using Equation (16), where W_{wet} is the weight of sample after immersed in water and W_{dry} is the dry weight of the sample.

$$\text{percent change} = \frac{(W_{\text{wet}} - W_{\text{dry}})}{W_{\text{dry}}} \times 100 \quad (16)$$

Thereafter, the samples were allowed to gain mass until they reached an equilibrium state. The water uptake kinetics were model by using Fick's theory of dispersion. The diffusion coefficient D (m²/s) for shorter immersion time of nanocomposite samples with respect to the ability of moisture/water to penetrate the samples was deduced from Fick's law, as in Equation (17). Where M_t is the water uptake at a lower immersion time, M_{∞} is the maximum mass gained, L (m) is the thickness of the sample and time t (s).

$$\frac{M_t}{M_\infty} = 2 \times \left(\sqrt{\frac{D t}{\pi L^2}} \right) \quad (17)$$

Chapter 4 Results and Discussion

This chapter consists of the results and discussions of the doctoral thesis based on the appended three articles.

4.1 Pulp-Fiber Composites

As an initial part of the investigation, wood-pulp fibers derived from softwood were used to reinforce polyamide 6 (PA6) matrix. Although, cellulose nanofibrils (CNF) offer greater potential as discussed in Chapter 1, cellulose pulp fibers (diameter $\sim 30\ \mu\text{m}$) have various cost and processing advantages. When compared to CNF, pulp fibers have lower costs, lower viscosity in suspensions, shorter dewatering time, and etc. In this section, pulp fiber composites are used to prepare PA6-pulp fiber composites. The results presented in this section are from Article I and the investigative outcomes are further used to design nanocomposites with CNF elucidated in the later sections.

4.1.1 Effect of Fiber Orientation on the Mechanical Properties

High purity cellulose pulp fibers were used to produce composites with PA6 and five different wt% formulations (5, 10, 15, 20, and 25 wt%) were prepared. The materials were melt compounded in the high speed kinetic mixer (GELIMAT®) and then produced into test samples using injection moulding. To analyse the effect of fiber orientation on the mechanical properties of the composites, a square mould (**Figure 4.1(v)**) was injected with the compounded composite and later test samples were cut at different angles/orientations with respect to the injection flow (**Figure 4.1(i-iv)**). The pulp fibers, during processing (injection) are expected to align themselves in the direction of the injection flow imparting anisotropic

properties to the resulting composites.^{132,133} A similar model where the injection process was simulated shows the fiber orientation inside the square mould (**Figure 4.1(vi)**). Pulp fibers with high degree of orientation impart high stiffness to the composite in the longitudinal direction, mimicking the microfibrils in the plant cell wall. Flow induced alignment and good distribution of fibers within the matrix allow for greater control of the composites' microstructure when designing such biocomposites.¹³⁴

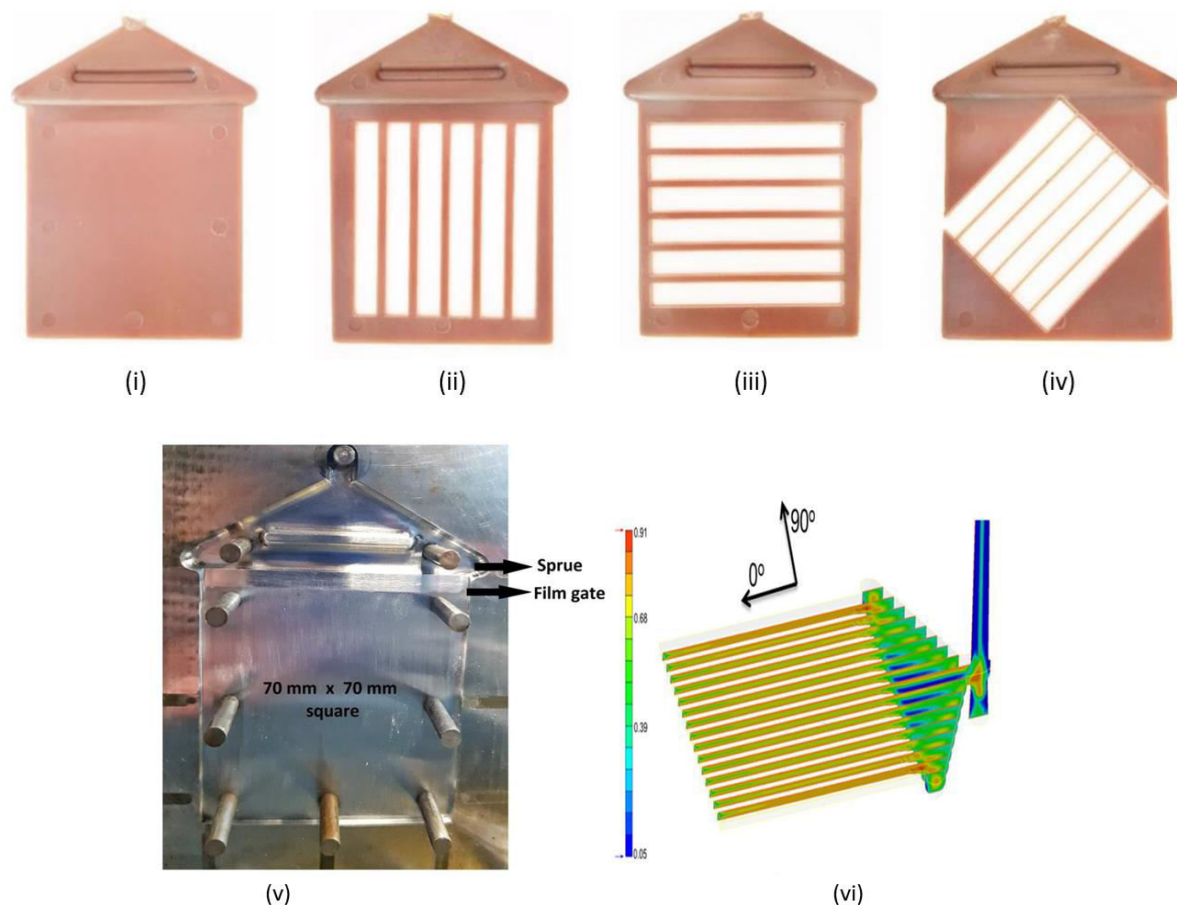


Figure 4.1 (i) Square samples of dimensions (L x B x T) 70 x 70 x 1.5 mm, and square samples from which (ii) 0°, (iii) 90°, and (iv) 45° oriented test specimens were laser cut. (v) Square mould used for injection moulding and (vi) Flow simulation showing the orientation of the pulp fibers within the square mould. Figure adapted from Article I.

4.1.1.1 Mechanical Properties

The summary of the tensile and flexural properties for dry samples are listed in **Table 1**. The pulp fiber/PA6 composites obtained showed better mechanical properties. The

mechanical properties increased with the increase in pulp fiber content in comparison to neat PA6. As expected, the composite specimens oriented in the direction of the injection flow exhibited higher mechanical properties, compared to the other two orientations for all formulations respectively.

Table 1. Summary of tensile properties of pulp fiber composites showing the variation of yield strength with respect to fiber orientation with the matrix for dry samples. Table adapted from Article I.

Sample Pulp (wt%)	Yield Strength σ (MPa)			Young's Modulus E (GPa)	Strain at Break (%)	Flexural Strength σ_F (MPa)	Flexural Modulus E_F (GPa)
	0°	45°	90°	0°	0°		
Neat PA6	— 53.3 —			3.01	17.8	103.2	2.5
5	60.6	56.2	54.5	3.3	7.1	105	2.6
10	60.5	57.7	54.8	3.5	6.5	107.9	2.8
15	61.4	59.5	55.3	3.8	4.9	111	3.01
20	66.2	58.2	53.3	4.2	4.5	112.2	3.6
25	64.8	60.5	53.1	4.6	4.0	113.6	3.8

The assessment of fiber orientation on the composites' mechanical properties was analysed based on the yield strength results. For the oriented sample's gauge length was too small for our extensometer to measure the modulus. However, the modulus and the deformation strain were measured from dog-bone samples prepared according to ASTM D638 standard. For the pulp fiber composites, the tensile properties increased with the increase of pulp fibers. The maximum yield strength was obtained for 20 wt% formulation and the maximum elastic modulus was obtained for 25 wt% formulation. The tensile strength values obtained for the 0° oriented samples were higher than the values for the other two oriented samples, with the least values obtained for 90° oriented samples. Naturally, cellulose microfibrils have higher specific strength in the longitudinal direction and this property is inherited in the pulp fiber composites

as well. The aspect ratio of pulp fibers, along with the good dispersion and distribution within the PA6 matrix aid in the enhancement of mechanical properties. For 45° and 90° oriented samples, the strength tends to decrease because of the increased amount of transverse fibers which provide low cross-sectional strength which tends to behave as defects under the elongation load. Further, the incorporation of pulp fibers into PA6 matrix restricts the elastic deformation of PA6 resulting in composites with higher modulus.¹³⁵ The strong interaction between cellulose (carboxyl groups) and PA6 (amide groups) allows effective stress transfer under loading and notably, the strains at yield are reduced. These reductions in strain indicate that the pulp fibers were well dispersed and stiffened the composites. Flexural testes were carried out on samples according to ASTM D790 standard. Consequently, due to the stiffness of the composites, the flexural properties also increased with the addition of pulp fiber content. High magnification images (**Figure 4.2**) obtained from SEM analysis show that there is good wetting between the pulp fibers and PA6 matrix supporting the reinforcing effect of pulp fibers. The moisture content in never dried pulp fibers aid in interfacial bonding, due to the partial hydrolysis of PA6 caused by moisture at high temperature, generating carboxylic acid end groups which are compatible with the (-OH) groups forming ester bonds.¹³⁶ Minor intermittent voids are can also be observed.

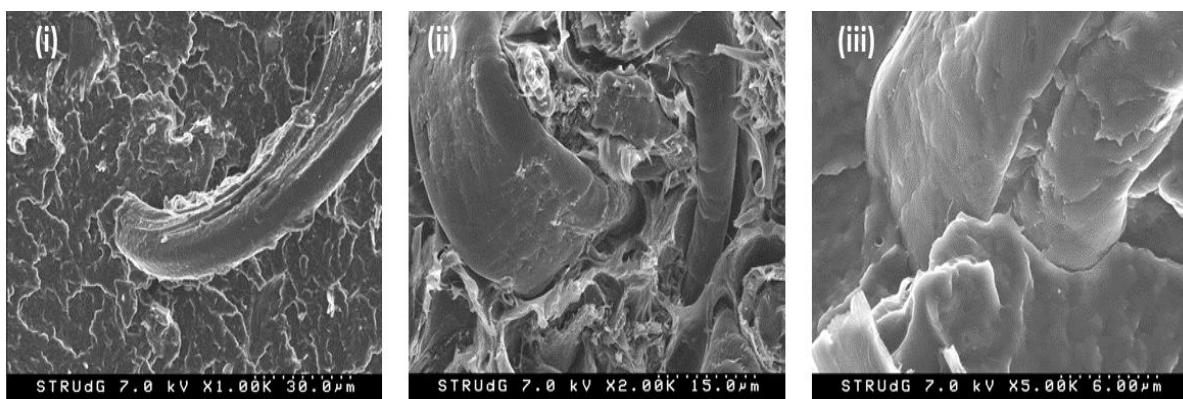


Figure 4.2 Cross-sectional images of 25 wt% pulp fiber composites at various magnification levels indicating good wetting between fibers and matrix. Figure adapted from Article I.

4.1.2 Hygro-Mechanical Properties

With both PA6 and cellulose pulp fibers being hydrophilic in nature, the properties of the composites are altered with moisture absorption. Pulp fiber/PA6 composites were studied

for hygro-mechanical stability by conditioning the test samples at 23°C and relative humidity 50% for a period of 48 hours (ASTM D618 13) prior to testing. The mechanical properties reduced for the moisture conditioned samples (**Table 2**). Composites showed decent hygro-mechanical stability when compared to neat PA6. The tensile modulus reduces to 4.4 GPa from 4.6 GPa at relative humidity 50% for the 25 wt% formulation. Similarly, flexural modulus reduced to 3.1 GPa to 3.8 GPa for the 25 wt% formulation. Hydration of composites due to humidity reduces the intrinsic stiffness of the fibers. Moisture is likely to be accumulated at the fiber/matrix interface and weakens the adhesion. However, the tensile modulus reduction of ~0.2 GPa is considerably a minor reduction and is also much higher than the modulus of conditioned neat PA6. This is due to the successful saturation of the PA6 matrix into the random pulp fiber reinforcement network and favourable interactions at the interface. Further, the effect of moisture on glass transition temperature, and mechanical properties of CNF nanocomposites are discussed in the later sections.

Table 2. Summary of the mechanical properties for the PA6-pulp fiber composites after 48-hour conditioning of samples at 23° and relative humidity 50%. Table adapted from Article I.

Sample Pulp (wt%)	Yield Strength σ (MPa)			Young's Modulus E (GPA)	Strain at Break (%)	Flexural Strength σ_F (MPa)	Flexural Modulus E_F (GPA)
	0°	45°	90°	0°	0°		
Neat PA6	—	48.8	—	2.9	16	90.2	2.1
5	55.8	54.5	54	3.2	4.8	94.2	2.2
10	57.6	56.2	53.1	3.4	4.8	95.4	2.3
15	59.4	57.2	52.9	3.7	4.05	98.5	2.5
20	57.6	55.4	51.5	4.1	3.7	101.5	2.8
25	57.3	55.8	51.3	4.4	3.8	106.5	3.1

4.2 Nanocomposites via Solvent Casting

This section focuses on CNF/thermoplastic composites with PA6 as polymer. CNF are long fibril like structures which form percolated/entangles network when filtered from water. A solvent casting processing method, similar to a prepreg-based approach is adopted to produce nanocomposites with high CNF composition up to 50 wt%. Effect of high CNF content, specific surface area and fibril-matrix interface of the composites are studied. The tensile mechanical properties of the nanocomposite films were improved. The results presented in this section are selected from Article III. The differences in the reinforcement effect of cellulose pulp fiber and CNF are also analysed.

4.2.1 Processing Approach

PA6/CNF nanocomposites were prepared by an impregnation-based approach using solvent casting. A dilute colloidal CNF suspension was filter to obtain a CNF nanopaper template. Formic acid was used as the solvent for dissolving PA6, as it accounts for negligible polymer degradation at a dissolving temperature of 30°C promoted by the weak acid characteristics.^{137,138} In addition, CNF has good dispersion in water and hence, a water/formic acid mixed system was adopted to impregnate dissolved PA6 in dispersed CNF. Furthermore, formic acid functions as a protic solvent and it can disrupt the hydrogen bonding in aggregated CNFs, hence, more effectively dispersing them.⁷⁷ Moreover, CNF in formic acid medium results in esterification of hydroxyl entities upon evaporation/casting.¹³⁹ Both PA6 solution and CNF suspension in formic acid/water medium were prepared as a first step. The nanocomposite films were produced by diluting the CNF dispersion in water into formic acid containing 20 wt% of dissolved PA6. Homogenous impregnation of CNF was facilitated the Ultra-turrax. An advantage of this process is that CNF/polymer ratio in the final composites can be conveniently tuned by controlling the dissolved polymer content in the impregnating solution.

4.2.2 Dispersion, High Specific Surface Area and CNF Network

The prepared nanocomposite films showed no signs of optical agglomeration or defects (Figure 4.3 (iv & vii)). This indicated that the films had homogenous distribution and good

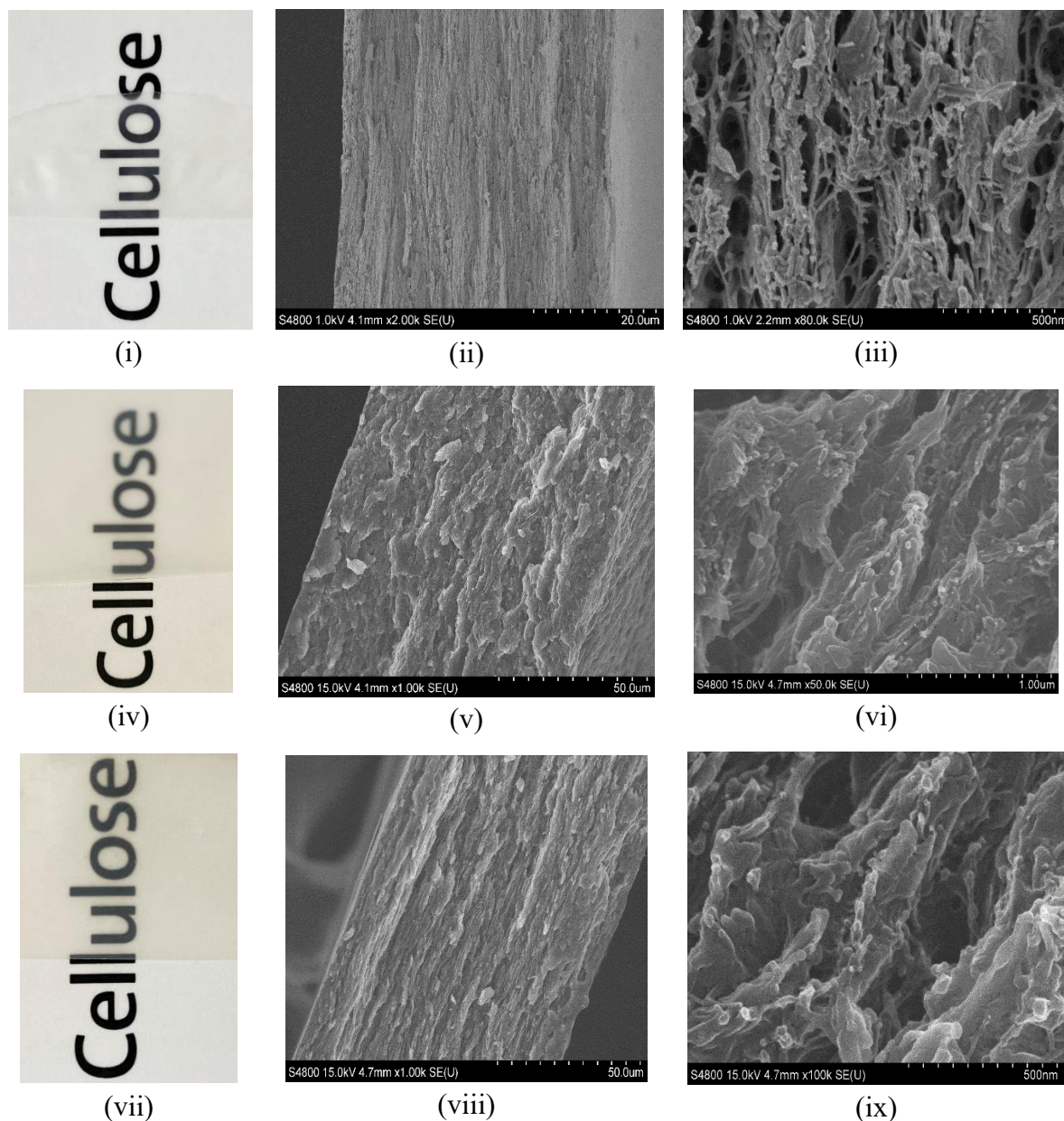


Figure 4.3 Cross-sectional SEM images of PA6/CNF nanocomposites films: (ii & iii) CNF nanopaper, (v & vi) 20 wt%, and (viii & ix) 50 wt% formulations. These images are adapted from Article III. Casted CNF nanocomposite films: (i) neat CNF nanopaper film, (iv) 20 wt%, and (vii) 50 wt% formulations.

dispersion. When the CNF colloidal suspension is filtered, CNFs form physical entanglements with a random in plane orientation of nanofibrils (**Figure 4.3 (ii)**). Layered structures are a feature of the nanocomposites too, since, the processing involves removal of solvent mixture through evaporation. The layers are distinct in the nanocomposites as well (**Figure 4.3 (v & viii)**). For CNF nanopaper, the hydroxyl groups on the CNF results in hydrogen bonding between individual CNFs and hence creating a 3D percolated network (**Figure 4.3 (iii)**). This network formation is apparent in the higher magnifications of the nanocomposites as well (**Figure 4.3 (vi & ix)**), where the nanofibrils are surrounded but the strands of PA6 which have deformed under elongation. Besides, this corroborates that the CNF network was successfully impregnated by the PA6 matrix. Nanocomposite films prepared by casting CNF and PA6 mixture in formic acid had showed high optical transparency. In fact, the transparency increased with the addition of CNF. A favourable interface between CNF and PA6 matrix assists in dispersion of CNFs and relatively void-free packing in film. The absence of CNF agglomerates aided by dispersion to a large content, prevents scattering of light thereby, improving transparency. The electrostatic repulsion between the nanofibrils due to the negative charged surface density is also key in dispersing the CNF within the matrix. Storage modulus

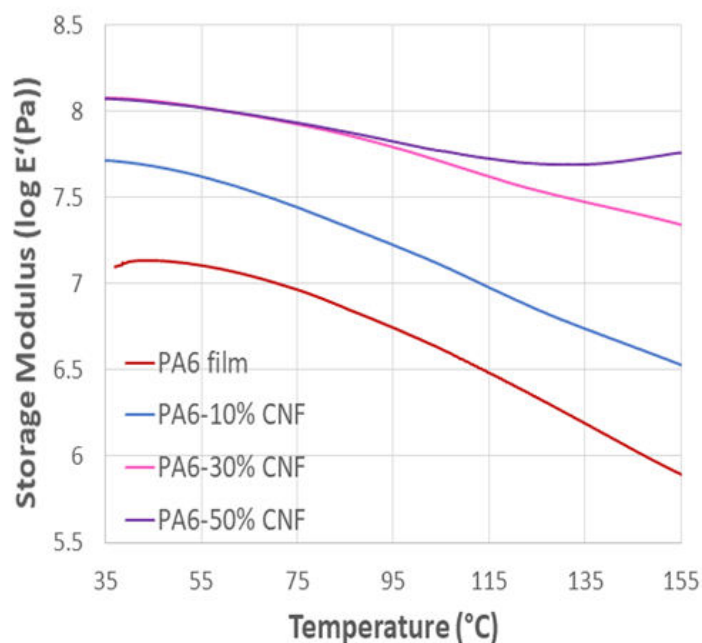


Figure 4.4 Storage modulus as a function of temperature for PA6/CNF nanocomposites (10, 30 and 50 wt% formulations). Figure from Article III.

as a function of temperature in PA6/CNF nanocomposites is shown in **Figure 4.4**. The modulus for neat PA6 stays constant up until 50 °C and later drops significantly corresponding to the glass transition region of PA6. For the nanocomposites, the storage modulus was significantly enhanced within the same temperature range, asserting that the CNF was well dispersed in the PA6 matrix. The increase in storage modulus is reminiscent even at higher temperatures, this effect is a result of the 3D percolated network within the rubbery matrix constraining the long-range motion of polymer chains.^{53,140} The tensile strength and modulus of the nanocomposite films was improved significantly with the addition of CNF. Again, this is attributed to the uniform dispersion and high surface area of the fibres and strong interaction between the CNF and PA6 matrix, promoting effective stress transfer. The tensile mechanical properties are discussed further in in the later section.

4.2.2.1 Mechanical Properties

In this section, the uniaxial tensile properties are discussed. Furthermore, micromechanical models are used to estimate the tensile strength and modulus of the CNF in different formulations of nanocomposites. The relation of CNF network reinforcement and mechanical properties of the nanocomposites are discussed. Representative stress strain curves are plotted in **Figure 4.5** and the results are summarized in **Table 3**. From the curves (**Figure 4.5**), it is palpable that the modulus and strength increased with the addition of CNF to the neat PA6. Ultimate strength of 124 MPa and modulus of 4.2 GPa was obtained for the 50 wt% formulation of nanocomposite. The tensile values are greater than previously reported values using cellulose or plant-based fibers for PA6 matrix.^{75,82,89,103,111,112,141–143} The trend in contrast to several of the mentioned studies on PA6 and cellulose (micro and nano) composites is characterized by strength increase for lower formulation of CNF content and then decreases for higher CNF content due to cellulose agglomeration. In our study, the impregnation in a solvent mixture necessitated by high speed dispersing (Ultra-turrax) and then casting allowed incorporating high CNF content (up to 50 wt%) in form of 3D percolated network, without causing extensive agglomerations. For CNF nanocomposites produced by melt processing approach, which is discussed in the next section, high content CNF nanocomposites (up to 25 wt%) with improved mechanical properties were prepared as well, demonstrating that the

processing approaches adopted in our study allowed for producing high-performance biocomposites of cellulose nanofibrils and a technical polymer such as polyamide-6.

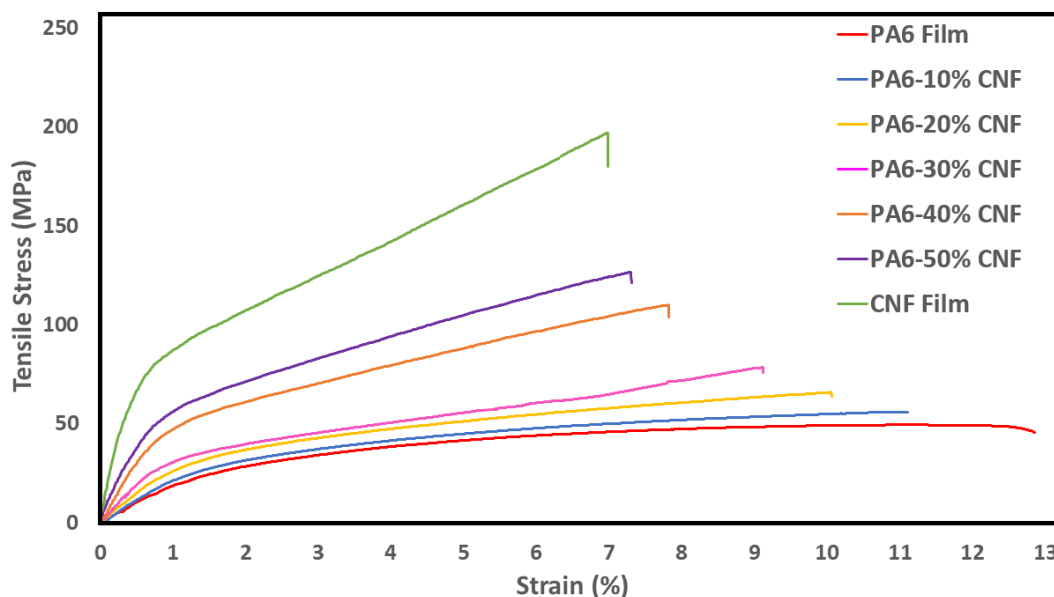


Figure 4.5 Characteristic stress-strain curves from uniaxial tensile tests for PA6/CNF nanocomposites with relative humidity 50%. Figure adapted from Article III.

Table 3. Summary of the tensile mechanical properties for the PA6/CNF nanocomposites at relative humidity 50%. Table from Article III.

CNF Content (wt. %)	Mean Thickness (μm)	Tensile Strength (MPa)	Elastic Modulus (GPa)	Strain at Break (%)
Neat PA6	96.2 ± 8.4	46.3 ± 2.35	1.52 ± 0.08	12.6 ± 0.42
10	111 ± 7.3	54.1 ± 2.87	1.85 ± 0.05	11.1 ± 1.72
20	108.6 ± 1.9	67.3 ± 1.60	2.30 ± 0.08	10.1 ± 1.69
30	116.8 ± 6.3	78.4 ± 0.35	3.48 ± 0.47	9.2 ± 0.49
40	91.3 ± 3.0	110.5 ± 7.80	4.10 ± 0.26	7.8 ± 1.17
50	99.8 ± 2.9	123.9 ± 6.12	4.20 ± 0.27	7.3 ± 0.50
CNF film	15.4 ± 0.8	200.9 ± 6.73	12.23 ± 0.39	6.9 ± 0.82

The stress-strain curves for the PA6/CNF nanocomposites follow the characteristics of the CNF nanopaper, where typical initial linear region (elastic response), followed by corresponding yielding at lower strain and subsequent plastic deformation (strain hardening) until sample fractures. Nanocomposites undergo significant plastic deformation which is especially apparent for high CNF content nanocomposites. Favourable strain hardening region if CNF network is retained, resulting in high strain to failure and higher ultimate strength. The reinforcement mechanism in plastic region are dominated by the CNF network and improves ductility and strength.¹⁴⁴ In addition, polymers with low yield and high ductility allows for stronger effects of deformation. Hence, in some studies the tensile strength of the PA6 composite is doubled for smaller concentrations of CNF content.⁸⁹ At relative humidity 50%, neat PA6 has a modulus of 1.5 GPa, which increases to 4.2 GPa for 50 wt% formulation of nanocomposite (**Table 3**). The effective contribution of CNF to the composite modulus can be estimated using micromechanical models mentioned in Chapter 2. The yield strength was estimated using a RoM model (Equation (1)) and the composite modulus was estimated from Cox-Krenchel (Equations (2) & (3)) and Tsai-Pagano models (Equations (4)-(6)). The RoM model overestimates the tensile strength value (σ_{NC}) for the nanocomposites (**Figure 4.6 (i)**). RoM is a basic micromechanical model and does not take into account the effect of CNF network in high fiber weight fraction composites. Overall, for high fiber volume fraction nanocomposites, the predicted values should be considered purely theoretical since the nanocellulose might not exist as a dense nanopaper network but as a 3D percolated network of CNF.⁶⁸ However, for the elastic moduli (E_{NC}) of the nanocomposites, the values calculated from the models form a fitting upper and lower bounds for the experimental values of moduli (**Figure 4.6 (ii)**). The experimental values perform better than the values obtained from Cox-Krenchel model. This model is considered a good method to approximate the elastic modulus as it takes into account the aspect ratio of CNFs. However, the Tsai-Pagano model overestimates the modulus values for the 10 wt%, 20 wt% and 50 wt% formulations of nanocomposites, suggesting that the potential CNF network on the reinforcement effect was not fully utilized. Overall, these models indicate that the reinforcement effect was strongest for 30 wt% and 40 wt% formulations implying that good impregnation of PA6 within CNF network. For the 50 wt% formulation, the reinforcement effect was underutilised maybe due to the CNF agglomerates in high CNF content network.

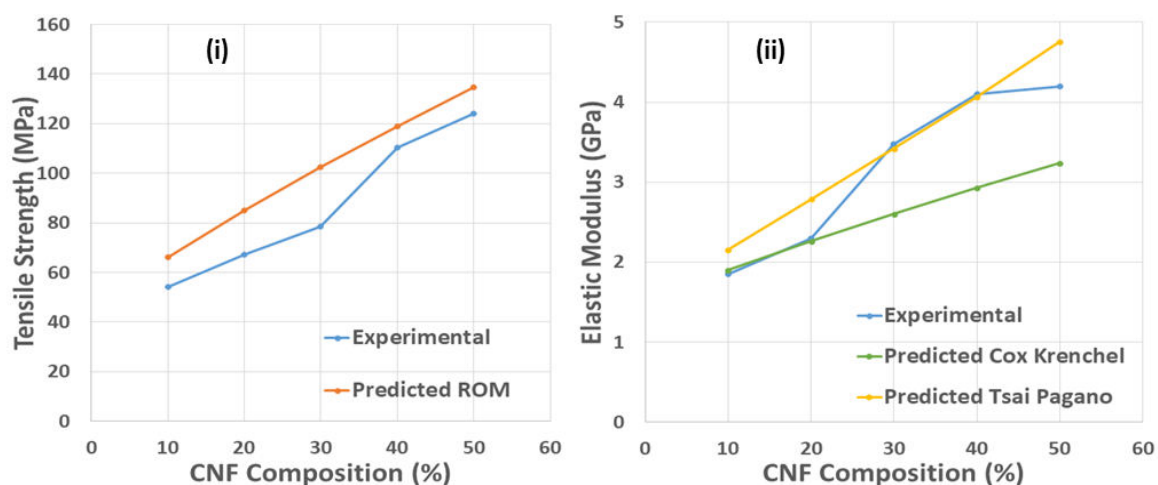


Figure 4.6 Experimental and theoretically predicted values for (i) tensile strength and (ii) elastic moduli for PA6-CNF nanocomposites. Figure from Article III.

4.2.2.2 Glass Transition Temperature (T_g) and Crystallinity

The glass transition temperature (T_g), other thermal parameters and the crystallinity (χ_c) of the PA6/CNF nanocomposites obtained from DSC analysis are shown in T_g for nanocomposites shifts to a higher temperature, indicating strong interactions at the interface, which constrain the molecular mobility in the vicinity of CNF. For lower formulation of CNF, the increase of T_g is due to better dispersion and stronger interactions at the interface.¹⁴⁵ In our case, the CNF content in the nanocomposites are high and the CNF network is stabilized by physical entanglement as well as CNF percolated network crosslinks from secondary interactions such as hydrogen bonds. Storage modulus as a function of temperature for PA6/CNF nanocomposites obtained from dynamical mechanical analysis was shown in Figure 4.4. The neat PA6 shows constant modulus until 50 °C, after which modulus decreases corresponding to the polymer glass transition. CNF nanocomposites have higher modulus than neat polymer, and the reinforcement is more amplified in the rubbery state i.e. $T > T_g$. The strong improvement is due to the CNF network structure, which retains mechanical stiffness above the polymer T_g . 3D percolated networks of CNF formed due to hydrogen bonding results in strong improvements in the nanocomposites' modulus above the polymer T_g . Altogether, the increased T_g reported for CNF-PA6 nanocomposites in this study could be attributed to the

higher CNF content which is dispersed well with the composites signifying that the fraction of PA6 polymer affected by the CNF is much larger.⁹⁰ The decrease in the crystallinity for the nanocomposite samples is also attributed to the vast surface on nanofibrils, and its' effect on the mobility of chains of polymer matrix. In some studies, CNF acted as nucleating sites for crystallization.¹¹⁰ The nucleating effect significantly contributes to the formation of trans-crystalline layers around nanofibers thus, resulting in increase in crystallinity.¹⁴⁶ Nevertheless, the addition of CNF constrains the mobility of polymer chains hindering the crystal growth. This is more influential in high CNF composition composites, as in our case, strong interactions between polar amide groups of PA6 and hydroxyl groups of CNF resulted in constrained segmental mobility of PA6 chain. This restricted conformational freedom for the PA6 polymer decreased the degree of crystallinity.

Table 4, the T_g for nanocomposites shifts to a higher temperature, indicating strong interactions at the interface, which constrain the molecular mobility in the vicinity of CNF. For lower formulation of CNF, the increase of T_g is due to better dispersion and stronger interactions at the interface.¹⁴⁵ In our case, the CNF content in the nanocomposites are high and the CNF network is stabilized by physical entanglement as well as CNF percolated network crosslinks from secondary interactions such as hydrogen bonds. Storage modulus as a function of temperature for PA6/CNF nanocomposites obtained from dynamical mechanical analysis was shown in Figure 4.4. The neat PA6 shows constant modulus until 50 °C, after which modulus decreases corresponding to the polymer glass transition. CNF nanocomposites have higher modulus than neat polymer, and the reinforcement is more amplified in the rubbery state i.e. $T > T_g$. The strong improvement is due to the CNF network structure, which retains mechanical stiffness above the polymer T_g . 3D percolated networks of CNF formed due to hydrogen bonding results in strong improvements in the nanocomposites' modulus above the polymer T_g . Altogether, the increased T_g reported for CNF-PA6 nanocomposites in this study could be attributed to the higher CNF content which is dispersed well with the composites signifying that the fraction of PA6 polymer affected by the CNF is much larger.⁹⁰ The decrease in the crystallinity for the nanocomposite samples is also attributed to the vast surface on nanofibrils, and its' effect on the mobility of chains of polymer matrix. In some studies, CNF acted as nucleating sites for crystallization.¹¹⁰ The nucleating effect significantly contributes to the

formation of trans-crystalline layers around nanofibers thus, resulting in increase in crystallinity.¹⁴⁶ Nevertheless, the addition of CNF constrains the mobility of polymer chains hindering the crystal growth. This is more influential in high CNF composition composites, as in our case, strong interactions between polar amide groups of PA6 and hydroxyl groups of CNF resulted in constrained segmental mobility of PA6 chain. This restricted conformational freedom for the PA6 polymer decreased the degree of crystallinity.

Table 4. Thermal parameters and degree of crystallinity for the PA6 polymer in the plain matrix and in the PA6-CNF nanocomposites. Table from Article III.

CNF Composition (wt. %)	<i>T_g</i> (°C)	<i>T_m</i> (°C)	<i>T_c</i> (°C)	ΔH_{Sample} (J/s)	χ_c (%)
Neat PA6 powder	43.4	223.2	193.7	120.4	52.3
Neat PA6 film	44.2	223.2	194.0	114.9	49.9
10	48.4	220.3	190.3	101.6	49.1
20	50.2	218.7	189.3	81.4	44.2
30	51.0	217.2	188.0	68.3	42.4
40	53.6	217.0	187.2	54.9	39.8
50	50.9	213.8	182.5	43.7	38.0

4.2.3 Cellulose Pulp Fibers vs. CNF as Reinforcement

To further our understanding of the relationship between cellulose structure and the physical properties of the respective composites, it would be of interest to compare the mechanical properties of pulp fiber composites with CNF nanocomposites. The increments of the tensile strength and modulus with respect to neat polymer values for a common weight formulation of the composites are assessed. Since 20 wt% formulation was prepared for both pulp fiber and CNF composites, the mechanical properties of corresponding to this formulation is compared. For the pulp fiber composite, the 20 wt% formulation showed ~18% improvement in yield strength and ~41% improvement in elastic modulus. Under similar testing parameters, the 20 wt% CNF nanocomposite exhibited ~45% improved yield strength and ~51% improved elastic modulus. In contrast, the enhancement for the tensile properties of CNF nanocomposites

are higher than pulp-fiber composites. In pulp fiber composites, there is likely to be poor stress transfer between the microfibrils-PA6 matrix interface. However, in CNF nanocomposites, the CNF interactions forming a percolated network, which is then impregnated with matrix and utilised as an effective reinforcement. In addition, the plastic deformation in CNF nanocomposites is dominated by strain hardening of the CNF network, so that the ultimate strength is substantially enhanced. Moreover, CNF provide higher surface area for the matrix to form primary and secondary interaction which further increase the interfacial adhesion and allows for efficient stress transfer. In pulp-fiber composites, the fiber/matrix interface may initiate early debonding under stress, thus, leading to lower strain to failure. Therefore, the plastic deformation may or may not be dominated by the strain hardening for pulp-fiber composites. Even though, the size of the fibers are in microscale, strain hardening is unique to and a characteristic behaviour of the CNF network.¹⁴⁷ Fundamentally, this highlights the importance of CNF and/or CNF network in order to produce high ductility and high ultimate strength polymer matrix-based cellulose composites.

4.3 Nanocomposites for Industrial Scale Melt Processing

This section focuses on CNF/PA6 polymer nanocomposites produced by melt processing techniques. On an industrial scale, it is still a challenge for CNF-based biocomposites to become mainstream. The current day plastic industry involves majorly thermal processing methods such as extrusion, injection moulding, compression moulding and etcetera to produce composites. However, involving high processing temperatures is a major risk for the thermal stability of cellulose (CNF and CNC). CNF nanocomposites prepared via solvent casting, discussed in the previous section has many disadvantages at an industrial production scale such as; the use of large amounts of solvent could generate chemical waste. In addition, the complex geometries require specialized equipment to be casted whereas similar parts can be easily produced by injection moulding with negligible shrinkage. In this study we produce CNF-PA6 nanocomposites in order for it to be scalable at an industrial level. Developing a method to produce such nanocomposites by making use of the currently normative processing methods (melt processing) in the industry gives rise to various cost saving advantages. This section briefly discusses an approach to develop mechanically strong

and thermally stable PA6 and CNF nanocomposites in order to be produced at an industrial scale. The results presented in this section are selected from Article II.

4.3.1 Processing Approach

A total of three different weight formulations of nanocomposites were prepared: 5 wt%, 15 wt% and 25 wt% CNF content formulations of PA6/CNF nanocomposites. A major obstacle for melt processing PA6/CNF nanocomposites is the high melting temperature of PA6 (~220 °C) which is close to the onset temperature of CNF. To overcome this and produce high-performance biocomposites, GELIMAT[®] mixer (discussed in Chapter 1) was used to homogeneously compound PA6 and CNF. Ability of the Gelimat to compound materials in extremely less time (<60 s) allows for shorter period of exposure of CNF at high processing temperatures, thus, preserving thermal stability of CNF within the composite. To further improve the scalability no dispersing agent and/or binding agent were used in the process. The compatibility of CNF and PA6 and the direct melt mixing of the composites allowed us to eliminate the use any coupling agent and dispersive agent.¹⁴⁸ A schematic of the complete processing method adopted to produce PA6/CNF nanocomposites is shown in **Figure 4.7**.

In brief, PA6 powder and enzymatic CNF gel was mixed thoroughly according to the respective formulations and set to dry. The dried mixture was then melt compounded in the thermo-kinetic mixer (Gelimat). The compounded mixture was then milled into pellets which was then followed by compression moulding at 230 °C into films (0.3-0.5 mm thickness). Dog-bone samples from this film were cut according to ASTM D638 (Type V) standard for mechanical testing. The processes resulted in a slight brownish colour change of for all the formulations of nanocomposites with expectedly, colour intensity increasing with increase in CNF content. Also, the films showed no optical aggregation of CNF. The discoloration of the prepared nanocomposite films (pressed samples) was due to the onset thermal degradation temperature of the CNF. This degradation is characterized by a slow, mild reaction and is mainly attributed to the dehydration of composite and formation of peroxides, which may catalyse the cellulose degradation.¹⁴⁹ However, this degradation does not affect the thermal stability of CNF and the mechanical integrity of the nanocomposites.

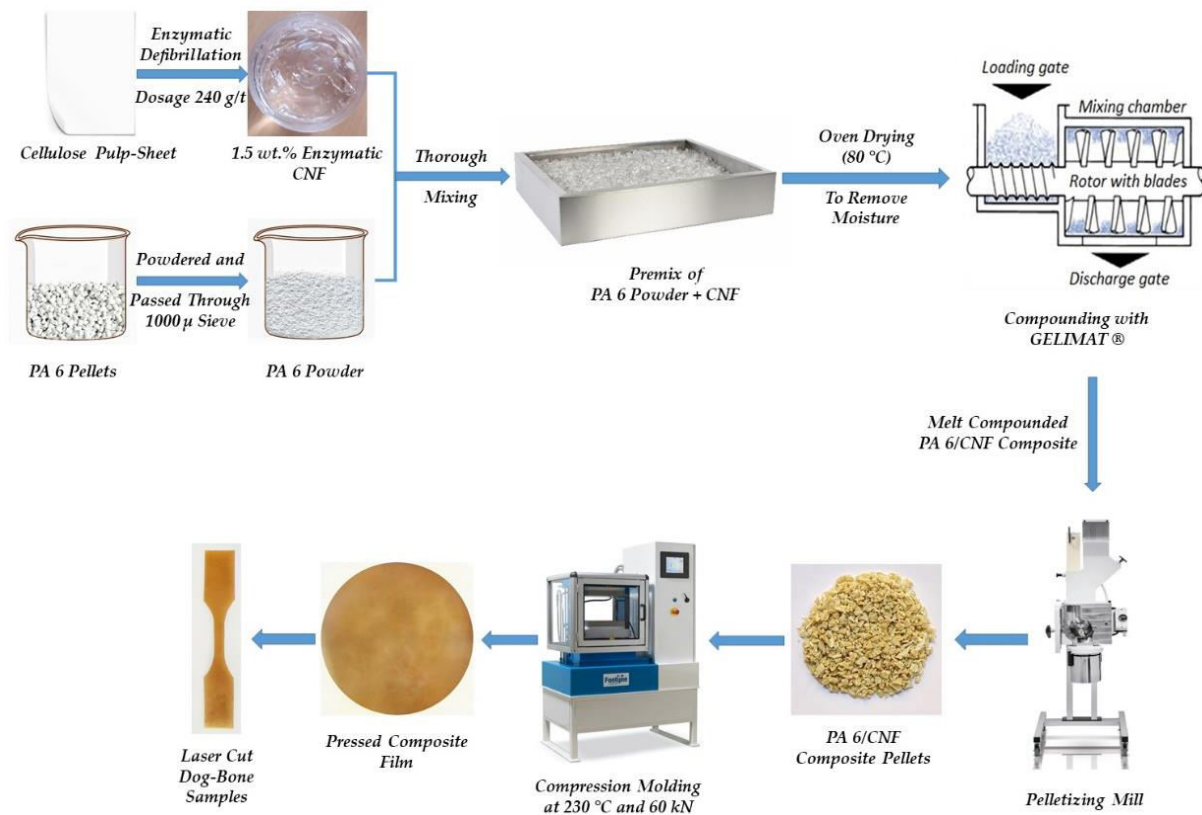


Figure 4.7 Schematic of the complete manufacturing process for the PA6/CNF nanocomposites. This figure is taken from Article II.

4.3.2 Hygro-Mechanical Stability and Interfacial Effects

CNF are inherently hygroscopic and absorb moisture when exposed to humid environment. Moisture is preferentially accumulated at the disordered regions of the CNF and on the fibril surface, reducing the intrinsic properties and acting as plasticizer for network deformation.¹⁵⁰ This has an adverse effect on the mechanical properties, especially modulus and yield strength.¹⁵¹ The PA6/CNF nanocomposites were characterized for tensile mechanical properties at two different relative humidities to further our understanding of the CNF-matrix interface. The mechanical properties of nanocomposites at dry conditions ($\sim 0\%$ relative humidity (RH)) and the 48-hour conditioned (at 50% RH) are shown in **Table 5**.

Table 5. Summary of the uniaxial tests for PA6/CNF nanocomposites at dry sample conditions and at relative humidity (RH 50%). For standard deviations of values, refer to Article II. This table was adopted from Article II.

CNF (wt %)	Mean Thickness		Yield Strength		Elastic Modulus		Strain at Break	
	(mm)		(MPa)		(GPa)		(%)	
	Dry	RH 50%	Dry	RH 50%	Dry	RH 50%	Dry	RH 50%
PA 6	0.46	0.48	50.8	47.8	2.2	2.1	9.8	10.4
5	0.35	0.29	56.5	53.6	3.9	3.5	2.3	2.5
15	0.30	0.25	65.6	61.7	4.8	4.3	1.6	1.8
25	0.25	0.31	77.7	73.2	5.6	5.4	1.2	1.3

Mechanical properties for the nanocomposites were significantly improved with the addition of CNF. The improvement is directly correlated to the dispersion of CNF and strong interface adhesion. Strain at break for the nanocomposites decreased suggesting that good wetting and interaction between CNF and PA6 necessitating effective stress transfer.¹⁵² The nanofibril interaction leading to formation of the percolated CNF network, was effectively impregnated with the PA6 matrix by using this method. Unsuccessful impregnation of matrix in CNF network lead to poor reinforcement and embrittlement of the nanocomposite, which was not prominent in our case.¹⁴¹ The improvement in tensile mechanical properties also stipulates that there was no excessive nanofiller-nanofiller interaction which prevent the effective impregnation of matrix into the CNF network.

Considering the elastic modulus and the yield strength of the PA6/CNF nanocomposites, the values for the RH 50% samples are comparable to the dry sample values, with the RH 50% samples showing minor decrease in strength and modulus values. For neat PA6, the yield strength and modulus accounted for 5.9% and 4.5% reduction in values from dry to conditioned samples. On an average, the yield strength reduced about 3.8% and the modulus reduced 8.1% in value for all the formulations of PA6/CNF nanocomposites. Moisture can enter at a molecular scale in between the CNF-matrix interface. The secondary interaction due to the larger surface area of CNF will be weakened due to the moisture accumulation.¹⁵³ The presence of moisture at the interface, facilitates sliding of the fibril and deteriorates the

CNF network contributions to stress upon loading.¹⁵⁴ Nevertheless, the reduction in modulus and strength values is less severe for CNF nanocomposites due to the strong interactions of CNF (hydroxyl groups) and PA6 matrix (amide groups). It is notable that the PA6/CNF nanocomposites have extraordinary mechanical stability towards moisture absorption. The higher strain to failure for RH 50% formulations is significant of favourable strain hardening of CNF network. The yield strength and modulus values are not severely affected by moisture because the CNF network framework is retained at relative humidity levels and favourable plastic deformation from the network preserves the uniaxial mechanical properties at high relative humidity. Additionally, it can be speculated that the high surface charge opens the supramolecular structure, portions of which may have not been impregnated by matrix.¹⁵⁵ Hydroxyls in these un-impregnated regions cause moisture sensitivity at high relative humidity.⁴⁹ Polyelectrolyte and conductimetric titration revealed the cationic demand of 258 $\mu\text{eq. g/g}$ and the carboxyl group content of 54 $\mu\text{mol COOH/g}$, respectively, for the adopted enzymatic CNF. Hence, it can be concluded that there is an optimum in fiber charge for hygro-mechanical stability, even though mechanical properties for our nanocomposites were enhanced.

Since there was only a small reduction in modulus value (-3.6 %) at RH 50% for the 25 wt% formulation, the effect of CNF content on the water absorption of the nanocomposites was studied. Water uptake study was carried out gravimetrically over a 24-h period. Mass measurements were noted periodically at 0 h, 0.5 h, 1 h, 3 h, 6 h, 12 h, 18 h and 24 h to determine the water absorption in the nanocomposites. In our case, two main interactions can be conjectured; (a) The interaction between the water molecules and the amide groups of the PA6 and then (b) interaction of water molecules with the hydrophilic CNF. With the former dominating the moisture absorption process in nanocomposite samples as the water uptake for nanocomposite samples decreased as function of CNF content but remained lower than the neat PA6 (**Figure 4.8**). The strong hydrogen bonds between the CNF and PA6 along with CNF-CNF interaction and other secondary interactions are already competing with water molecules.¹⁵⁶ This hinders the diffusion of water molecules within the nanocomposites. Further, diffusion coefficient (D) was calculated for lower immersion times using Fick's law (Equation (17)). The diffusion coefficient decreased with the increase of CNF composition in

the nanocomposites. The 25 wt% had the lowest diffusion coefficient and can be related to the lower mobility of PA6 chains restricted by the CNF reinforcement. Nevertheless, hydrogen bonding between the nanofibers and PA6 matrix can also have a negative effect on the diffusion of water through the composite samples.

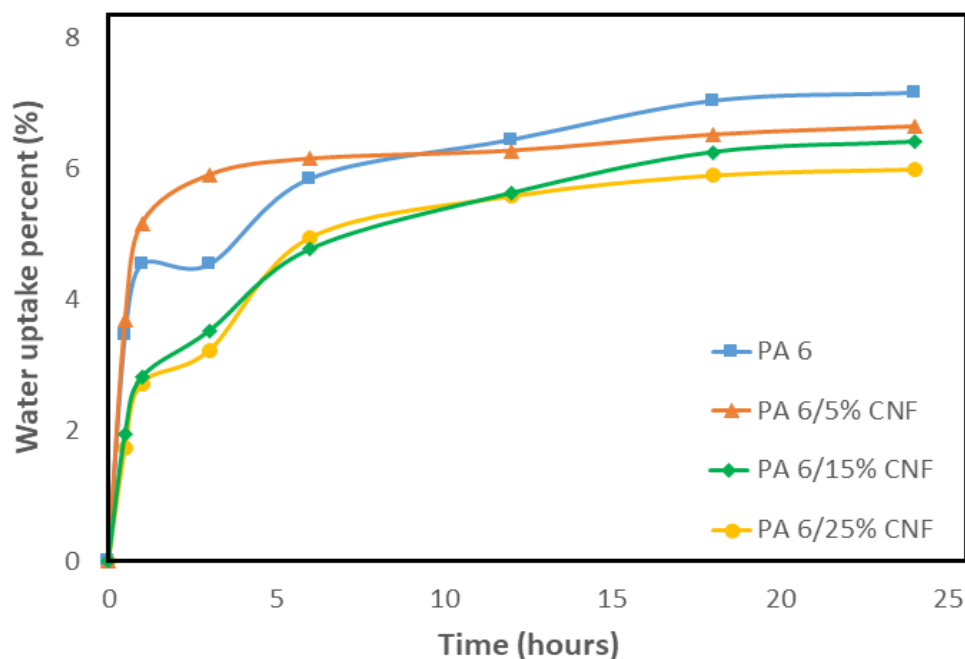


Figure 4.8 Water absorption percent as a function of CNF content versus time for PA6/CNF nanocomposites at room temperature. This figure is adopted from Article II.

4.3.3 Capillary Rheological Properties

It is important to optimize the processing conditions and to understand the rheological behaviour of the CNF nanocomposites to be scalable for production on an industrial level. This can be done by characterizing the samples for capillary rheological properties. The methodology used to determine the capillary rheological properties is discussed in Chapter 2. A rheogram representing variation of dynamic viscosity (μ) versus shear rate (γ) can be obtained without having to use a sophisticated rheometer. A rheogram for the nanocomposite samples at 230 °C is shown in **Figure 4.9**. The MFI values for the neat PA6 and nanocomposite samples can be found in the Supplementary Materials of Article II. Relevant processing shear rates involved can be characterized by analysing the flow behaviour of composite melts through

a capillary and evaluate the process-ability of the CNF nanocomposites. In addition, capillary rheological characterization by applied pressure closely resembles injection moulding process. The nanocomposites displayed similar shear thinning behaviour and PA6/CNF nanocomposites behave as pseudo-plastic fluids (non-Newtonian behaviour) which is confirmed by decreasing viscosity with increasing true shear rates. Moreover, pseudo-plastic behaviour is enhanced by the addition of CNF in the nanocomposites.

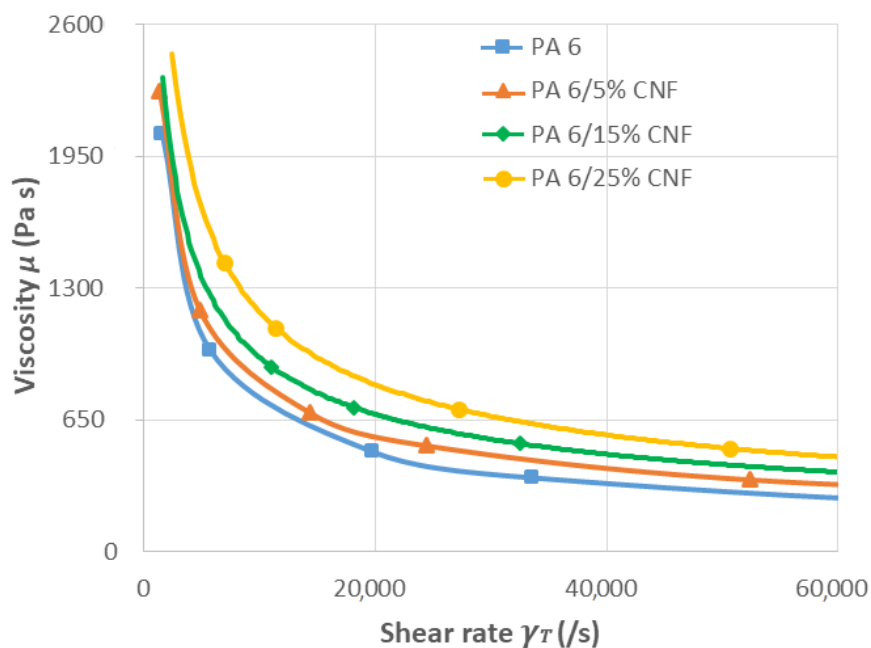


Figure 4.9 Rheogram representing viscosity and true shear rate at 230 °C for the PA6/CNF nanocomposites. This figure is taken from Article II.

For the nanocomposite samples, the viscosities increased with increase in CNF content with the highest viscosity seen for the 25 wt % formulation. At lower formulations (5 wt %), the CNF for the most part may be like free particles and the nanocomposite melt is characterized by higher mobility. At larger formulations (15 wt% and 25 wt %), the CNF disturbs the normal flow of nanocomposite melts and hinders the melt mobility causing high shear stresses, which is attributed to the hydrodynamic effect.^{79,157} The viscosity was increased marginally for the nanocomposites when compared to neat PA6. This is due the processing method employed and the aspect ratio of the CNF, which align themselves along the composite melt flow direction.¹⁵⁸ However, increase in dynamic viscosity of CNF nanocomposites are a

characteristic of well dispersed CNF and the presence of a percolating network. Furthermore, rheological behaviour is beneficial for process optimization and adjust processing conditions to improve the productivity.

Chapter 5 Summary of Results

This chapter contains a brief summary of major results based on the details found in appended Articles I to III.

The results obtained from the cellulose pulp fiber composites (Article I) indicated a positive influence on the tensile and flexural mechanical properties with respect to increase in the composition of pulp fibers. A Maximum tensile strength of 66.17 MPa and modulus of 4.6 GPa was measured for 20 wt% and 25 wt% samples of cellulose pulp-PA6 composites respectively. This constituted to an increase of strength by 24% and increase of modulus by 25% when compared to the values of neat PA6. Moreover, pulp fiber composites samples depicted decent hygro-mechanical stability when compared to dry samples. Lower strain values of the composite samples with the increase in cellulose composition indicate the prominent reinforcing effect of cellulose due to strong interfacial bonding between fibers and PA6 matrix without the use of any bonding agents. Likewise, maximum value of flexural resistance of 113.6 MPa and flexural modulus of 3.84 GPa was obtained for 25 wt% cellulose pulp-PA6 composites which associated to an increase in value of 57% and 8% respectively when compared to neat PA6. Additionally, testing of different oriented samples indicate that the parallel fiber orientation with respect to the injection flow exhibit higher values of tensile strength. The adhesion between the cellulose pulp-fibers and PA6 matrix was further demonstrated through SEM analysis which also indicated lack of major defects or agglomerations confirming that the compounding method had been effective. The extreme short processing times, allows the composite mixture to be thermally compounded with negligible degrading effect on the cellulose pulp fibers. This single step, quick compounding process (GELIMAT) is suitable for temperature-time dependent materials such as cellulose in the preparation of cellulose reinforced polymer composites.

For CNF nanocomposites prepared by solvent casting approach (Article III), nanocomposite films of enzymatically derived CNF with PA6 as matrix were successfully prepared by adopting a green solvent casting method (mixture of formic acid and water). High formulations of CNF nanocomposites up to 50 wt% in composition were prepared and characterized. The enzymatic CNF provided excellent reinforcement effect for the composites and solvent casting enabled good dispersion of CNF allowing for excellent stress transfer through strong interface adhesion between PA6 and CNF. The tensile properties increased with the addition of CNF demonstrating excellent reinforcement effect. A maximum values of tensile strength of 124 MPa and modulus of 4.2 GPa were obtained for 50 wt% CNF formulation. In general, the nanocomposite films were uniform, indicating good dispersion of CNF in the PA6 matrix, and no agglomeration was seen with the corresponding SEM micrographs. FTIR analysis revealed the molecular interactions between the CNF and PA6 through hydrogen bonds with OH-groups of cellulose. TGA results illustrated that the nanocomposites' thermal stability slightly decreased with the addition of CNF. DSC revealed that the glass transition temperature increased slightly with the increase in CNF composition. In our case, the addition of CNF surfaces did not act as nucleating sites and restricted crystal growth thereby, decreasing the polymer crystallinity. A maximum crystallinity of ~49% was obtained for 10% CNF formulation. The nanocomposites had superior thermo-mechanical stability with an increase in CNF composition. This study presented an environmentally friendly and energy-efficient laboratory method to produce high CNF content nanocomposites with PA6.

CNF nanocomposites were prepared by melt processing approach (as described in Article II) using a high speed thermo-kinetic mixer (GELIMAT), and this study provided a methodology to produce CNF reinforced polymer composites which can be integrated at an industrial level. Good dispersion was obtained by adopting prior premixing and compounding procedure. Given the short compounding time of the Gelimat as discussed previously, the thermal integrity of CNF was not compromised during the procedure. Formulation up to 25 wt% of CNF was prepared and characterized. The mechanical properties were improved significantly with the addition of CNF, where the 25 wt% formulation exhibiting the highest tensile values, with Young's modulus of 5.6 GPa and tensile strength of ~78 MPa. In addition,

nanocomposite samples showed good hygro-mechanical properties with slight reduction in tensile values when compared to dry samples. Water uptake study indicated that the water uptake reduced with the addition of CNF due to the hydrogen bonds between the PA 6 and CNF, which hindered the diffusion of water molecules. DSC analysis revealed that the degree of crystallinity reduced for the nanocomposites as the addition of CNF constrained the polymer chain hindering crystal growth. TGA expectedly implied that the thermal stability of nanocomposites reduced slightly for the nanocomposites. The capillary rheological study indicated that the dynamic viscosity increased with the addition of CNF. SEM micrographs showed homogenous interface morphology of fractured samples with hardly any fiber pull-out. Further, this study provides useful prospects on sustainable materials and a methodology for developing high performance nanocellulose reinforced polymer composites with high CNF content

In general, PA6 with its material properties has become a hot commodity especially in the automobile industry. This combined with the tremendous emphasis on enhancing the mechanical properties using natural nanofillers. CNF with its high specific strength, aspect ratio and compatibility with PA6 become a tangible eco-friendly and sustainable choice of reinforcement. From the studies discussed so far, we conclude that different cellulosic materials effect the physical properties of cellulose-based composites due to various factors such as particle size, particle shape, dispersion, distribution, thermal stability, cellulose surface morphology and cellulose surface energy.

Conclusion

Biocomposites with high content of cellulose pulp fibers and cellulose nanofibers were prepared. Various effects from the incorporation CNF with the different cellulose/PA6 matrix system were investigated. In cellulose pulp-fiber/polyamide 6 (PA6) composites obtained by melt compounding and injection moulding, unique characteristics of the pulp-fiber/PA6 biocomposites were discussed and the findings include (a) Strongly increased mechanical properties of the biocomposites. (b) Effect of fiber orientation on the final property of the biocomposites governed by the flow of polymer composites melt. (c) Good dispersion and interaction between the PA6 and cellulose fibers providing for overall strength increase with increased in cellulose pulp content.

In PA6/CNF nanocomposites, nanocellulose dispersion was further improved even for high content of CNF formulations in the biocomposites due to a greener effective solvent casting method. Formulations upto 50 wt.% of CNF derived via environmentally friendly enzymatic methods were prepared using a green solvent mixture of formic acid and water. As the parameter of temperature is circumvented, thermal stability of CNF was retained completely. (a) Nanocomposites showed improved optical transparency and significantly improved tensile strength (up to 2.7x) and elastic modulus (up to 3x) due to strain hardening and corresponding ductility of CNF network biocomposites. (b) With the addition of CNF, glass transition temperature occurred a higher temperature and degree of crystallinity decreased indicating that the addition of CNF hinders the PA6 crystal growth. (c) Improved thermo-mechanical properties due to well dispersed CNF particles which provide high surface area for the polymer matrix to form strong interfacial adhesion. (d) The strong interfacial adhesion was associated to the formation of hydrogen bonds between the amide groups PA6 and OH groups of CNF. (e) Increased hygro-mechanical stability of CNF-based composites from matrix/interface tailoring.

In PA6/CNF nanocomposites produced by melt compounding and compression moulding, high specific surface area due to well dispersed CNF led to several interesting results providing a methodology to produce these biocomposites scaled to an industrial level. By this processing strategy, (a) Successful impregnation of polymer into the 3D percolated network was achieved even for high content CNF biocomposites. (b) Good dispersion and strong interfacial bonding led to higher mechanical properties. (c) Rheological behaviour of biocomposites was influenced by the addition of CNF with higher dynamic viscosity for higher CNF formulations. (d) Water absorption of the biocomposites reduced with the addition of CNF as hydrogen bonds between PA6 and CNF hindered the diffusion of diffusion water molecules. (e) The CNF did not manage to provide any nucleating sites for PA6, affecting crystal growth in biocomposites and decreasing the crystallinity of CNF.

The CNF network is crucial in imparting high mechanical performance to the biocomposites. CNF network dominated the plastic deformation in the nanocomposites, even at higher relative humidity. Hence there is no severe reduction in the strength and modulus values at a higher relative humidity. The mechanical improvements were more significant for the CNF biocomposites when compared to cellulose pulp fiber biocomposites, thus, showcasing the importance of nanoscale distribution and network.

Nanocomposites from polyamide-6 and high content of cellulose nanofibers were successfully prepared in this work, with remarkable improvement in the mechanical performance compared to the net matrix, for both Young's modulus and tensile strength. This in itself is an outstanding achievement, as compared for the literature up today. Moreover, the used methodology stands for industrial scalability and feasible processes towards the use renewable and more sustainable products.

Future Outlook

Cellulose nanofibers show great promise as (nano)reinforcement materials for polymeric matrices. Important characteristics and parameters that influence the macroscopic properties of cellulose-based composites with PA6 matrix has been highlighted in this thesis. The future development of CNF reinforcements is based on understanding how the natural materials work. A high degree of dispersion is one of the most important parameters. Well dispersed CNF provide high specific surface area to facilitate filler /polymer interface dynamics. Moving forward, the surface functionalization characteristic of CNFs should be made use of to produce hybrid composites with PA6 for specific applications such as flame retardancy.

The study and use of nanocellulose materials is said to increase in the recent future, with the current trend on 'greener materials' and increased industrial interest in sustainable materials.¹⁵⁹ Despite, the advantages of cellulosic materials in the field of nanocomposites, the practical transition from laboratory scale to an industrial scale requires development of suitable technologies. One such methodology to produce such CNF nanocomposites on an industrial level is discussed in this thesis. However, in the long term, synergistic approaches and advancements will enable to manufacture high performing bionanocomposites. Strategies to further our understanding of bio-based nanostructure, synthesis, and methods to incorporate them in bio-based composites will create the next generation of bio-based materials.

References

1. Martins F, Felgueiras C, Smitková M. Fossil fuel energy consumption in European countries. *Energy Procedia*. 2018;153:107-111.
2. Ragauskas AJ, Williams CK, Davison BH, et al. The path forward for biofuels and biomaterials. *Science (80-)*. 2006;311(5760):484-489.
3. Kollmann FFP, Kuenzi EW, Stamm AJ. *Principles of Wood Science and Technology: II Wood Based Materials*. Springer Science & Business Media; 2012.
4. Hurmekoski E, Jonsson R, Korhonen J, et al. Diversification of the forest industries: role of new wood-based products. *Can J For Res*. 2018;48(12):1417-1432.
5. Saito T, Kuramae R, Wohler J, Berglund LA, Isogai A. An ultrastrong nanofibrillar biomaterial: the strength of single cellulose nanofibrils revealed via sonication-induced fragmentation. *Biomacromolecules*. 2013;14(1):248-253.
6. Hubbe MA, Rojas OJ, Lucia LA, Sain M. Cellulosic nanocomposites: a review. *BioResources*. 2008;3(3):929-980.
7. Bhatnagar A, Sain M. Processing of cellulose nanofiber-reinforced composites. *J Reinf Plast Compos*. 2005;24(12):1259-1268.
8. Dufresne A. Nanocellulose: a new ageless bionanomaterial. *Mater today*. 2013;16(6):220-227.
9. Siqueira G, Bras J, Dufresne A. Cellulosic bionanocomposites: a review of preparation, properties and applications. *Polymers (Basel)*. 2010;2(4):728-765.
10. Bandyopadhyay-Ghosh S, Ghosh SB, Sain M. The use of biobased nanofibres in composites. In: *Biofiber Reinforcements in Composite Materials*. Elsevier; 2015:571-

- 647.
11. Postek MT, Vladár A, Dagata J, et al. Development of the metrology and imaging of cellulose nanocrystals. *Meas Sci Technol*. 2011;22(2). doi:10.1088/0957-0233/22/2/024005
 12. Fernandes AN, Thomas LH, Altaner CM, et al. Nanostructure of cellulose microfibrils in spruce wood. *Proc Natl Acad Sci*. 2011;108(47):E1195-E1203.
 13. Martins MA, Teixeira EM, Corrêa AC, Ferreira M, Mattoso LHC. Extraction and characterization of cellulose whiskers from commercial cotton fibers. *J Mater Sci*. 2011;46(24):7858-7864.
 14. Astruc J, Nagalakshmaiah M, Laroche G, Grandbois M, Elkoun S, Robert M. Isolation of cellulose-II nanospheres from flax stems and their physical and morphological properties. *Carbohydr Polym*. 2017;178:352-359.
 15. Morán JI, Alvarez VA, Cyras VP, Vázquez A. Extraction of cellulose and preparation of nanocellulose from sisal fibers. *Cellulose*. 2008;15(1):149-159.
 16. Liu R, Yu H, Huang Y. Structure and morphology of cellulose in wheat straw. *Cellulose*. 2005;12(1):25-34.
 17. Zhao Y, Moser C, Lindström ME, Henriksson G, Li J. Cellulose nanofibers from softwood, hardwood, and tunicate: preparation–structure–film performance interrelation. *ACS Appl Mater Interfaces*. 2017;9(15):13508-13519.
 18. Ross P, Mayer R, Benziman M. Cellulose biosynthesis and function in bacteria. *Microbiol Mol Biol Rev*. 1991;55(1):35-58.
 19. Mihranyan A. Cellulose from cladophorales green algae: From environmental problem to high-tech composite materials. *J Appl Polym Sci*. 2011;119(4):2449-2460.
 20. Jonoobi M, Oladi R, Davoudpour Y, et al. Different preparation methods and properties of nanostructured cellulose from various natural resources and residues: a review. *Cellulose*. 2015;22(2):935-969.

21. Herrick FW, Casebier RL, Hamilton JK, Sandberg KR. Microfibrillated cellulose: morphology and accessibility. In: *J. Appl. Polym. Sci.: Appl. Polym. Symp.*; (United States). Vol 37. ITT Rayonier Inc., Shelton, WA; 1983.
22. Lawrence D, Vandecar K. The impact of tropical deforestation on climate and links to agricultural productivity. *Nat Clim Chang*. 2014;5:27-36.
23. Brown AJ. Brown on acetic ferment. *J Chem Soc Trans*. 1886;49:432-439.
24. Campano C, Balea A, Blanco A, Negro C. Enhancement of the fermentation process and properties of bacterial cellulose: a review. *Cellulose*. 2016;23(1):57-91.
25. Chawla PR, Bajaj IB, Survase SA, Singhal RS. Microbial cellulose: fermentative production and applications. *Food Technol Biotechnol*. 2009;47(2):107-124.
26. Hornung M, Ludwig M, Gerrard AM, Schmauder H. Optimizing the production of bacterial cellulose in surface culture: Evaluation of substrate mass transfer influences on the bioreaction (Part 1). *Eng Life Sci*. 2006;6(6):537-545.
27. Torres FG, Arroyo JJ, Troncoso OP. Bacterial cellulose nanocomposites: An all-nano type of material. *Mater Sci Eng C*. 2019;98:1277-1293.
28. Salidkul N, Mongkolthananaruk W, Faungnawakij K, Pinitsoontorn S. Hard magnetic membrane based on bacterial cellulose–Barium ferrite nanocomposites. *Carbohydr Polym*. 2021;264:118016.
29. Saito T, Kimura S, Nishiyama Y, Isogai A. Cellulose nanofibers prepared by TEMPO-mediated oxidation of native cellulose. *Biomacromolecules*. 2007;8(8):2485-2491.
30. Saito T, Nishiyama Y, Putaux J-L, Vignon M, Isogai A. Homogeneous suspensions of individualized microfibrils from TEMPO-catalyzed oxidation of native cellulose. *Biomacromolecules*. 2006;7(6):1687-1691.
31. Shinoda R, Saito T, Okita Y, Isogai A. Relationship between length and degree of polymerization of TEMPO-oxidized cellulose nanofibrils. *Biomacromolecules*. 2012;13(3):842-849.

-
32. Ho TTT, Zimmermann T, Hauert R, Caseri W. Preparation and characterization of cationic nanofibrillated cellulose from etherification and high-shear disintegration processes. *Cellulose*. 2011;18(6):1391-1406.
 33. Pei A, Butchosa N, Berglund LA, Zhou Q. Surface quaternized cellulose nanofibrils with high water absorbency and adsorption capacity for anionic dyes. *Soft Matter*. 2013;9(6):2047-2055.
 34. Wågberg L, Decher G, Norgren M, Lindström T, Ankerfors M, Axnäs K. The build-up of polyelectrolyte multilayers of microfibrillated cellulose and cationic polyelectrolytes. *Langmuir*. 2008;24(3):784-795.
 35. Iwamoto S, Abe K, Yano H. The effect of hemicelluloses on wood pulp nanofibrillation and nanofiber network characteristics. *Biomacromolecules*. 2008;9(3):1022-1026.
 36. Pääkkö M, Ankerfors M, Kosonen H, et al. Enzymatic hydrolysis combined with mechanical shearing and high-pressure homogenization for nanoscale cellulose fibrils and strong gels. *Biomacromolecules*. 2007;8(6):1934-1941.
 37. Yang X, Reid MS, Olsén P, Berglund LA. Eco-friendly cellulose nanofibrils designed by nature: effects from preserving native state. *ACS Nano*. 2019;14(1):724-735.
 38. Huang P, Wang C, Huang Y, Wu M. Structure and Properties of Cellulose Nanofibrils. *Nanocellulose From Fundam to Adv Mater*. 2019:53-80.
 39. Novak BM. Hybrid nanocomposite materials—between inorganic glasses and organic polymers. *Adv Mater*. 1993;5(6):422-433.
 40. Eichhorn SJ, Dufresne A, Aranguren M, et al. Current international research into cellulose nanofibres and nanocomposites. *J Mater Sci*. 2010;45(1):1-33.
 41. Sehaqui H, Liu A, Zhou Q, Berglund LA. Fast preparation procedure for large, flat cellulose and cellulose/inorganic nanopaper structures. *Biomacromolecules*. 2010;11(9):2195-2198.
 42. Henriksson M, Berglund LA, Isaksson P, Lindstrom T, Nishino T. Cellulose nanopaper

- structures of high toughness. *Biomacromolecules*. 2008;9(6):1579-1585.
43. Wu T, Zeng Z, Siqueira G, et al. Dual-porous cellulose nanofibril aerogels via modular drying and cross-linking. *Nanoscale*. 2020;12(13):7383-7394.
 44. Sehaqui H, Zhou Q, Ikkala O, Berglund LA. Strong and tough cellulose nanopaper with high specific surface area and porosity. *Biomacromolecules*. 2011;12(10):3638-3644.
 45. Fukuzumi H, Saito T, Iwata T, Kumamoto Y, Isogai A. Transparent and high gas barrier films of cellulose nanofibers prepared by TEMPO-mediated oxidation. *Biomacromolecules*. 2009;10(1):162-165.
 46. Nogi M, Iwamoto S, Nakagaito AN, Yano H. Optically transparent nanofiber paper. *Adv Mater*. 2009;21(16):1595-1598.
 47. Xu X, Zhou J, Jiang L, et al. Highly transparent, low-haze, hybrid cellulose nanopaper as electrodes for flexible electronics. *Nanoscale*. 2016;8(24):12294-12306.
 48. Benítez AJ, Torres-Rendon J, Poutanen M, Walther A. Humidity and multiscale structure govern mechanical properties and deformation modes in films of native cellulose nanofibrils. *Biomacromolecules*. 2013;14(12):4497-4506.
 49. Ansari MF. Nanostructured Cellulose Biocomposites : Effects from dispersion, network and interface. *TRITA-CHE-Report NV - 201619*. 2016. <http://urn.kb.se/resolve?urn=urn:nbn:se:kth:diva-185723>.
 50. Parit M, Aksoy B, Jiang Z. Towards standardization of laboratory preparation procedure for uniform cellulose nanopapers. *Cellulose*. 2018;25(5):2915-2924.
 51. Baez C, Considine J, Rowlands R. Influence of drying restraint on physical and mechanical properties of nanofibrillated cellulose films. *Cellulose*. 2014;21(1):347-356.
 52. Favier V, Chanzy H, Cavailé J. Polymer nanocomposites reinforced by cellulose whiskers. *Macromolecules*. 1995;28(18):6365-6367.
 53. Favier V, Canova GR, Cavailé JY, Chanzy H, Dufresne A, Gauthier C. Nanocomposite materials from latex and cellulose whiskers. *Polym Adv Technol*. 1995;6(5):351-355.

-
54. Azizi Samir MAS, Alloin F, Sanchez J-Y, El Kissi N, Dufresne A. Preparation of cellulose whiskers reinforced nanocomposites from an organic medium suspension. *Macromolecules*. 2004;37(4):1386-1393.
 55. Boujemaoui A, Carlsson L, Malmström E, et al. Facile preparation route for nanostructured composites: surface-initiated ring-opening polymerization of ϵ -caprolactone from high-surface-area nanopaper. *ACS Appl Mater Interfaces*. 2012;4(6):3191-3198.
 56. Alila S, Boufi S, Belgacem MN, Beneventi D. Adsorption of a cationic surfactant onto cellulosic fibers I. Surface charge effects. *Langmuir*. 2005;21(18):8106-8113.
 57. Belgacem MN, Gandini A. The surface modification of cellulose fibres for use as reinforcing elements in composite materials. *Compos Interfaces*. 2005;12(1-2):41-75.
 58. Thakur VK, Thakur MK. Processing and characterization of natural cellulose fibers/thermoset polymer composites. *Carbohydr Polym*. 2014;109:102-117.
 59. Fink H, Ganster J. Novel Thermoplastic Composites from Commodity Polymers and Man-Made Cellulose Fibers. In: *Macromolecular Symposia*. Vol 244. Wiley Online Library; 2006:107-118.
 60. Oksman K, Mathew AP, Bondeson D, Kvien I. Manufacturing process of cellulose whiskers/poly(lactic acid) nanocomposites. *Compos Sci Technol*. 2006;66(15):2776-2784.
 61. Moon RJ, Martini A, Nairn J, Simonsen J, Youngblood J. Cellulose nanomaterials review: structure, properties and nanocomposites. *Chem Soc Rev*. 2011;40(7):3941-3994.
 62. Oksman K, Aitomäki Y, Mathew AP, et al. Review of the recent developments in cellulose nanocomposite processing. *Compos Part A Appl Sci Manuf*. 2016;83:2-18.
 63. Wang L, Gardner DJ, Wang J, et al. Towards the scale-up production of cellulose nanocomposites using melt processing: A critical review on structure-processing-property relationships. *Compos Part B Eng*. 2020:108297.

-
64. Yang J, Xu F. Synergistic Reinforcing Mechanisms in Cellulose Nanofibrils Composite Hydrogels: Interfacial Dynamics, Energy Dissipation, and Damage Resistance. *Biomacromolecules*. 2017;18(8):2623-2632. doi:10.1021/acs.biomac.7b00730
 65. Cox HL. The elasticity and strength of paper and other fibrous materials. *Br J Appl Phys*. 1952;3(3):72.
 66. Nairn JA. On the use of shear-lag methods for analysis of stress transfer in unidirectional composites. *Mech Mater*. 1997;26(2):63-80.
 67. Favier V, Cavaille JY, Canova GR, Shrivastava SC. Mechanical percolation in cellulose whisker nanocomposites. *Polym Eng Sci*. 1997;37(10):1732-1739.
 68. Lee KY, Aitomäki Y, Berglund LA, Oksman K, Bismarck A. On the use of nanocellulose as reinforcement in polymer matrix composites. *Compos Sci Technol*. 2014;105:15-27. doi:10.1016/j.compscitech.2014.08.032
 69. Nadiv R, Shtein M, Shachar G, Varenik M, Regev O. Optimal nanomaterial concentration: harnessing percolation theory to enhance polymer nanocomposite performance. *Nanotechnology*. 2017;28(30):305701.
 70. Ogunsona EO, Misra M, Mohanty AK. Sustainable biocomposites from biobased polyamide 6, 10 and biocarbon from pyrolyzed miscanthus fibers. *J Appl Polym Sci*. 2017;134(4).
 71. Armoun S, Panthapulakkal S, Scheel J, Tjong J, Sain M. Sustainable and lightweight biopolyamide hybrid composites for greener auto parts. *Can J Chem Eng*. 2016;94(11):2052-2060.
 72. Miao C, Hamad WY. Cellulose reinforced polymer composites and nanocomposites: A critical review. *Cellulose*. 2013;20(5):2221-2262. doi:10.1007/s10570-013-0007-3
 73. Holbery J, Houston D. Natural-fiber-reinforced polymer composites in automotive applications. *Jom*. 2006;58(11):80-86.
 74. Elsabbagh A, Steuernagel L, Ring J. Natural Fibre/PA6 composites with flame

-
- retardance properties: Extrusion and characterisation. *Compos Part B Eng.* 2017;108:325-333.
75. Peng Y, Gardner DJ, Han Y. Characterization of mechanical and morphological properties of cellulose reinforced polyamide 6 composites. *Cellulose.* 2015;22(5):3199-3215.
76. Ogunsona EO, Codou A, Misra M, Mohanty AK. A critical review on the fabrication processes and performance of polyamide biocomposites from a biofiller perspective. *Mater Today Sustain.* 2019;5:100014.
77. Qua EH, Hornsby PR. Preparation and characterisation of nanocellulose reinforced polyamide-6. *Plast rubber Compos.* 2011;40(6-7):300-306.
78. Corrêa AC, de Morais Teixeira E, Carmona VB, et al. Obtaining nanocomposites of polyamide 6 and cellulose whiskers via extrusion and injection molding. *Cellulose.* 2014;21(1):311-322.
79. Kiziltas A, Nazari B, Gardner DJ, Bousfield DW. Polyamide 6–Cellulose Composites: Effect of Cellulose Composition on Melt Rheology and Crystallization Behavior. *Polym Eng Sci.* 2014;54(4):739-746. doi:doi:10.1002/pen.23603
80. Mendez JA, Vilaseca F, Pelach MA, et al. Evaluation of the reinforcing effect of ground wood pulp in the preparation of polypropylene-based composites coupled with maleic anhydride grafted polypropylene. *J Appl Polym Sci.* 2007;105(6):3588-3596.
81. Thumm A, Dickson AR. The influence of fibre length and damage on the mechanical performance of polypropylene/wood pulp composites. *Compos Part A Appl Sci Manuf.* 2013;46:45-52.
82. Lee J-A, Yoon M-J, Lee E-S, Lim D-Y, Kim K-Y. Preparation and characterization of cellulose nanofibers (CNFs) from microcrystalline cellulose (MCC) and CNF/polyamide 6 composites. *Macromol Res.* 2014;22(7):738-745.
83. Abacha N, Kubouchi M, Sakai T. Diffusion behavior of water in polyamide 6 organoclay nanocomposites. *Express Polym Lett.* 2009;3(4):245-255.

-
84. Khoshkava V, Kamal MR. Effect of surface energy on dispersion and mechanical properties of polymer/nanocrystalline cellulose nanocomposites. *Biomacromolecules*. 2013;14(9):3155-3163.
 85. Jonoobi M, Aitomäki Y, Mathew AP, Oksman K. Thermoplastic polymer impregnation of cellulose nanofibre networks: morphology, mechanical and optical properties. *Compos Part A Appl Sci Manuf*. 2014;58:30-35.
 86. Sharma A, Thakur M, Bhattacharya M, Mandal T, Goswami S. Commercial application of cellulose nano-composites—A review. *Biotechnol Reports*. 2019;21:e00316.
 87. Osong SH, Norgren S, Engstrand P. Processing of wood-based microfibrillated cellulose and nanofibrillated cellulose, and applications relating to papermaking: a review. *Cellulose*. 2016;23(1):93-123.
 88. Sanchez-Garcia MD, Gimenez E, Lagaron JM. Morphology and barrier properties of solvent cast composites of thermoplastic biopolymers and purified cellulose fibers. *Carbohydr Polym*. 2008;71(2):235-244.
 89. Qua EH, Hornsby PR. Preparation and characterisation of nanocellulose reinforced polyamide-6. *Plast Rubber Compos*. 2011;40(6-7):300-306. doi:10.1179/1743289810Y.0000000019
 90. Henriksson M, Fogelström L, Berglund LA, Johansson M, Hult A. Novel nanocomposite concept based on cross-linking of hyperbranched polymers in reactive cellulose nanopaper templates. *Compos Sci Technol*. 2011;71(1):13-17.
 91. Sanjay MR, Madhu P, Jawaid M, Senthamarai kanna n P, Senthil S, Pradeep S. Characterization and properties of natural fiber polymer composites: A comprehensive review. *J Clean Prod*. 2018;172:566-581.
 92. Iwatake A, Nogi M, Yano H. Cellulose nanofiber-reinforced polylactic acid. *Compos Sci Technol*. 2008;68(9):2103-2106.
 93. Bondeson D, Oksman K. Dispersion and characteristics of surfactant modified cellulose whiskers nanocomposites. *Compos Interfaces*. 2007;14(7-9):617-630.

-
94. Zheng T, Pilla S. Melt Processing of Cellulose Nanocrystal-Filled Composites: Toward Reinforcement and Foam Nucleation. *Ind Eng Chem Res.* 2020;59(18):8511-8531.
 95. DUSATEC Inc. Mixing Ultrahigh-speed Thermokinetic Gelimat™ Technology.
 96. Gopakumar TG, Pagé D. Compounding of nanocomposites by thermokinetic mixing. *J Appl Polym Sci.* 2005;96(5):1557-1563.
 97. Ansari F, Granda LA, Joffe R, Berglund LA, Vilaseca F. Experimental evaluation of anisotropy in injection molded polypropylene/wood fiber biocomposites. *Compos Part A Appl Sci Manuf.* 2017;96:147-154.
 98. Sessini V, Haseeb B, Boldizar A, Lo Re G. Sustainable pathway towards large scale melt processing of the new generation of renewable cellulose-polyamide composites. *RSC Adv.* 2020;11(2):637-656. doi:10.1039/d0ra07141b
 99. Klason C, Kubat J, Strömvall H-E. The efficiency of cellulosic fillers in common thermoplastics. Part 1. Filling without processing aids or coupling agents. *Int J Polym Mater.* 1984;10(3):159-187.
 100. Jacobson R, Caulfield D, Sears K, Underwood J. Low temperature processing of ultra-pure cellulose fibers into nylon 6 and other thermoplastics. In: *Sixth International Conference on Woodfiber-Plastic Composites: May 15-16, 2001... Madison, Wisconsin. Madison, WI: Forest Products Society, C2002: P. 127-133: ISBN: 0892529181. ; 2002:127-133.*
 101. Chen J, Gardner DJ. Dynamic mechanical properties of extruded nylon-wood composites. *Polym Compos.* 2008;29(4):372-379.
 102. El-Sabbagh A, Steuernagel L, Ziegmann G, Meiners D, Toepfer O. Processing parameters and characterisation of flax fibre reinforced engineering plastic composites with flame retardant fillers. *Compos Part B Eng.* 2014;62:12-18.
 103. Alonso-Montemayor FJ, Tarrés Q, Oliver-Ortega H, et al. Enhancing the Mechanical Performance of Bleached Hemp Fibers Reinforced Polyamide 6 Composites: A Competitive Alternative to Commodity Composites. *Polymers (Basel).*

- 2020;12(5):1041.
104. Annandarajah C, Langhorst A, Kiziltas A, Grewell D, Mielewski D, Montazami R. Hybrid cellulose-glass fiber composites for automotive applications. *Materials (Basel)*. 2019;12(19):3189.
 105. Melo RP, Rosa MP da, Beck PH, Tienne LGP, Marques M de F V. Thermal, morphological and mechanical properties of composites based on polyamide 6 with cellulose, silica and their hybrids from rice husk. *J Compos Mater*. 2020:0021998320978290.
 106. Liang S, Nouri H, Lafranche E. Thermo-compression forming of flax fibre-reinforced polyamide 6 composites: influence of the fibre thermal degradation on mechanical properties. *J Mater Sci*. 2015;50(23):7660-7672.
 107. Mariano M, El Kissi N, Dufresne A. Cellulose nanocrystals and related nanocomposites: Review of some properties and challenges. *J Polym Sci Part B Polym Phys*. 2014;52(12):791-806.
 108. Kashani Rahimi S, Otaigbe JU. Polyamide 6 nanocomposites incorporating cellulose nanocrystals prepared by In situ ring-opening polymerization: Viscoelasticity, creep behavior, and melt rheological properties. *Polym Eng Sci*. 2016;56(9):1045-1060. doi:<https://doi.org/10.1002/pen.24335>
 109. Aitha S, Vasanthan N. Effect of cellulose nanocrystals on crystallization, morphology and phase transition of polyamide 6. *Compos Interfaces*. 2020;27(4):371-384.
 110. Lee J-C, Lee J-A, Lim D-Y, Kim K-Y. Fabrication of cellulose nanofiber reinforced thermoplastic composites. *Fibers Polym*. 2018;19(8):1753-1759.
 111. Semba T, Ito A, Kitagawa K, et al. Polyamide 6 composites reinforced with nanofibrillated cellulose formed during compounding: Effect of acetyl group degree of substitution. *Compos Part A Appl Sci Manuf*. 2021;145:106385.
 112. Joshi MK, Tiwari AP, Maharjan B, et al. Cellulose reinforced nylon-6 nanofibrous membrane: Fabrication strategies, physicochemical characterizations, wicking

- properties and biomimetic mineralization. *Carbohydr Polym.* 2016;147:104-113.
113. Xiang M, Yang R, Yang J, Zhou S, Zhou J, Dong S. Fabrication of polyamide 6/reduced graphene oxide nano-composites by conductive cellulose skeleton structure and its conductive behavior. *Compos Part B Eng.* 2019;167:533-543.
114. Garcia-Ramirez M, Cavaille JY, Dupeyre D, Peguy A. Cellulose-polyamide 66 blends. I. Processing and characterization. *J Polym Sci Part B Polym Phys.* 1994;32(8):1437-1448.
115. Ramirez MG, Cavaillé JY, Dufresne A, Tékély P. Cellulose-polyamide 66 blends. Part II: Mechanical behavior. *J Polym Sci Part B Polym Phys.* 1995;33(15):2109-2124.
116. Peng SX, Shrestha S, Youngblood JP. Crystal structure transformation and induction of shear banding in Polyamide 11 by surface modified Cellulose Nanocrystals. *Polymer (Guildf).* 2017;114:88-102.
117. Oliver-Ortega H, Méndez JA, Reixach R, Espinach FX, Ardanuy M, Mutjé P. Towards more sustainable material formulations: A comparative assessment of PA11-SGW flexural performance versus oil-based composites. *Polymers (Basel).* 2018;10(4):440.
118. Zierdt P, Kulkarni G, Theumer T. Mechanical and Thermo-Mechanical Properties of Discontinuously and Continuously Processed Biogenic Wood-Plastic Composites from Polyamide 11 and Chemically Modified Beech Particles. In: *Macromolecular Symposia.* Vol 373. Wiley Online Library; 2017:1600118.
119. Rohner S, Humphry J, Chaléat CM, et al. Mechanical properties of polyamide 11 reinforced with cellulose nanofibres from *Triodia pungens*. *Cellulose.* 2018;25(4):2367-2380.
120. Semba T, Ito A, Kitagawa K, Nakatani T, Yano H, Sato A. Thermoplastic composites of polyamide-12 reinforced by cellulose nanofibers with cationic surface modification. *J Appl Polym Sci.* 2014;131(20). doi:<https://doi.org/10.1002/app.40920>
121. Nicharat A, Sapkota J, Weder C, Foster EJ. Melt processing of polyamide 12 and cellulose nanocrystals nanocomposites. *J Appl Polym Sci.* 2015;132(45).

-
122. Santos PA, Spinacé MAS, Feroselli KKG, De Paoli M-A. Polyamide-6/vegetal fiber composite prepared by extrusion and injection molding. *Compos Part A Appl Sci Manuf.* 2007;38(12):2404-2411.
 123. Henriksson M, Henriksson G, Berglund LA, Lindström T. An environmentally friendly method for enzyme-assisted preparation of microfibrillated cellulose (MFC) nanofibers. *Eur Polym J.* 2007;43(8):3434-3441.
 124. Kong I, Tshai KY, Hoque ME. Manufacturing of natural fibre-reinforced polymer composites by solvent casting method. In: *Manufacturing of Natural Fibre Reinforced Polymer Composites.* Springer; 2015:331-349.
 125. Agarwal BD, Broutman LJ, Bert CW. Analysis and performance of fiber composites. 1981.
 126. Krenchel H. Fibre reinforcement; theoretical and practical investigations of the elasticity and strength of fibre-reinforced materials. 1964.
 127. Vilaseca F, Del Rey R, Serrat R, Alba J, Mutje P, Espinach FX. Macro and micro-mechanics behavior of stiffness in alkaline treated hemp core fibres polypropylene-based composites. *Compos Part B Eng.* 2018;144:118-125.
 128. Wu Q, Liu X, Berglund LA. An unusual crystallization behavior in polyamide 6/montmorillonite nanocomposites. *Macromol Rapid Commun.* 2001;22(17):1438-1440.
 129. Millot C, Fillot L-A, Lame O, Sotta P, Seguela R. Assessment of polyamide-6 crystallinity by DSC. *J Therm Anal Calorim.* 2015;122(1):307-314.
 130. Shenoy A V, Saini DR, Nadkarni VM. Melt rheology of polymer blends from melt flow index. *Int J Polym Mater.* 1984;10(3):213-235.
 131. Guillot P, Colin A. Determination of the flow curve of complex fluids using the Rabinowitsch–Mooney equation in sensorless microrheometer. *Microfluid Nanofluidics.* 2014;17(3):605-611.

-
132. Håkansson KMO, Fall AB, Lundell F, et al. Hydrodynamic alignment and assembly of nanofibrils resulting in strong cellulose filaments. *Nat Commun.* 2014;5(1):1-10.
 133. Kamada A, Levin A, Toprakcioglu Z, et al. Modulating the Mechanical Performance of Macroscale Fibers through Shear-Induced Alignment and Assembly of Protein Nanofibrils. *Small.* 2020;16(9):1904190.
 134. Mittal N, Ansari F, Gowda. V K, et al. Multiscale control of nanocellulose assembly: transferring remarkable nanoscale fibril mechanics to macroscale fibers. *ACS Nano.* 2018;12(7):6378-6388.
 135. Fernandes FC, Gadioli R, Yassitepe E, De Paoli M. Polyamide-6 composites reinforced with cellulose fibers and fabricated by extrusion: Effect of fiber bleaching on mechanical properties and stability. *Polym Compos.* 2017;38(2):299-308.
 136. Santos PA, Spinacé MAS, Feroselli KKG, De Paoli MA. Polyamide-6/vegetal fiber composite prepared by extrusion and injection molding. *Compos Part A Appl Sci Manuf.* 2007;38(12):2404-2411. doi:10.1016/j.compositesa.2007.08.011
 137. Hocker S, Rhudy AK, Ginsburg G, Kranbuehl DE. Polyamide hydrolysis accelerated by small weak organic acids. *Polymer (Guildf).* 2014;55(20):5057-5064.
 138. Nirmala R, Panth HR, Yi C, et al. Effect of solvents on high aspect ratio polyamide-6 nanofibers via electrospinning. *Macromol Res.* 2010;18(8):759-765.
 139. Van den Berg O, Capadona JR, Weder C. Preparation of homogeneous dispersions of tunicate cellulose whiskers in organic solvents. *Biomacromolecules.* 2007;8(4):1353-1357.
 140. Aydemir D, Kiziltas A, Kiziltas EE, Gardner DJ, Gunduz G. Heat treated wood–nylon 6 composites. *Compos Part B Eng.* 2015;68:414-423.
 141. Krishna S, Patel CM. Computational and experimental study of mechanical properties of Nylon 6 nanocomposites reinforced with nanomilled cellulose. *Mech Mater.* 2020;143:103318.

-
142. Shao M-W, Huang J-J, Chen Y-X, Hwang S-S. Synthesis and characterization of the microcellular injection molded PA6/flax and the PA6/graphene nanocomposites. In: *IOP Conference Series: Materials Science and Engineering*. Vol 542. IOP Publishing; 2019:12067.
 143. Sucharitpong T, Lam NT, Sukyai P. Production of Nylon-6/Cellulose Nanocrystal Composite Films Using Solvent Dissolution. *Sugar Tech*. 2020;22(2):328-339.
 144. Benítez AJ, Walther A. Cellulose nanofibril nanopapers and bioinspired nanocomposites: a review to understand the mechanical property space. *J Mater Chem A*. 2017;5(31):16003-16024.
 145. Ray D, Sain S. In situ processing of cellulose nanocomposites. *Compos Part A Appl Sci Manuf*. 2016;83:19-37.
 146. Norrrahim MNF, Mohd Kasim NA, Knight VF, et al. Performance evaluation of cellulose nanofiber reinforced polymer composites. *Funct Compos Struct*. 2021;3(2):24001. doi:10.1088/2631-6331/abef6
 147. Hisseine OA, Tagnit-Hamou A. Nanocellulose for ecological nanoengineered strain-hardening cementitious composites incorporating high-volume ground-glass pozzolans. *Cem Concr Compos*. 2020;112:103662.
 148. Müller K, Zollfrank C. Ionic liquid aided solution-precipitation method to prepare polymer blends from cellulose with polyesters or polyamide. *Eur Polym J*. 2020;133:109743.
 149. Borsoi C, Zimmermann MVG, Zattera AJ, Santana RMC, Ferreira CA. Thermal degradation behavior of cellulose nanofibers and nanowhiskers. *J Therm Anal Calorim*. 2016;126(3):1867-1878.
 150. Perkins EL, Batchelor WJ. Water interaction in paper cellulose fibres as investigated by NMR pulsed field gradient. *Carbohydr Polym*. 2012;87(1):361-367.
 151. Prakobna K, Terenzi C, Zhou Q, Furó I, Berglund LA. Core-shell cellulose nanofibers for biocomposites—Nanostructural effects in hydrated state. *Carbohydr Polym*.

-
- 2015;125:92-102.
152. Faruk O, Bledzki AK, Fink H, Sain M. Progress report on natural fiber reinforced composites. *Macromol Mater Eng.* 2014;299(1):9-26.
153. Ansari F, Lindh EL, Furo I, Johansson MKG, Berglund LA. Interface tailoring through covalent hydroxyl-epoxy bonds improves hygromechanical stability in nanocellulose materials. *Compos Sci Technol.* 2016;134:175-183.
154. Safari S, van de Ven TGM. Effect of water vapor adsorption on electrical properties of carbon nanotube/nanocrystalline cellulose composites. *ACS Appl Mater Interfaces.* 2016;8(14):9483-9489.
155. Svensson A, Larsson PT, Salazar-Alvarez G, Wågberg L. Preparation of dry ultra-porous cellulosic fibres: Characterization and possible initial uses. *Carbohydr Polym.* 2013;92(1):775-783.
156. Venkatraman P, Gohn AM, Rhoades AM, Foster EJ. Developing high performance PA 11/cellulose nanocomposites for industrial-scale melt processing. *Compos Part B Eng.* 2019;174:106988.
157. Lundell F, Prahl Wittberg L. Hydrodynamic alignment of Nano-Fibrillated Cellulose in extensional flow. *Bull Am Phys Soc.* 2012;57.
158. Mittal N, Lundell F, Soderberg D. Hydrodynamic alignment and assembly of nano-fibrillated cellulose in the laminar extensional flow: Effects of solidifying agents. In: *APS Division of Fluid Dynamics Meeting Abstracts.* ; 2015:L39-011.
159. Milanez DH, Amaral RM do, Faria LIL de, Gregolin JAR. Assessing nanocellulose developments using science and technology indicators. *Mater Res.* 2013;16(3):635-641.

Appendix A Appended Articles

A.1

Article I

Sridhara, P.K. and Vilaseca, F., 2020. Assessment of fiber orientation on the mechanical properties of PA6/cellulose composite. Applied Sciences, 10(16), p.5565. DOI: 10.3390/app10165565

Journal Impact Factor: 2.679 (2020), Journal Rank: JCR – Q2 (38/91 in Engineering, Multidisciplinary)

Article

Assessment of Fiber Orientation on the Mechanical Properties of PA6/Cellulose Composite

Pruthvi K. Sridhara ¹ and Fabiola Vilaseca ^{1,2,*} 

¹ Advanced Biomaterials and Nanotechnology, Department of Chemical Engineering, University of Girona, 17003 Girona, Spain; pruthvi.sridhara@udg.edu

² Department of Fiber and Polymer Technology, KTH Royal Institute of Technology, SE-10044 Stockholm, Sweden

* Correspondence: fabiola.vilaseca@udg.edu

Received: 22 July 2020; Accepted: 10 August 2020; Published: 11 August 2020



Abstract: Cellulose is being considered as a suitable renewable reinforcement for materials production. In particular, cellulose based composites are attracting global interest for their unique and intrinsic properties such as strength to weight ratio, dimensional stability and low thermal expansion and contraction. This article investigates the preparation of cellulose pulp fibers with polyamide-6 (PA6) polymer and the effect of fiber orientation within the matrix on the final properties of the biocomposite. Cellulose pulp fibers were melt compounded with PA6 using a thermo-kinetic mixer. Different formulations were prepared and the compounds were manufactured into test samples by injection molding. Mechanical characterization revealed that elastic modulus and the flexural properties increased linearly with the fiber composition. The effect of fiber orientation was examined from square samples out of which individual specimens were cut at different directions with respect to the flow direction. The contributions related to fiber content and effect of fiber orientation on the tensile properties assessed lent positively towards parallel oriented samples (0°) with respect to flow direction. Furthermore, the cellulose network within the biocomposite revealed the superior interfacial properties between the cellulose and PA6 matrix when observed under a scanning electron microscope.

Keywords: cellulose; polyamide-6; dispersion; orientation; interface

1. Introduction

Cellulose is the most abundant natural polymer in the world. Due to the demand for biodegradable and renewal materials caused due to threats such as global warming and plastic pollution, there has been a tremendous interest during the past decade in biocomposites derived from cellulose and thermoplastic polymers [1]. From an engineering materials perspective, celluloses form the major load bearing component in wood cell walls with high strength of about ~3 GPa and a potential modulus ~138 GPa with respect to the longitudinal direction [2]. Extensive research and a number of publications on the terms cellulose and biocomposites have increased drastically in recent years [3]. Many cellulose reinforced composites have potential applications in the automotive component industry, construction and packaging [4–6]. This is due to the sustainability, availability, low density, high specific strength and stiffness of natural fibers which can be compared to that of glass fibers [7–9]. To date, almost 50% of a vehicle's internal parts are made out of polymeric materials and the global average weight of plastic in a modern day passenger vehicle is 105 kg accounting for 10–12% of the vehicle weight [4]. As government regulations and automotive makers are trending towards fuel economy, high efficiency, and cleaner ways of operating with reduced CO₂ levels, the demand for biocomposites is expected to increase [10,11]. Cellulose fibrils impart improvement in dimensional stability and physical and thermal properties of the cellulose reinforced biocomposites and have

excellent potential as a reinforcement material for thermoplastic composites because of their mechanical properties and low thermal expansion coefficient [12].

Few studies have been published examining the natural fibers reinforced polyamide-6 (PA6) composites preparation through the injection molding technique for the automotive industry [13]. Natural fiber reinforced composites are mainly confined to commodity or standard polymers such as polyolefins due to the challenges of high processing temperatures [10,14–16]. Commonly, polypropylene (PP), polyethylene (PE) and polyoxymethylene are reinforced with natural short fibers and subsequently reveal excellent mechanical properties but these polymers habitually require coupling agents such as maleic anhydride grafted polypropylene (MAPP) and/or dispersing agents such as diglyme, during their preparation processes, respectively [17–20]. Biobased polymer like polylactic acid (PLA) has also been studied as a matrix for natural fibers reinforcement, but PLA-natural fiber composites exhibit poor adhesion at the fiber-matrix interface. Various studies have indicated a decrease in the final properties of the PLA-natural fiber composite and, moreover, have given the thermal characteristics of PLA, it tends to degrade in some compounding processes such as repeated extrusion [21–23].

Engineering polymers such as polyamides are in exigency in the automobile industry accounting to their eco-friendly nature. Recent studies emphasizing on increasing the properties of polyamides reinforced with cellulosic materials are promising for our study [24,25]. Polyamide-11 (PA11) would be an obvious choice of matrix to work on, as 100% bio-based PA11 is commercially available and many investigations published are successful in obtaining composites with high mechanical properties [24,26]. However, polyamide-6 (PA6) or nylon-6 is a more attractive engineering polymer provided that PA6 is competing with thermoset plastics and metals for “under the hood” automotive applications due to their resistance to high temperature, oils and corrosive chemicals, relative strength to weight ratio and recyclability [16]. The use of natural fibers in PA6 matrix not only provides better physical and mechanical properties to the composite but also there is excellent compatibility between the fibers and the matrix due to the hydrophilic nature of PA6, thus eliminating the need for any coupling agent [7,16]. In North America, the market size of nylon-6 is estimated to grow as a result of environmental concerns by the plastic industry (Figure 1). This forecast is supported by the increase in demand for environmentally friendly wood based plastic composites. Correspondingly, PA6 has been considered as conventional matrix material for natural fiber-reinforced composites because of its beneficial thermo-mechanical properties [27].

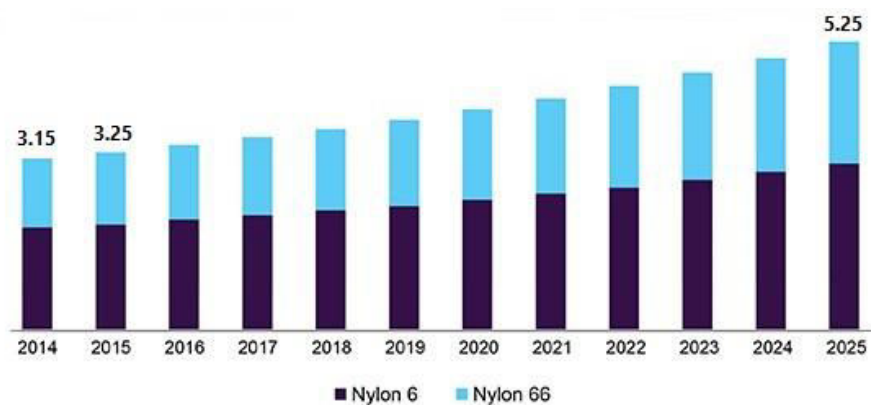


Figure 1. USA nylon 6 and 66 market size, by product, 2014–2025 (USD Billion) [source: [grandviewresearch.com](https://www.grandviewresearch.com)].

With a view to increasing the mechanical properties of the final composite, it is important to understand the mechanics of microstructure of the composite. Von misses’ criteria can be used to deduce that the strength of the composite is limited by the strength of the matrix [28]. The intrinsic tensile properties of the cellulose fibers can be imparted to the composites if there is qualitative interfacial bonding between the matrix and cellulose fibers. Addition to this, high degree of fiber

orientation, fiber dispersion and distribution and shorter processing times are key factors to achieve PA6-cellulose composites [29].

Melt processing techniques for preparation of natural fibers thermoplastic composites has simplified scaling and shortening time for composite formation [30]. The morphology and properties of PA6 composites are significantly affected by the type of melt processing technique and also depends on the amount of shear produced [31]. The most common melt processing technique is the twin screw extrusion process through which high degree of filler dispersion can be obtained and thus, significant reinforcement and greater properties of the composites [32,33]. However, cycle time is long and optimizing the extruder mixing conditions is a difficult task [34], which might lead to thermal degradation of the natural cellulose fibers. Even though there are some limitations such as level of dispersion and distribution or interfacial bonding with the matrix, these limitations can be overcome by melt processing with the Gelimat[®] mixer [35]. Gelimat is a compounder/mixer based on the principle of high speed thermo-kinetic mixing. A final compound with excellent dispersion quality can be obtained in one cycle due to the high shear rate generated by the rotor [35]. The Gelimat equipment and a schematic of the Gelimat mixer is shown in Figure 2. When compared with the twin screw extruder, the Gelimat mixer produces higher dispersion [36] and the fiber length remains longer when compared to extruder or internal mixers, consequently improving strength of the composite [37]. Some studies indicate that several passes are required to obtain a biocomposite using an extruder with satisfactory dispersion level exposing the natural fibers to longer levels of processing time hence prone to thermal degradation [38,39]. Instead, Gelimat kinetic-mixer compounds at shorter processing time and it helps fibrillation of fibers due to the high shear rate induced [30,40]. These factors make it very suitable to manufacture extremely time-temperature sensitive biocomposites of cellulose and polymers such as polyamide-6.

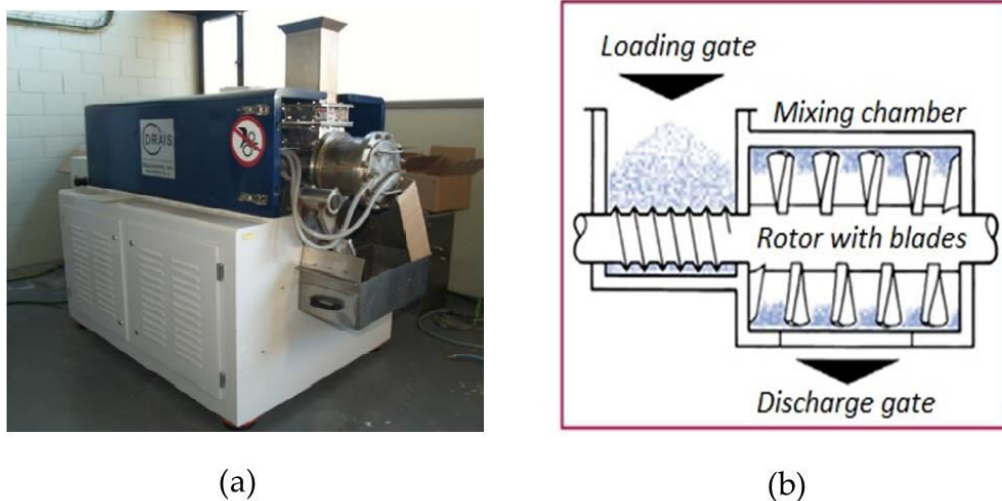


Figure 2. (a) Gelimat[®] equipment, and (b) Schematic of Gelimat compounder.

In this study the feasibility of reinforcing PA6 matrix with cellulose fibers by melt compounding with a thermo-kinetic mixer was studied. The thermal degradation temperature of cellulose together with the higher processing temperatures of PA6 are challenges for this study [14]. PA6 cellulose composites were prepared in the Gelimat mixer and injected to test samples. For analyzing the effect of fiber orientation on the mechanical properties of the composites, a square mold (Figure 3a) for injecting test samples was used and test specimens oriented at different direction with respect to the flow were laser cut from the square samples for all compositions. A simulation of the injection process shows the fiber orientation indicated by color and the scale bar represented by orientation factor (Figure 3b). The alignment of cellulose pulp fibers within the PA6 matrix is dictated by the

direction of injection flow and alignment occurs parallel to the flow [41]. Natural wood pulp fibers with high degree of orientation impart high levels of stiffness to the biocomposite [42]. Many studies have analyzed the ability of flow stream with fibers to produce homogenous aligned fibrils at the nano and micro scale [8,43,44]. In addition, flow induced alignment has good distribution due to the electrostatic repulsion between the fibrils [8,42]. Such control of internal morphology gives advantages in expanding the anisotropic properties of biocomposites [44].

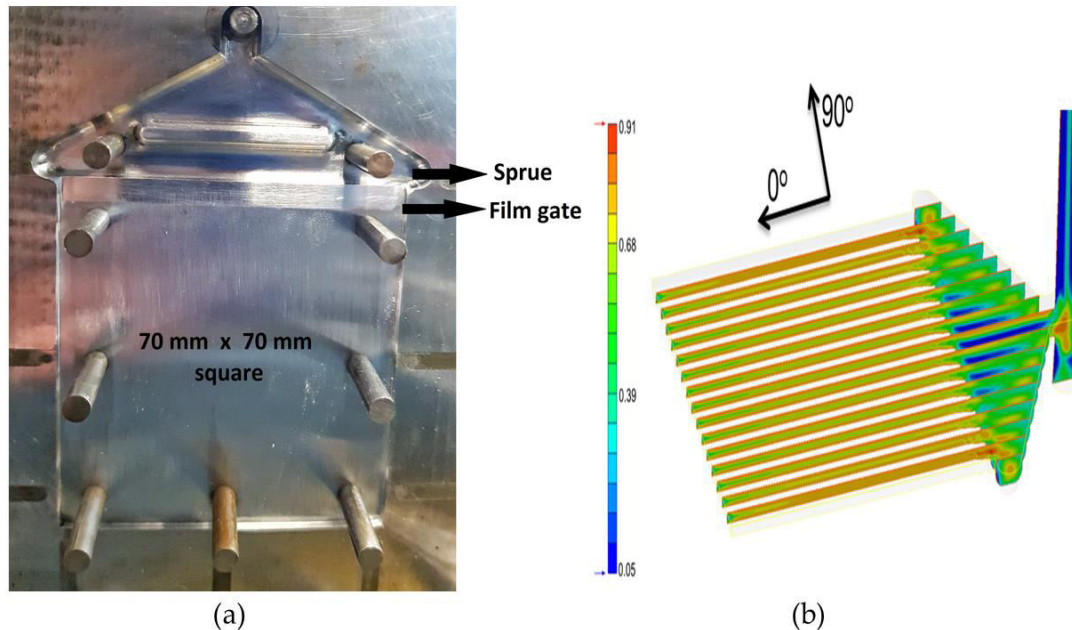


Figure 3. (a) Square mold, and (b) Flow simulation using Moldex[®] 3 D with scale bare depicting orientation factor.

2. Materials and Methods

Cellulose was obtained as a commercial product in the form of sheets (>97% cellulose content) by the company Domsjö Fabriker (Örnsköldsvik, Sweden). It is made out of softwood, primarily from the northern parts of Sweden and Latvia. Initially, the thermal degradation temperature of the cellulose pulp fibers was determined by thermogravimetric analysis using a Mettler Toledo TGA851 equipment. Commercially available PA6 (RADILON S 24 E 100 NAT) of 1140 kg/m³ density was purchased from Radici Plastics Iberica SL (Barcelona, Spain) in the form of natural colored pellets. This grade of PA6 has low material viscosity index (125 mL/g) and is suitable for efficient processing with injection molding. A purging agent Ultra Purge 5150 from Chem-Trend (Entzheim, France) was used for cleaning the injection chamber and screw from impurities and also to avoid contamination before the injection process of our composites. The mixing chamber of the Gelimat was cleaned by running it with just the PA6 prior to composite compounding process to avoid contamination.

2.1. Cellulose Pulp-PA6 Composites Preparation

To prepare different compositions of pulp composites, batches of PA6 were dried for 8 h in 80 °C before they were compounded in the Gelimat[®] (Draiswerke G5 S, Ramsey, NJ, USA) (Figure 2a) to remove the moisture content. Non-dried cellulose sheets were micro-shredded using a paper disintegrator before the melt compounding process.

The mixing chamber of the Gelimat was cleaned with PA6 to avoid contamination. The rotor was set to 300 rpm and non-dry micro-shredded cellulose was introduced first into the mixing chamber through the loading gate (Figure 2b). Non-dried pulp fibers were used to avoid fiber hornification [45]. Dry PA6 pellets were then introduced and the loading gate was closed. The speed of the rotor blades

was then increased gradually up to 2300–2600 rpm to consolidate the mixture to reach a melting temperature of 220 °C thus resulting the mixing time of less than 15–20 s at this temperature. As soon as there was a drop in the current (amperes) drawn by the rotor, compounding of the mixture was completed and then the discharge gate was opened while rotor speed reduced. The discharged compounded mixture collected in the discharge cabin was then carefully rolled flat with the help of a heavy roller and cooled immediately to prevent any thermal degradation. When the flattened composite had completely cooled down to room temperature, it was then broken into smaller pieces to be introduced into the pelletizer and pellets were prepared prior to injection process. Finally, the composites pellets were dried for 8 h at 80 °C before processing them into test specimens using injection molding.

The injection machine (ARBURG AllRounder 220 M) was set to the parameters shown in Table 1 and then injection chamber was purged from contaminants and impurities before starting the injection process for the composites. The composites were injected into a square shaped mold. The injected square samples are shown in the Figure 4a. Later, the test specimens were obtained from the square samples by using a laser cutting. Three different orientations of the test samples were laser cut from the square samples: (i) perpendicular, (ii) parallel, and (iii) at 45° with respect to the injection flow (Figure 4b).

Table 1. Injection molding parameters for pulp composites.

Parameter	Value/s
Temperature profile	210, 215, 220, 225, and 230 °C
Mold temperature	60 °C
Injection pressure	575–650 bars



Figure 4. (a) Square sample with dimension 70 × 70 × 1.5 mm, and (b) Square samples from which oriented specimens are laser cut, (from left to right) parallel (0°), perpendicular (90°) and 45° oriented cut.

2.2. Composite Characterization

2.2.1. Mechanical Testing

Tensile tests were performed using a universal testing machine type Instron™ 1122 (IDM Test, San Sebastián, Spain) fitted with a load cell of 5 kN and operating at 2 mm/min. For tensile testing, specimens were cut to 65 × 6 × 1.5 mm for all compositions at different orientation (0°, 45° and 90°). Flexural testing samples were prepared according to the standard ASTM D790 and tensile modulus samples were prepared according to ASTM D638 by using an extensometer (MFA2–Velbert, Germany). All the tests were conducted at room temperature condition (23 ± 2 °C) and relative humidity (50 ± 5%) for dry samples. The same was repeated for 48-h conditioned specimens using a Dycometal (Barcelona, Spain) climatic chamber at 23 °C and 50% relative humidity for 48 h, according to ASTM D618 13 standard, for all composition. A minimum of five samples were tested for each formulation.

2.2.2. SEM Analysis

The morphology of fractured samples was observed under a scanning electron microscope (Zeiss DSM 960A, Jena, Germany) to characterize the interaction between fibers and PA6 matrix. The samples were coated with gold using a sputter prior to measurement and observed at an accelerated voltage of 7 kV.

3. Results and Discussion

3.1. Thermogravimetric Analysis of Cellulose Pulp Fibers

Thermogravimetric analysis (TGA) of cellulose pulp fibers provide important information for means to avoid thermal degradation during composite processing. The TGA curve and its first derivative (DTG) curve are shown in Figure 5. About 5% mass loss due to the evaporation of absorbed moisture was observed from 80 °C. The initial mass loss peak started at 320 °C with the maximum mass loss at 346 °C, as shown in the DTG curve (Figure 5). The use of pure cellulose is then beneficial to allow the processing temperature of PA6 of 230 °C without degradation of the pure cellulose fibers. The composites were compounded well under this temperature (220 °C) in the Gelimat and manufactured at an injection temperature not exceeding 230/235 °C, with high injection pressure.

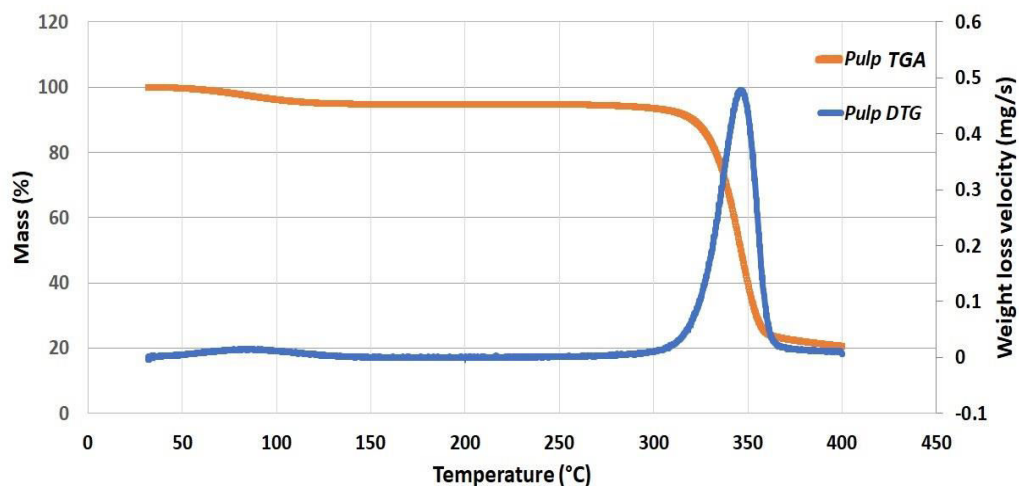


Figure 5. TGA curve, and DTG for the current cellulose pulp fibers.

3.2. Mechanical Analysis

3.2.1. Tensile Strength of Oriented Specimens

PA6-cellulose pulp composites with cellulose composition of 5, 10, 15, 20, and 25% were prepared, and shown in Figure 6. These pellets were manufactured into test specimens using injection molding. The samples turned light brown with respect to the increasing order of pulp cellulose composition.



Figure 6. Cellulose pulp composite pellets indicating their respective cellulose composition prepared from Gelimat mixer and later pelletized prior to injection.

The mean values of tensile strengths of the oriented specimens are shown in the Figure 7a for dry samples and in Figure 7b for 48-h conditioned samples, conditioned at temperature ($23 \pm 2 \text{ }^\circ\text{C}$) and relative humidity ($50 \pm 5\%$). The control sample of dry PA6 had a tensile strength of 53.30 MPa. For all formulations, the properties were in accordance to the cellulose fiber orientation inside the composite. It is worth mentioning that 25 wt % of cellulose fiber was the maximum amount of fiber reinforcement affordable for the PA6 matrix. Higher amounts of cellulose fibers were not allowed as the PA6 matrix did not show proper fiber distribution and fiber wrapping along the composite material.

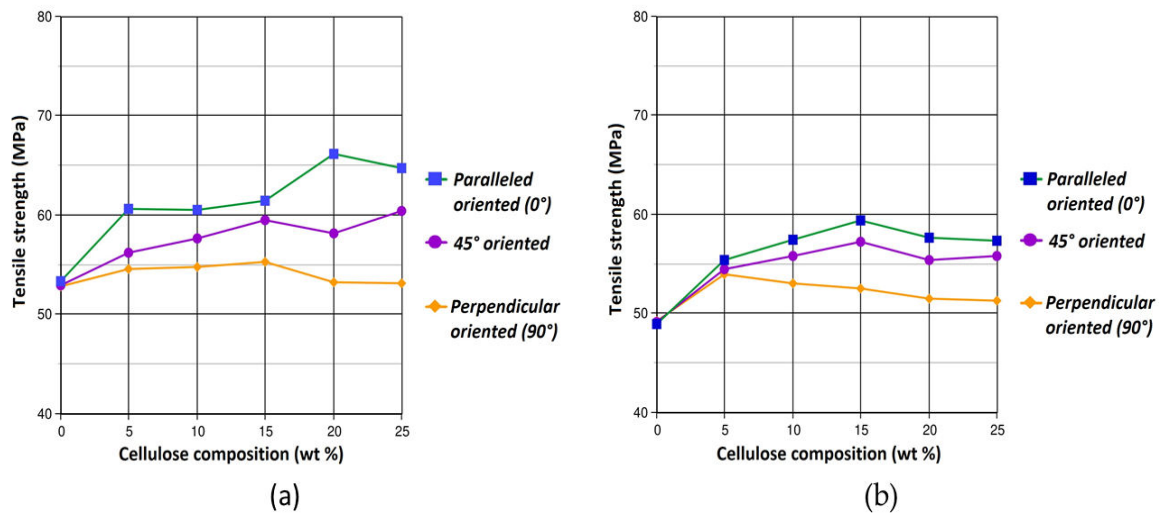


Figure 7. Tensile strength of oriented samples, (a) dry samples and (b) 48-h conditioned samples.

Parallel oriented specimens (0°) displayed the best results substantiating the wood pulp fiber composites with high orientation in longitudinal alignment have higher mechanical properties [42]. The tensile strength increased gradually with respect to increase in pulp cellulose composition. The maximum value of 66.17 MPa was obtained for 20% composition followed by 64.76 MPa for 25% composition for dry samples. These tensile strength value corresponds to a 24% higher than the values of the control sample. For 45° oriented samples, the values of tensile strength values were

intermediate between 0° and 90° oriented samples with the highest value being 60.44 MPa for dry sample of 25% composition. The 90° oriented samples exhibited the least values as the elongation took place perpendicular to the fibers alignment, this is because of the anisotropic properties defined by morphology of composites [44]. All the tensile strength values for 48-h conditioned samples showed lower values than the dry ones since the samples absorb moisture during the 48-h conditioning in the climatic chamber and water molecules behave as plasticizer in the course of tensile testing. Here, the maximum tensile strength values were found at 15 wt % cellulose content, with an increment from 48.8 to 59.4 MPa in value with respect to the neat PA6 conditioned. For perpendicular oriented fibers, the strength tends to decrease with the fiber content due to the increase amount of transverse fibers with very low cross section strength that tends to behave as defects along the measurement direction.

3.2.2. Tensile Modulus of Elasticity

The control sample of PA6 for tensile modulus of elasticity (TMOE) test had a value of 3.01 GPa. The control sample subjected to elongation initially responded with elastic deformation, viscoelasticity followed by the yield point. The samples were allowed to deform after yielding resulting in necking and propagation of necking until fracture to measure the elongation at break. The TMOE increased significantly for the composites and its increase is linear to increase in cellulose composition. The maximum TMOE was obtained for 25% composition samples with their values being 4.6 GPa and 4.4 GPa for dry and 48-h conditioned samples respectively (Figure 8b). These TMOE values are equivalent to 53% higher than those of the control sample. The incorporation of cellulose pulp fibers into PA6 matrix restricts the elastic deformation of PA6 resulting in composites with high TMOE [14,46]. Due to this, pulp cellulose–PA6 composites when subjected to tensile load displayed notably lower strains at yield point when compared to the control sample. The significant drop in strain levels at break is shown in Figure 8a. Higher compositions of cellulose pulp fibers contribute to more relative surface area for the PA6 matrix to adhere to, owing to the high dispersion and distribution of fibers within the matrix imparted during Gelimat compounding. Thereby, forming stronger interfacial bonds and incidentally increasing the tensile strength and TMOE [47,48].

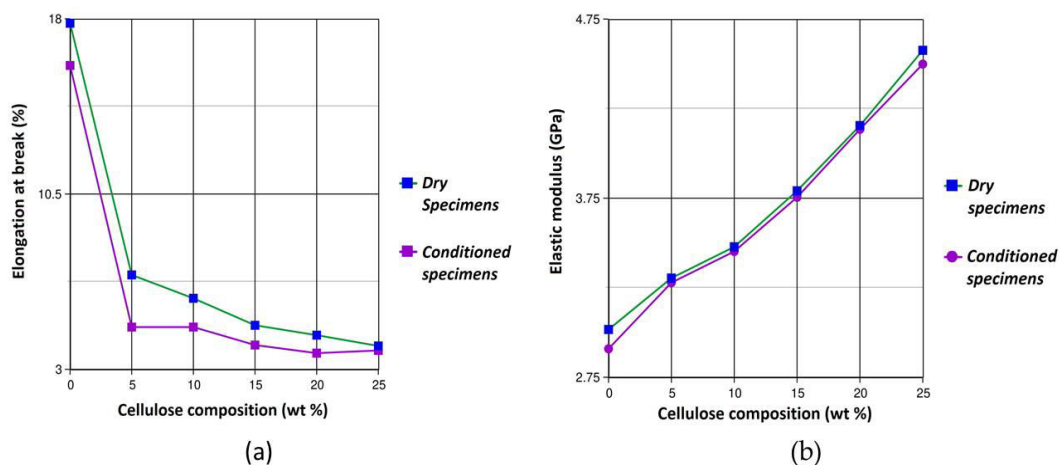


Figure 8. (a) Elongation at break (indicating low strain at break for composites compared to control sample), and (b) Tensile modulus of elasticity plot for all compositions.

There was a slight decrease of tensile strength from 66.17 MPa to 64.76 MPa from 20% to 25% cellulose composition for the dry samples and 59.40 MPa to 57.29 MPa from 15% to 25% composition for 48-h conditioned samples. Though these were small decrease in the values, this may be due to lack of wetting and interaction between the fibers and PA6 matrix [14]. In such cases, the lack of interaction weakens the reinforcing effect of the fibers within the PA6 matrix [49]. The reinforcing effect remain dominant for TMOE and improvements were seen linearly with increase in composition (Figure 8b).

This linear increase in stiffness depends on the fiber composition, dispersion and distribution of the pulp fibers within the PA6 matrix [50].

Stress strain curves for control sample (neat PA6) and the different compositions of cellulose pulp-PA6 composites deduced from the experimental data are shown in Figure 9. The deformation behavior during elongation for all the samples is observed. Naturally, the presence of fibrils reduces the elongation in the composites when compared to the neat PA6 attributable to the reinforcing effect of cellulose fibers in the matrix [29]. In addition, increase in the cellulose composition supplements to stiffening the composites. Further, it can be testified from Figure 8a that as fiber composition increases, the strain at the point of deformation decreases thanks to the strong interfacial bonding between fiber and matrix.

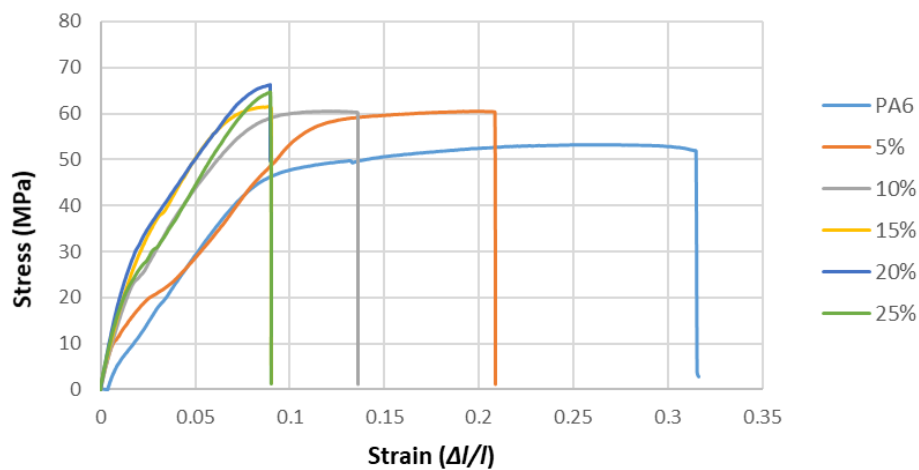


Figure 9. Stress-strain curves of neat PA6 and cellulose pulp-PA6 composites.

3.2.3. Flexural Resistance and Flexural Modulus of Elasticity

The flexural resistance and flexural modulus of elasticity (MOE) for all the composites are shown in Figure 10. The flexural resistance and flexural MOE for the PA6 control sample were 105 MPa and 2.45 GPa for dry samples and 90.19 MPa and 2.08 GPa for 48-h conditioned samples respectively. The flexural MOE had significant improvements and the flexural resistance had gradual improvements with respect to increase in cellulose composition.

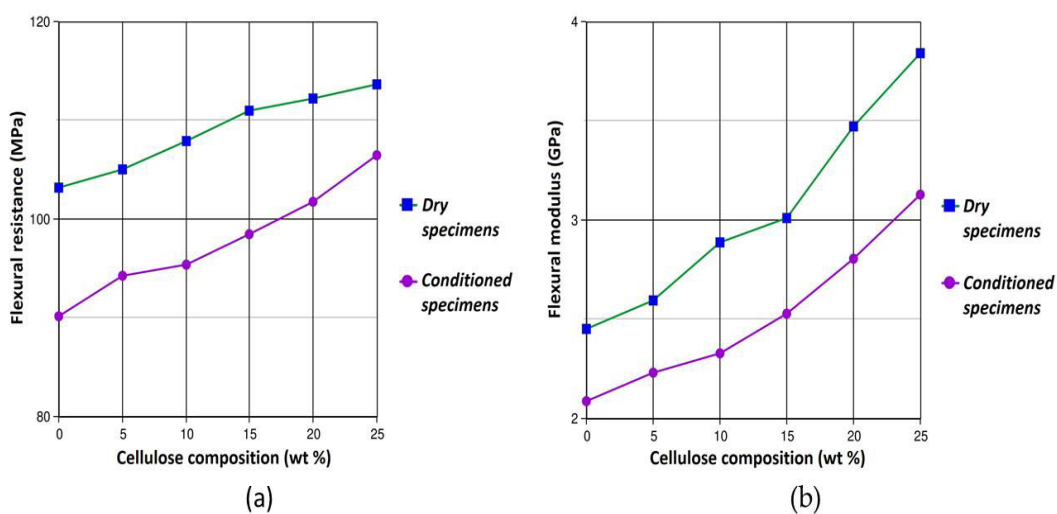


Figure 10. (a) Flexural resistance and (b) flexural modulus of elasticity (MOE) of the pulp cellulose composites.

The highest values of flexural resistance and flexural MOE were obtained for 25% composition with the values being 113.6 MPa and 3.84 GPa for dry samples and 106.5 MPa and 3.13 GPa for conditioned samples respectively. These values correspond to an 8% increase in flexural resistance (Figure 10a) and 57% increase in flexural MOE (Figure 10b).

3.3. SEM Analysis

The morphology of 5%, 15% and 25% in composition cellulose pulp fiber composites were observed under SEM. The fractured surfaces of samples used for tensile testing were examined to study the interfacial bonding between pulp fibers and PA6 matrix sequentially. All the fractured samples were allowed to reach equilibrium weight at room temperature and atmospheric conditions prior to SEM analysis. The SEM micrographs for 25% cellulose pulp-PA6 composite are shown in Figure 11.

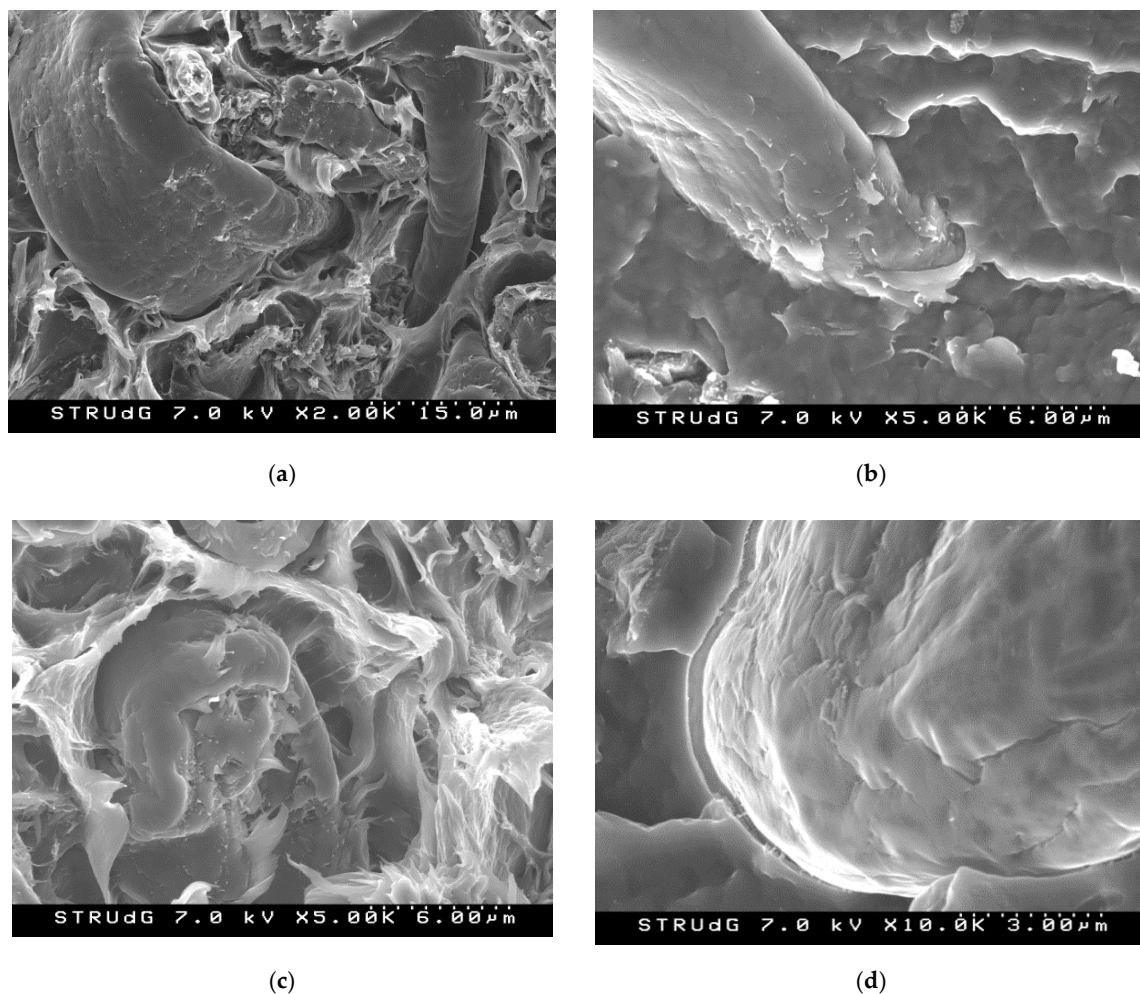


Figure 11. SEM micrographs of fracture surfaces of 25% cellulose pulp composite tested under tensile load at different magnification levels.

The SEM images reveal that there was good wetting of cellulose pulp fibers within the PA6 matrix, denoting that the cellulose fibril surfaces are saturated by the PA6 matrix. Simultaneously in Figure 11a, it is observed that pulp fiber (micro fibers) were well dispersed and no agglomerations were observed. At higher magnifications (Figure 11b–d), the adhesion between the polymer and the pulp fibers might be due to the chemical affinity between both components favoring the interface compatibility. The hydrophilic nature of PA6 makes the adhesion between pulp fibers and PA6 matrix strong [7,51]. The attraction between PA6 and cellulose fibers makes dispersion and distribution more

effective, as it was validated by the improvements of tensile and flexural properties of the composites. Some authors have explained the chemical interaction between PA6 matrix and cellulose fibers in the partial hydrolysis of PA6 in presence of moisture and high temperature. The moisture content prior to compounding process in (non-dried) fibers aid in interfacial bonding, due to the partial hydrolysis of PA6 caused by moisture at high temperature, generating carboxylic acid end groups which are compatible with the (-OH) groups forming ester bonds [45]. The reinforcing effect of cellulose materials is determined by the stress transfer through the interfacial adhesion [14]. The PA6 matrix showed surface distortion characteristic of ductile deformation after reaching to a level that the interfacial adhesion cannot resist and the fibers were broken at the surface. No fiber pullout was observed as seen from Figure 11c.

3.4. Summary

The results obtained from the tensile testing of different oriented samples draw positive conclusions that the composites with parallel fiber orientation with respect to the injection flow exhibit higher values tensile strength. Maximum tensile strength (66.17 MPa) and a maximum TMOE (4.6 GPa) was seen in 20% and 25% cellulose pulp-PA6 composite associating to 24% and 25% increase in values respectively when compared to neat PA6. Similarly, maximum flexural resistance (113.6 MPa) and maximum flexural MOE (3.84 GPa) was attained for 25% cellulose pulp-PA6 composites associating to 57% and 8% higher values than those of neat PA6 respectively.

Previously conducted research on PA6-cellulose materials depicts no major increments in the mechanical properties of the final composite [50,52]. The tensile and flexural values obtained in this study are without the use of any lubricants or process stabilizers and are comparable to the results of those in the bibliography [7,10,53]. Different cellulosic materials effect the tensile and flexural properties of cellulose based composites due to various factors such as particle size, particle shape, distribution, thermal stability, particle surface morphology and particle surface energy [54,55]. Lower strain values with the increase in cellulose composition indicate the prominent reinforcing effect of cellulose due to strong interfacial bonding between fibers and PA6 matrix [14,29]. The adhesion between pure cellulose fibers and PA6 matrix is further demonstrated through SEM analysis. Lack of defects indicate that the compounding method has been effective. Thanks to extreme short processing times, the thermal stresses subjected on the cellulose fibers have negligible degrading effect. This single step, quick compounding process constitutes to high fiber length when compared to studies which involve multiple thermal compounding steps/cycles [25,49]. This aspect is boon on an industrial level where the promotion of renewable materials is hindered due to complex nature procedures involved in manufacturing biocomposites.

4. Conclusions

Cellulose pulp fibers were used to reinforce PA6 matrix to produce cellulose pulp-PA6 composites from melt compounding with the thermokinetic mixer- Gelimat and injection molding without the use of any coupling agent. The feasibility of conventional manufacturing processes is a very important consideration for industrial level to promote use of renewable materials. This study provides a novel method with a single step compounding procedure and injection molding keeping the industry in mind. The Gelimat minimizes the exposure of cellulose fibers at high temperature inhibiting thermal degradation and the injected samples exhibit high mechanical properties as a consequence of low thermal stresses imposed on the cellulose fibers along with imparting excellent dispersion and distribution of fibers within the PA6 matrix.

Overall, composite compositions of up to 25% in weight of cellulose pulp fiber were prepared and all the formulations showed improved tensile and flexural properties due to the reduced fluidity of PA6 and increased stiffness of the composites when cellulose fibers were incorporated into the PA6 matrix. Also, the SEM micrograph showed good wetting of pulp fibers within the PA6 matrix, without any agglomerations and no pullout of fibers indicating the superiority of the interfacial bonding between

the fibers and the PA6 matrix. This demonstrates that the Gelimat equipment is able to compound cellulose-PA6 materials thoroughly with good mechanical properties of the final biocomposite.

This study corroborates that the fiber orientation in injection molded samples is dictated by the forces exerted by the injection flow on the cellulose fiber. The tensile tests of different oriented samples revealed that the fibers aligned in parallel (0°) to the injection flow had the highest values of tensile properties. The flexural tests of parallel oriented samples revealed that the flexural rigidity increases linearly with cellulose composition. TMOE tests revealed low strain at break with respect to cellulose composition indicating the effect of reinforcement. Flow induced natural fibers alignment with high orientation produce biocomposites with high levels of stiffness imparting anisotropic properties to the biocomposite. Moving forward, the potential of this research design can be further explored onto PA6-cellulose nanocomposites and hybrid nanocomposites.

Author Contributions: Conceptualization, P.K.S. and F.V.; methodology, P.K.S. and F.V.; software, P.K.S.; validation, P.K.S. and F.V.; formal analysis, P.K.S. and F.V.; investigation, P.K.S.; resources, P.K.S. and F.V.; data curation, P.K.S.; writing—original draft preparation, P.K.S.; writing—review and editing, P.K.S. and F.V.; visualization, P.K.S.; supervision, F.V.; project administration, F.V.; funding acquisition, F.V. All authors have read and agreed to the published version of the manuscript.

Funding: This research was funded within the Biocomposites Program by Knut and Alice Wallenberg Foundation (Sweden) and the UdG grant (IFUdG 2017).

Acknowledgments: The authors want to thank LEPAMAP Group of the University of Girona (UdG) for helping in the use of laboratory equipment, as well as to the administrative help from the EQATA Department and the OITT service of UdG.

Conflicts of Interest: The authors declare no conflict of interest.

References

1. Kargarzadeh, H.; Mariano, M.; Huang, J.; Lin, N.; Ahmad, I.; Dufresne, A.; Thomas, S. Recent developments on nanocellulose reinforced polymer nanocomposites: A review. *Polymer* **2017**, *132*, 368–393. [[CrossRef](#)]
2. Saito, T.; Kuramae, R.; Wohlert, J.; Berglund, L.A.; Isogai, A. An ultrastrong nanofibrillar biomaterial: The strength of single cellulose nanofibrils revealed via sonication-induced fragmentation. *Biomacromolecules* **2013**, *14*, 248–253. [[CrossRef](#)] [[PubMed](#)]
3. Lee, K.Y.; Aitomäki, Y.; Berglund, L.A.; Oksman, K.; Bismarck, A. On the use of nanocellulose as reinforcement in polymer matrix composites. *Compos. Sci. Technol.* **2014**, *105*, 15–27. [[CrossRef](#)]
4. Furtado, S.C.R.; Araújo, A.L.; Silva, A.; Alves, C.; Ribeiro, A.M.R. Natural fibre-reinforced composite parts for automotive applications. *Int. J. Automot. Compos.* **2014**, *1*, 18. [[CrossRef](#)]
5. Rudeiros-Fernández, J.L.; Thomason, J.L.; Liggat, J.J.; Soliman, M. Characterisation of the mechanical and thermal degradation behaviour of natural fibres for lightweight automotive applications. In Proceedings of the ICCM International Conferences on Composite Materials 2013, Montreal, QC, Canada, 28 July–2 August 2013; Volume 1, pp. 8142–8153.
6. Njuguna, J.; Wambua, P.; Pielichowski, K. Natural Fibre-Reinforced Polymer Composites and Nanocomposites for Automotive Applications. In *Cellulose Fibers: Bio- and Nano-Polymer Composites*; Springer: Berlin/Heidelberg, Germany, 2011; pp. 661–700. ISBN 9783642173707.
7. de Arcaya, P.A.; Retegi, A.; Arbelaz, A.; Kenny, J.M.; Mondragon, I. Mechanical properties of natural fibers/polyamides composites. *Polym. Compos.* **2008**, *30*, 257–264. [[CrossRef](#)]
8. Hakansson, K.M.O.; Fall, A.B.; Lundell, F.; Yu, S.; Krywka, C.; Roth, S.V.; Santoro, G.; Kvick, M.; Prah Wittberg, L.; Wagberg, L.; et al. Hydrodynamic alignment and assembly of nanofibrils resulting in strong cellulose filaments. *Nat. Commun.* **2014**, *5*, 1–10.
9. Rogovina, S.Z.; Prut, E.V.; Berlin, A.A. Composite Materials Based on Synthetic Polymers Reinforced with Natural Fibers. *Polym. Sci.-Ser. A* **2019**, *61*, 417–438. [[CrossRef](#)]
10. Ozen, E.; Kiziltas, A.; Kiziltas, E.E.; Gardner, D.J. Natural fiber blend—Nylon 6 composites. *Polym. Compos.* **2013**, *34*, 544–553. [[CrossRef](#)]
11. Dunne, R.; Desai, D.; Sadiku, R.; Jayaramudu, J. A review of natural fibres, their sustainability and automotive applications. *J. Reinf. Plast. Compos.* **2016**, *35*, 1041–1050. [[CrossRef](#)]

12. Lee, J.A.; Yoon, M.J.; Lee, E.S.; Lim, D.Y.; Kim, K.Y. Preparation and characterization of cellulose nanofibers (CNFs) from microcrystalline cellulose (MCC) and CNF/polyamide 6 composites. *Macromol. Res.* **2014**, *22*, 738–745. [[CrossRef](#)]
13. Annandarajah, C.; Langhorst, A.; Kiziltas, A.; Grewell, D.; Mielewski, D.; Montazami, R. Hybrid cellulose-glass fiber composites for automotive applications. *Materials* **2019**, *12*, 3189. [[CrossRef](#)] [[PubMed](#)]
14. Peng, Y.; Gardner, D.J.; Han, Y. Characterization of mechanical and morphological properties of cellulose reinforced polyamide 6 composites. *Cellulose* **2015**, *22*, 3199–3215. [[CrossRef](#)]
15. Xu, S.; Yi, S.; He, J.; Wang, H.; Fang, Y.; Wang, Q. Preparation and properties of a novel microcrystalline cellulose-filled composites based on polyamide 6/high-density polyethylene. *Materials* **2017**, *10*, 808. [[CrossRef](#)] [[PubMed](#)]
16. Corrêa, A.C.; de Moraes Teixeira, E.; Carmona, V.B.; Teodoro, K.B.R.; Ribeiro, C.; Mattoso, L.H.C.; Marconcini, J.M. Obtaining nanocomposites of polyamide 6 and cellulose whiskers via extrusion and injection molding. *Cellulose* **2014**, *21*, 311–322. [[CrossRef](#)]
17. Delgado-Aguilar, M.; Tarrés, Q.; de Marques, M.F.V.; Espinach, F.X.; Julián, F.; Mutjé, P.; Vilaseca, F. Explorative study on the use of Curauá reinforced polypropylene composites for the automotive industry. *Materials* **2019**, *12*, 4185. [[CrossRef](#)]
18. Reixach, R.; Espinach, F.X.; Arbat, G.; Julián, F.; Delgado-Aguilar, M.; Puig, J.; Mutjé, P. Tensile properties of polypropylene composites reinforced with mechanical, thermomechanical, and chemi-thermomechanical pulps from orange pruning. *BioResources* **2015**, *10*, 4544–4556. [[CrossRef](#)]
19. Tarrés, Q.; Vilaseca, F.; Herrera-Franco, P.J.; Espinach, F.X.; Delgado-Aguilar, M.; Mutjé, P. Interface and micromechanical characterization of tensile strength of bio-based composites from polypropylene and henequen strands. *Ind. Crops Prod.* **2019**, *132*, 319–326. [[CrossRef](#)]
20. Espinach, F.X.; Granda, L.A.; Tarrés, Q.; Duran, J.; Fullana-i-Palmer, P.; Mutjé, P. Mechanical and micromechanical tensile strength of eucalyptus bleached fibers reinforced polyoxymethylene composites. *Compos. Part B Eng.* **2017**, *116*, 333–339. [[CrossRef](#)]
21. Siakeng, R.; Jawaid, M.; Ariffin, H.; Sapuan, S.M.; Asim, M.; Saba, N. Natural fiber reinforced polylactic acid composites: A review. *Polym. Compos.* **2019**, *40*, 446–463. [[CrossRef](#)]
22. Oksman, K.; Skrifvars, M.; Selin, J.F. Natural fibres as reinforcement in polylactic acid (PLA) composites. *Compos. Sci. Technol.* **2003**, *63*, 1317–1324. [[CrossRef](#)]
23. Mathew, A.P.; Oksman, K.; Sain, M. Mechanical properties of biodegradable composites from poly lactic acid (PLA) and microcrystalline cellulose (MCC). *J. Appl. Polym. Sci.* **2005**, *97*, 2014–2025. [[CrossRef](#)]
24. Venkatraman, P.; Gohn, A.M.; Rhoades, A.M.; Foster, E.J. Developing high performance PA 11/cellulose nanocomposites for industrial-scale melt processing. *Compos. Part B Eng.* **2019**, *174*, 106988. [[CrossRef](#)]
25. Alonso-Montemayor, F.J.; Tarrés, Q.; Oliver-Ortega, H.; Espinach, F.X.; Narro-Céspedes, R.I.; Castañeda-Facio, A.O.; Delgado-Aguilar, M. Enhancing the mechanical performance of bleached hemp fibers reinforced polyamide 6 composites: A competitive alternative to commodity composites. *Polymers* **2020**, *12*, 1041. [[CrossRef](#)] [[PubMed](#)]
26. Oliver-Ortega, H.; Granda, L.A.; Espinach, F.X.; Menez, J.A.; Julian, F.; Mutje, P. Tensile properties and micromechanical analysis of stone groundwood from softwood reinforced bio-based polyamide11 composites. *Compos. Sci. Technol.* **2016**, *132*, 123–130. [[CrossRef](#)]
27. Kiziltas, A.; Nazari, B.; Gardner, D.J.; Bousfield, D.W. Polyamide 6–Cellulose Composites: Effect of Cellulose Composition on Melt Rheology and Crystallization Behavior. *Polym. Eng. Sci.* **2014**, *54*, 739–746. [[CrossRef](#)]
28. Salem, S.; Oliver-Ortega, H.; Espinach, F.X.; Hamed, K.B.; Nasri, N.; Alcalà, M.; Mutjé, P. Study on the Tensile Strength and Micromechanical Analysis of Alfa Fibers Reinforced High Density Polyethylene Composites. *Fibers Polym.* **2019**, *20*, 602–610. [[CrossRef](#)]
29. Rezaee Niaraki, P.; Krause, A. Correlation between physical bonding and mechanical properties of wood–Plastic composites: Part 2: Effect of thermodynamic factors on interfacial bonding at wood–polymer interface. *J. Adhes. Sci. Technol.* **2020**, *34*, 756–768. [[CrossRef](#)]
30. Ray, D.; Sain, S. In situ processing of cellulose nanocomposites. *Compos. Part A Appl. Sci. Manuf.* **2016**, *83*, 19–37. [[CrossRef](#)]
31. Chavarria, F.; Shah, R.K.; Hunter, D.L.; Paul, D.R. Effect of melt processing conditions on the morphology and properties of nylon 6 nanocomposites. *Polym. Eng. Sci.* **2007**, *47*, 1847–1864. [[CrossRef](#)]

32. Karsli, N.G.; Aytac, A. Tensile and thermomechanical properties of short carbon fiber reinforced polyamide 6 composites. *Compos. Part B Eng.* **2013**, *51*, 270–275. [[CrossRef](#)]
33. Chavarria, F.; Paul, D.R. Comparison of nanocomposites based on nylon 6 and nylon 66. *Polymer* **2004**, *45*, 8501–8515. [[CrossRef](#)]
34. Shah, R.K.; Paul, D.R. Organoclay degradation in melt processed polyethylene nanocomposites. *Polymer* **2006**, *47*, 4075–4084. [[CrossRef](#)]
35. Gopakumar, T.G.; Page, D.J.Y.S. Compounding of nanocomposites by thermokinetic mixing. *J. Appl. Polym. Sci.* **2005**, *96*, 1557–1563. [[CrossRef](#)]
36. Park, B.D.; Balatinecz, J.J. A Comparison of Compounding Processes for Wood-Fiber/Thermoplastic Composites. *Polymer* **2004**, *18*, 425–431. [[CrossRef](#)]
37. López, J.P.; Méndez, J.A.; Espinach, F.X.; Julián, F.; Mutjé, P.; Vilaseca, F. Tensile strength characteristics of polypropylene composites reinforced with stone groundwood fibers from softwood. *BioResources* **2012**, *7*, 3188–3200. [[CrossRef](#)]
38. Suzuki, K.; Okumura, H.; Kitagawa, K.; Sato, S.; Nakagaito, A.N.; Yano, H. Development of continuous process enabling nanofibrillation of pulp and melt compounding. *Cellulose* **2013**, *20*, 201–210. [[CrossRef](#)]
39. Ho, T.T.T.; Abe, K.; Zimmermann, T.; Yano, H. Nanofibrillation of pulp fibers by twin-screw extrusion. *Cellulose* **2015**, *22*, 421–433. [[CrossRef](#)]
40. Uetani, K.; Yano, H. Nanofibrillation of wood pulp using a high-speed blender. *Biomacromolecules* **2011**, *12*, 348–353. [[CrossRef](#)]
41. Kamada, A.; Mittal, N.; Söderberg, L.D.; Ingverud, T.; Ohm, W.; Roth, S.V.; Lundell, F.; Lendel, C. Flow-Assisted assembly of nanostructured protein microfibers. *Proc. Natl. Acad. Sci. USA* **2017**, *114*, 1232–1237. [[CrossRef](#)]
42. Mittal, N.; Ansari, F.; Gowda Krishne, V.; Brouzet, C.; Chen, P.; Larsson, P.T.; Roth, S.V.; Lundell, F.; Wågberg, L.; Kotov, N.A.; et al. Multiscale Control of Nanocellulose Assembly: Transferring Remarkable Nanoscale Fibril Mechanics to Macroscale Fibers. *ACS Nano* **2018**, *12*, 6378–6388. [[CrossRef](#)]
43. Hakansson, K.M.O.; Lundell, F.; Prah-Wittberg, L.; Söderberg, L.D. Nanofibril Alignment in Flow Focusing: Measurements and Calculations. *J. Phys. Chem. B* **2016**, *120*, 6674–6686. [[CrossRef](#)] [[PubMed](#)]
44. Kiriya, D.; Kawano, R.; Onoe, H.; Takeuchi, S. Microfluidic control of the internal morphology in nanofiber-based macroscopic cables. *Angew. Chemie-Int. Ed.* **2012**, *51*, 7942–7947. [[CrossRef](#)] [[PubMed](#)]
45. Santos, P.A.; Spinacé, M.A.S.; Feroselli, K.K.G.; De Paoli, M.A. Polyamide-6/vegetal fiber composite prepared by extrusion and injection molding. *Compos. Part A Appl. Sci. Manuf.* **2007**, *38*, 2404–2411. [[CrossRef](#)]
46. Fernandes, F.C.; Gadioli, R.; Yassitepe, E.; de Paoli, M.A. Polyamide-6 composites reinforced with cellulose fibers and fabricated by extrusion: Effect of fiber bleaching on mechanical properties and stability. *Polym. Compos.* **2017**, *38*, 299–308. [[CrossRef](#)]
47. Ku, H.; Wang, H.; Pattarachaiyakoop, N.; Trada, M. A review on the tensile properties of natural fiber reinforced polymer composites. *Compos. Part B Eng.* **2011**, *42*, 856–873. [[CrossRef](#)]
48. Faruk, O.; Bledzki, A.K.; Fink, H.P.; Sain, M. Progress report on natural fiber reinforced composites. *Macromol. Mater. Eng.* **2014**, *299*, 9–26. [[CrossRef](#)]
49. Feldmann, M.; Bledzki, A.K. Bio-based polyamides reinforced with cellulosic fibres—Processing and properties. *Compos. Sci. Technol.* **2014**, *100*, 113–120. [[CrossRef](#)]
50. Aydemir, D.; Kiziltas, A.; Erbas Kiziltas, E.; Gardner, D.J.; Gunduz, G. Heat treated wood-nylon 6 composites. *Compos. Part B Eng.* **2015**, *68*, 414–423. [[CrossRef](#)]
51. Tajvidi, M.; Feizmand, M.; Falk, R.H.; Felton, C. Effect of cellulose fiber reinforcement on the temperature dependent mechanical performance of nylon 6. *J. Reinf. Plast. Compos.* **2009**, *28*, 2781–2790. [[CrossRef](#)]
52. Xiaolin, X. Cellulose Fiber Reinforced Nylon 6 or Nylon 66. Ph.D. Thesis, Georgia Institute of Technology, Atlanta, GA, USA, December 2008.
53. Elsabbagh, A.; Steuernagel, L.; Ring, J. Natural Fibre/PA6 composites with flame retardance properties: Extrusion and characterisation. *Compos. Part B Eng.* **2017**, *108*, 325–333. [[CrossRef](#)]

54. Peng, Y.; Gardner, D.J.; Han, Y. Drying cellulose nanofibrils: In search of a suitable method. *Cellulose* **2012**, *19*, 91–102. [[CrossRef](#)]
55. Peng, Y.; Gardner, D.J.; Han, Y.; Kiziltas, A.; Cai, Z.; Tshabalala, M.A. Influence of drying method on the material properties of nanocellulose I: Thermostability and crystallinity. *Cellulose* **2013**, *20*, 2379–2392. [[CrossRef](#)]



© 2020 by the authors. Licensee MDPI, Basel, Switzerland. This article is an open access article distributed under the terms and conditions of the Creative Commons Attribution (CC BY) license (<http://creativecommons.org/licenses/by/4.0/>).

A.2 Article II

Sridhara, P.K. and Vilaseca, F., 2021. High Performance PA 6/Cellulose Nanocomposites in the Interest of Industrial Scale Melt Processing. *Polymers*, 13(9), p.1495. DOI: 10.3390/polym13091495

Journal Impact Factor: 4.329 (2020), Journal Rank: JCR – Q1 (18/88 in Polymer Science)

Article

High Performance PA 6/Cellulose Nanocomposites in the Interest of Industrial Scale Melt Processing

Pruthvi K. Sridhara  and Fabiola Vilaseca *

Advanced Biomaterials and Nanotechnology, Department of Chemical Engineering, University of Girona, 17003 Girona, Spain; pruthvi.sridhara@udg.edu

* Correspondence: fabiola.vilaseca@udg.edu; Tel.: +34-667-292-597

Abstract: On an industrial scale, it is a challenge to achieve cellulose based nanocomposites due to dispersion issues and high process temperatures sensitivity. The current study describes methods to develop mechanically strong and thermally stable polyamide 6 (PA 6) and cellulose nanofibers (CNF) composites capable of tolerating high processing temperatures. With PA 6 being a very technical polymer matrix to be reinforced with CNF, good dispersion can be achieved with a high speed kinetic mixer and also shield the CNF from excess thermal degradation by implementing extremely short processing time. This paper presents an industrially feasible method to produce PA 6/CNF nanocomposites with high CNF composition processed by a high speed kinetic mixer (GELIMAT[®]) followed by compression molding to obtain a homogenous and thermally stable nanocomposites aimed at high performance applications. PA 6 was reinforced with three different wt % formulations (5, 15 and 25 wt %) of cellulose nanofibers. The resulting nanocomposites exhibited significant increase in Young's modulus and ultimate strength with CNF content, owing to the effective melt processing and the surface charge density of the CNF, which necessitated the dispersion. The thermal stability and polymer crystallinity with respect to CNF composition for the PA 6/CNF nanocomposites were examined by TGA and DSC analysis. Rheology studies indicated that viscosity of the composites increased with increase in CNF composition. Overall, this work demonstrates industrially viable manufacturing processes to fabricate high performance PA 6/CNF nanocomposites.

Keywords: polyamide 6; cellulose nanofibers; nanocomposites; melt processing; mechanical properties; thermal properties



Citation: Sridhara, P.K.; Vilaseca, F. High Performance PA 6/Cellulose Nanocomposites in the Interest of Industrial Scale Melt Processing. *Polymers* **2021**, *13*, 1495. <https://doi.org/10.3390/polym13091495>

Academic Editor: Giulia Fredi

Received: 20 April 2021

Accepted: 3 May 2021

Published: 6 May 2021

Publisher's Note: MDPI stays neutral with regard to jurisdictional claims in published maps and institutional affiliations.



Copyright: © 2021 by the authors. Licensee MDPI, Basel, Switzerland. This article is an open access article distributed under the terms and conditions of the Creative Commons Attribution (CC BY) license (<https://creativecommons.org/licenses/by/4.0/>).

1. Introduction

Polyamide 6/nylon 6 (PA 6) is an engineering thermoplastic boasting good mechanical integrity, thermal properties, chemical and dimensional stability. In recent years, composites of PA 6 have gained tremendous interest in high performance and light weight replacement for metals and rubbers in the industrial sector especially in the automotive industry [1]. The performance of PA 6 can be further enhanced by reinforcing the polymer matrix with fibrous or crystalline filler [2]. Industrial interest has shifted towards eco-friendly and economic means to produce greener materials to reduce the impact of carbon footprint on the environment. Incorporating natural fibers to polymeric matrixes not only generates lower CO₂ emission, but also increases the biodegradability of the material [3]. Commonly used synthetic fibers such as glass and carbon fibers possess higher density than natural fibers, comparably to such synthetic fibers, natural fibers reinforcement can provide high specific mechanical properties to the polymer composites [4]. Further studies have revealed that incorporating natural fiber-fillers with their dimension in nanoscale, significantly improves the mechanical properties of neat polymers due to their high specific strength and high aspect ratio [5].

With cellulose being one of the most abundant natural polymer, reinforcing PA 6 with cellulosic nanofillers is an effective way to develop new composites, further widening the

potential of applications for polymeric composites [6]. There are two major families among nanocellulose: cellulose nanocrystals (CNC) and cellulose nanofibers (CNF). CNF are easily produced with high yield when compared to CNCs and, generally, CNF are more thermally stable than CNC when they are purified thoroughly from lignin and hemicellulose, which are thermally volatile constituents [7]. Enzymatically treatment of cellulose is one of the simplest and ecofriendly ways to defibrillate and extract CNF [8]. These CNF embody a swirled and flexible characteristic, and typically having their lengths in the range of 0.7–2 μm and diameters of around 5–30 nm, with majority of nanofibers with diameters within 15–30 nm [9,10]. As PA 6 and CNF are polar materials and are hydrophilic in nature, good interaction is formed between them making them compatible with each other [11].

CNF have a young's modulus of 24 GPa and tensile strength of 320 MPa [12]. These mechanical properties can be imparted to the end-use composite by dispersing them into polymer matrix by various processing methods. However, there are several challenges in reinforcing CNF with PA 6 matrix given the processing temperatures of PA 6 are close to the degradation onset temperatures of the CNF. On an industrial scale, it is important to optimize processing methods and modify materials if necessary, to produce high performance nanocomposites and to improve the scalability of the overall production. While processes like solvent casting have been successful in negating the degradation effect by not involving high temperatures, solvent casting process is most suited to small-scale or lab conditions and besides, extensive use of solvents generates chemical wastes making it not ecofriendly [13,14]. Conventional methods like melt processing, injection molding and compressing molding have already been well established in the current day industry. To this day, many researchers have been successful in melt processing cellulose composites with polyethylene (PE), polypropylene (PP), polyvinyl alcohol (PVA) and polylactic acid (PLA) [15]. Additionally, previous works within our group have successfully melt processed PA 6 composites with well dispersed microfibrillated/pulp fibers with improved mechanical properties and without compromising on thermal stability [16,17].

The obstacles of thermal stability can be overcome and good dispersion of CNF within the PA 6 matrix can be achieved by melt compounding with a high speed thermo-kinetic mixer such as a GELIMAT[®]. The schematic of a Gelimat mixing chamber is shown in Figure 1 [18]. The process involves exerting high shear rates on the materials, which increase the temperature of the compounding mixture and a final homogenous compound with excellent dispersion can be obtained [19]. Materials can be compounded in extremely less time (<60 s), therefore, the CNF are exposed to processing temperatures for a shorter period, thus, preserving thermal stability. Compared to twin screw extruder and Brabender[®], the Gelimat produces well dispersed and distributed composites [20]. Moreover, homogenous compounds can be obtained in a single cycle, whereas, similar levels of dispersion require two or three passes in an extruder. In our study, we push forward the scalable industrial method to produce high performance PA 6/CNF nanocomposites with high weight fraction of CNF. To further improve scalability and due to the matrix–nanofiber interface, no coupling and/or dispersing agent was used, which was used in some studies to improve processability [21]. Nanocomposite samples were produced using compression molding and characterized for tensile and thermal properties. Rheological behavior and water absorption was analyzed with the interest for industrial scale processing methods.

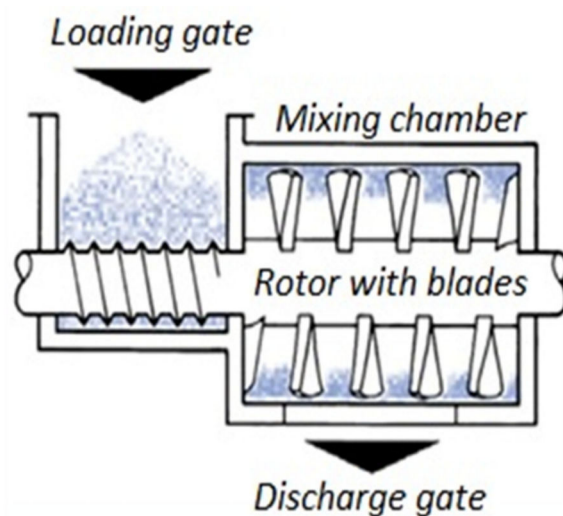


Figure 1. Schematic of GELIMAT® feeding and mixing chamber [18].

2. Materials and Methods

The PA 6 (density $\rho = 1.14 \text{ g/cm}^3$) was obtained commercially in pellet form from Radici Plastics Iberica SL (Barcelona, Spain). The PA 6 pellets were then powdered from Powder Plastics Europe SL (Valls, Spain) and the powdered PA 6 was passed through a 1000-micron sieve. The major particle size distribution of the powdered PA 6 ranged between 150 and 800 microns. For the rest of this paper, powdered PA 6 will be denoted as just PA 6. Cellulose was originally obtained in form of pulp sheets from Domsjö Fabriker (Örnsköldsvik, Sweden). These sheets were of high cellulose content (>97% pure cellulose) primarily derived from softwood. To prepare the CNF, an endoglucanase enzyme namely Novozyme 476 obtained from Novozymes® AS (Copenhagen, Denmark) was utilized to expedite the disintegration of cellulose pulp. The Schematic of the complete composites preparation process is depicted in Figure 2.

2.1. Processing of PA 6/CNF Nanocomposites

2.1.1. Preparation of CNF

The cellulose pulp was subjected to enzymatic treatment/disintegration as described by Heriksson et al. [8]. Initially, the cellulose pulp was broken up in distilled water and was amalgamated in a disintegrator (Papelquimia SA, Besalu, Spain) to form 3 wt % cellulose pulp fibers suspension. The cellulose pulp fibers were then mechanically subjected to a PFI mill (IDM Test SL, San Sebastian, Spain) at 1000 revolutions to increase the fibers swelling in water and provide adequate accessibility for the enzyme. The enzymatic treatment was carried out by dispersing the 3 wt % pulp fiber in 50 mM tris(hydroxymethyl)aminomethane/HCl buffer with pH 7 and 0.02 wt % enzyme. The fibers were incubated for 2 h at 50 °C and later washed on a Büchner funnel. This was followed by keeping the fibers at 80 °C for 30 min to stop the enzyme activity and was washed again. Additionally, the fibers were again subjected to the PFI mill at 4000 revolutions. After the enzyme treatment, 1.5 wt % of pretreated fibers solution in distilled water was prepared and subjected to homogenization (Panda Plus, GEA Niro Soavi, Parma, Italy). The fibers were passed through the homogenizer 6 times and a consistent CNF gel was procured.

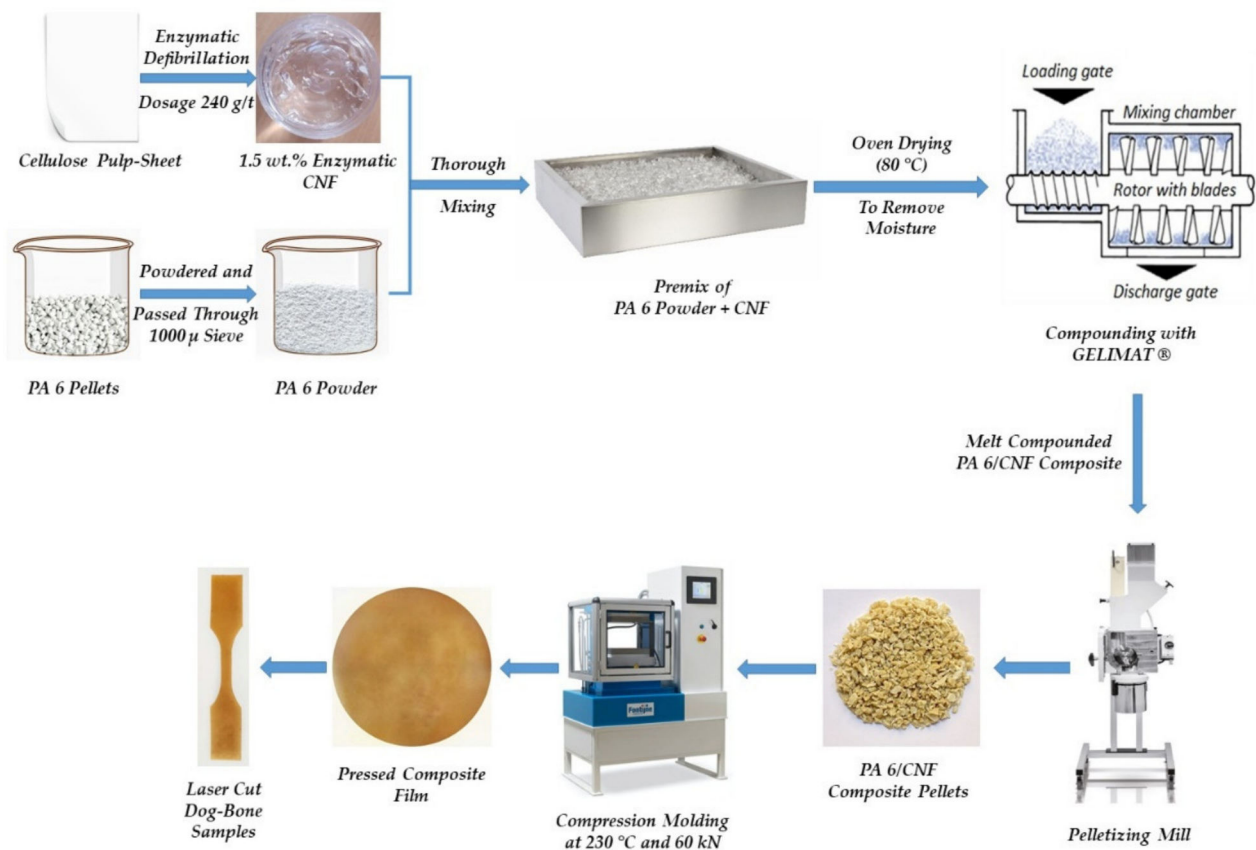


Figure 2. Schematic representation of the manufacture process for PA 6/CNF nanocomposites [18,22,23].

2.1.2. Melt Compounding

In order to prepare 5 wt %, 15 wt % and 25 wt % of PA 6/CNF nanocomposites, batches of PA 6 respectively were dried for 8 h in an 80 °C oven to remove any moisture content. Each batch of dry PA 6 was thoroughly mixed with the respective amount of CNF gel to obtain the corresponding CNF wt % formulation of the nanocomposite. These mixtures were then dried in a 60 °C oven until all the gel-moisture content was removed. The dry PA 6/CNF mixture was introduced into the Gelimat[®] (Draiswerke G5 S, Ramsey, NJ, USA) at a rotor speed of 300 rpm. The loading gate was shut and the rotor speed was increased to 2500 rpm. The action of the blades at such high speed allowed a mixture to reach melting temperature (220–230 °C) in less than 20 s. The completion of the compounding process was signified by the drop in current drawn by the rotor. Simultaneously, the discharge gate was opened and the compounded mixture was collected and cooled immediately using a cold bath. The compounding process was repeated to obtain the remaining formulations of the nanocomposites. Further, the compounded composite mixtures for all the formulations were produced into composite pellets respectively using a pelletizer (SM100, Retsch GmbH, Haan, Germany).

2.2. Characterization of PA 6/CNF Nanocomposites

2.2.1. Compression Molding

All the formulations of nanocomposites pellets obtained from the compounding process was compression molded into films using a laboratory hydraulic hot press (Fontijne Presses BV, Delft, The Netherlands) at 230 °C under a pressure of 60 kN for 10 min. Spacers with 0.5 mm thickness were positioned to control the thickness of the produced films. The obtained films were light brown in color and translucent with no optical signs of CNF aggregation. However, minute aggregation was observed in the 25 wt % formulation.

2.2.2. Mechanical Testing

PA 6/CNF nanocomposites were tensile tested using a 5 kN Instron[®] Type 1122 Test (Norwood, MA, USA) machine. Dog-bone shaped samples from the PA 6/CNF nanocomposites films were cut using a die as per ASTM D638 (Type V) specifications. The pressed dog-bone samples were tested under two parameters. Firstly, dry samples, where the dog-bone samples were dried in an 80 °C oven for 6 h prior to testing. Secondly, 48 h conditioned samples, where the samples were placed in a climatic chamber at 23 ± 2 °C and 50% ± 5% relative humidity for 48 h (ASTM D618 13) prior to testing. Tests were carried out at room temperature at a strain rate of 2 mm min⁻¹ and a gauge length of 30 mm. The thickness and width of the narrow section for each sample was measured using a digital micrometer (Starrett[®], Athol, MA, USA). Trials were repeated to establish statistical significance.

2.2.3. Conductometric and Polyelectrolyte Titration of CNF

The content of carboxyl groups of the CNFs was determined by conductometric titration as described by Saito et al. [22]. CNF was dispersed rigorously in deionized H₂O and 0.01 M HCl (Sigma Aldrich, Munich, Germany). The suspension was titrated with 0.5 M NaOH (Sigma Aldrich, Munich, Germany). Titration conductivity values were plotted against volume of NaOH added. The carboxyl content S (μMol/g) was calculated using Equation (1).

$$S = \frac{V_{NaOH} \cdot C_{NaOH}}{W_{CNF}} \cdot 10^6 \quad (1)$$

where V_{NaOH} is the added volume of NaOH, C_{NaOH} is the concentration of NaOH solution and W_{CNF} is the weight of dispersed CNF.

The surface charge of CNF was also characterized for cationic demand, which was determined by polyelectrolyte titration using a Mütek PCD04 (BTG SL, UK) charger analyzer. The titration was performed through surface adsorption of diallyldimethylammonium chloride, poly-DADMAC, (Sigma Aldrich, Munich, Germany, molecular weight: 107 kDa) and the excess was titrated with polyethenesodiumsulphonate, PES-Na, (BTG, Éclépens, Switzerland) an anionic standard polymer.

2.2.4. Rheology Study

The rheological behavior was studied using a melt flow indexer/MFI-type device (Ceast, Pianezza, Italy). Neat PA 6 and the compounded nanocomposite pellets were tested for MFI at 230 °C through a capillary (die) of specific diameter and length by pressure applied through dead weight M (kg) as per ASTM 1238-73. The geometrical dimensions of the MFI apparatus are: radius of the die $r = 1$ mm; radius of the heating cylinder $R = 4.75$ mm; length of the heating cylinder $L = 30$ mm (ISO 1133). The mass series was as follows: $M1-M2-M3.....M7$ (kg) = 1.2–2.16–3.8–5.0–7.16–10.0–12.16. For each mass used, five MFI values were measured for statistical significance.

Capillary rheological properties can be illustrated on a rheogram, which represents variation of dynamic viscosity μ (Pa s) versus shear rate γ (s⁻¹). To go from MFI (g/10 min) to viscosity, the equations governing the flow of fluids inside a capillary (die) was used [23].

The apparent shear rate γ depends on the volume flow rate Q (m³s⁻¹) and die radius r (m).

$$\gamma = \frac{4 \cdot Q}{\pi \cdot r^3} \quad (2)$$

The volume flow rate Q can be calculated using the MFI data and the respective hot density ρ (g cm⁻³) of the samples.

$$Q = \frac{600 \cdot MFI}{\rho \cdot t} \quad (3)$$

Hence,

$$\gamma = \frac{2400 \cdot MFI}{\pi \cdot r^3 \cdot \rho \cdot t} \quad (4)$$

The viscosity μ is defined as shear stress τ (Pa) divided by the shear rate γ . The shear stress τ depend on the pressure P exerted at die inlet, i.e., the force F exerted by the mass M placed on the MFI piston.

$$P = \frac{F}{\pi \cdot R^2} = \frac{M \cdot g}{\pi \cdot R^2} \quad (5)$$

Hence,

$$\tau = \frac{P \cdot F}{2 \cdot L} = \frac{M \cdot g \cdot r}{\pi \cdot R^2 \cdot 2 \cdot L} \quad (6)$$

The above Equations (4) and (6) are for Newtonian fluids. PA 6 and respective composite blends have non-Newtonian behavior. Therefore, the apparent shear rates were corrected using the Rabinowitsch shear rate correction [24]. A first realistic approach to the rheological behavior was presented by the power law symbolized by Oswald law (Equation (7)).

$$\tau_T = k \cdot \gamma_T^n \quad (7)$$

where τ_T is the true shear stress, k is a constant of the fluid and n is the flow index (pseudoplasticity index). To find out n , the curve $\text{Ln } \tau = f(\text{Ln } \gamma)$ was plotted from the calculated apparent stresses and shear rates obtained from the MFI data. With n being the slope and $\text{Ln } k$ the intercept, the necessary Rabinowitsch correction was performed for the apparent shear rate γ (Equation (8)).

$$\gamma_T = \frac{(3n + 1)}{4n} \cdot \gamma \quad (8)$$

where γ_T is the true shear rate, from which the true effective viscosity μ was calculated. Thus, the rheogram representing the rheological behavior of PA 6 and PA 6/CNF nanocomposites at 230 °C was obtained.

2.2.5. Water Absorption Study

Three dog-bone samples for each formulation were chosen to conduct periodic mass measurements when submerged in water over a 24-h period. The dry samples were weighed before placing them in distilled H₂O at room temperature. The samples were removed from the water and patted dry with Kimwipes® prior to weighing. Mass measurements were taken at 0 h, 0.5 h, 1 h, 3 h, 6 h, 12 h, 18 h and 24 h. The weight percentage change was calculated using Equation (9), where W_{wet} is the weight of sample after immersed in water and W_{dry} is the dry weight of the sample.

$$\text{percent change} = \frac{(W_{wet} - W_{dry})}{W_{dry}} \cdot 100 \quad (9)$$

The samples were allowed to gain mass until they reached an equilibrium state. The water uptake kinetics can be modelled analytically by using Fick's theory of dispersion. The diffusion coefficient D (m²s⁻¹) of the nanocomposite samples with respect to the ability of moisture/water to penetrate the samples was deduced from Fick's law. The diffusion coefficient was determined for shorter immersion time and thus, Fick's law is stated as in Equation (10). Where M_t (%) is the water uptake at a lower immersion time, M_∞ (%) is the maximum mass gained, L (m) is the thickness of the sample and time t (s).

$$\frac{M_t}{M_\infty} = 2 \cdot \left(\sqrt{\frac{D t}{\pi L^2}} \right) \quad (10)$$

2.2.6. Thermal Properties

Thermogravimetric analysis (TGA) was conducted using a Mettler Toledo TGA 851 equipment (Greifensee, Switzerland). The temperature ranged from 25 to 600 °C with a 10 °C/min heating rate. The tests were carried out by placing the samples in an open platinum pan within a nitrogen environment. All the results were recorded using the STAR^e thermal analysis software. Additionally, TGA at isothermal conditions (230 °C) for the CNF gel was performed to check for thermal stability of CNF at processing temperatures.

In addition to TGA, a differential scanning calorimeter (DSC) was performed with DSC Q2000 equipment (TA Instruments, New Castle, DE, USA). The DSC was run three times for each formulation and the dry samples ranging from 6 to 8 mg were placed in aluminum pans. The samples underwent a heating cycle from 30 to 260 °C with a heating rate of 10 °C/min. All the results were reported by a TA Universal Analysis software. The degree of crystallinity (χ_c) was calculated corresponding to the enthalpy of the melting endotherm using Equation (12), where ΔH_{sample} is the enthalpy of the melting endotherm of the sample from the heating cycle, $\Delta H_{polymer}$ is the melting enthalpy of PA 6 polymer in the sample, w_{CNF} is the weight fraction of the CNF in the sample and $\Delta H_{100\%}$ is the theoretical melting enthalpy of 100% crystalline PA6, which is equivalent to 230 J/g [25,26].

$$\Delta H_{polymer} = \Delta H_{sample} \cdot \left(\frac{1}{1 - \frac{w_{CNF}}{100}} \right) \quad (11)$$

$$\chi_c (\%) = \frac{\Delta H_{polymer}}{\Delta H_{100\%}} \cdot 100 \quad (12)$$

2.2.7. Scanning Electron Microscopy (SEM)

The morphology of fractured samples due to elongation from tensile testing was characterized under a S4800 electron microscope (Hitachi, Ibaraki, Japan). The 5 wt % and 25 wt % formulations of the PA 6/CNF nanocomposites were analyzed at an accelerated voltage of 15 kV to distinguish CNF and PA 6 matrix. The fractured surfaces were coated with a thin layer of gold with the help of a sputter prior to observation.

3. Results and Discussion

Samples were made for three different formulations of CNF composition: 5 wt %, 15 wt % and 25 wt %. The PA 6/CNF pellets and the respective homogeneous films obtained by Gelimat compounding and compression molding are shown in Figure 3. The processes resulted in a color change of slight brownish color and the films showed no optical aggregation of CNF. This discoloration of the pressed composite samples was expected due to the onset thermal degradation temperature of the CNF. This degradation is slow, mild and is mainly attributed to the dehydration of composite and formation of peroxides, which may catalyze the cellulose degradation [27,28]. However, our previous experience with pulp fiber composites suggest that it does not affect the mechanical integrity [16].

Mechanical properties of nanocomposites depend on many parameters like weight fraction of CNF, degree of dispersion of CNF and the size of the nanofibers. The mechanical behavior of the PA 6/CNF nanocomposites increased with the increase in CNF content with respect to neat PA 6. The best result for ultimate tensile strength (77.7 MPa) and modulus (5.6 GPa) was obtained for the 25 wt % formulation. All the data from the tensile tests are summarized in Table 1.

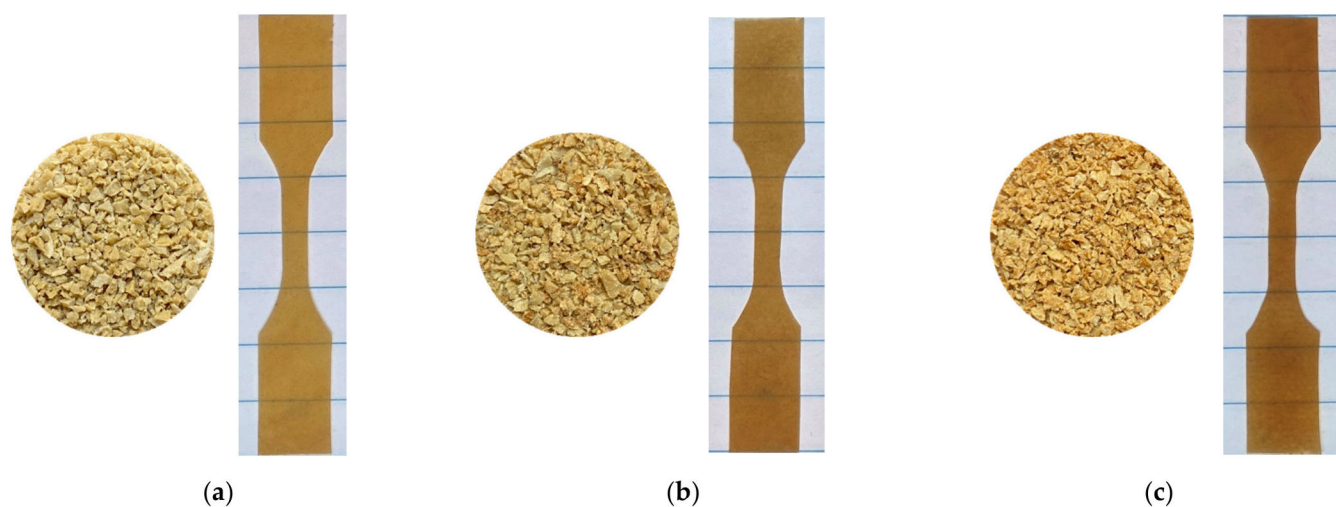


Figure 3. PA 6/CNF nanocomposites pellets and dog-bone samples for (a) 5 wt %, (b) 15 wt % and (c) 25 wt % formulations.

Table 1. Summary of tensile test results of dry and 48 h conditioned samples for neat PA 6 and all formulations of nanocomposites.

CNF Content (wt %)	Mean Thickness (mm)		Ultimate Strength (MPa)		Elastic Modulus (GPa)		Strain at Break (%)	
	Dry	48 h CC	Dry	48 h CC	Dry	48 h CC	Dry	48 h CC
Neat PA 6	0.46 ± 0.05	0.48 ± 0.03	50.8 ± 0.62	47.8 ± 1.1	2.2 ± 0.1	2.1 ± 0.3	9.8 ± 5.4	10.4 ± 5.6
5	0.35 ± 0.05	0.29 ± 0.06	56.5 ± 1.1	53.6 ± 0.7	3.9 ± 0.7	3.5 ± 0.7	2.3 ± 0.6	2.5 ± 0.5
15	0.30 ± 0.04	0.25 ± 0.08	65.6 ± 1.5	61.7 ± 2.1	4.8 ± 0.6	4.3 ± 0.3	1.6 ± 0.4	1.8 ± 0.2
25	0.25 ± 0.04	0.31 ± 0.03	77.7 ± 2.01	73.2 ± 2.5	5.6 ± 0.1	5.4 ± 0.4	1.2 ± 0.3	1.3 ± 0.1

The improvement in the mechanical properties are directly correlated to dispersion and distribution of CNF within the PA 6 matrix [29]. Additionally, the processing methods did not compromise on the thermal stability and the melt compounding improved the homogeneity of the nanocomposites. The compatibility of CNF-PA 6 and the direct melt mixing of the composites allowed us to suppress the use any coupling agent and dispersive agent. This increases the scalability of the entire process, which is important at an industrial level. The reduction of deformation (strain) at break for the nanocomposites indicated good wetting and interaction between the CNF and PA 6 matrix, which allowed effective stress transfer and improved the stiffness [30]. Some studies on polyamide cellulose composites indicated improvement in mechanical properties for lower nanocellulose concentrations, but for higher concentration the tensile properties diminished. This could be due to excessive nanofiller–nanofiller interaction leading to poor reinforcement and embrittlement of the overall sample [31]. Another reason could be that increased filler content makes the polymer difficult to penetrate the space between the nanofillers resulting in poor wetting and hindering stress transfer through the interface [32]. Overall, for such high fiber weight fraction nanocomposites, the CNF exists as a 3D percolated network due to the hydroxyl groups on CNF resulting in hydrogen bonding between them [33]. Our findings support the fact that high performance, high cellulose weight fraction composites can be obtained by optimizing processing methods, which means our processing method was successful in penetrating PA 6 in between the percolated network of CNF. Hence, is accountable for the improvement in mechanical properties of the nanocomposites.

The enhanced mechanical properties are directly related to how well the CNF is dispersed within the PA 6 matrix. The dispersibility is indeed dependent on the surface charge density of the CNF, which governs the electrostatic repulsion between the individual

fibers [34]. Polyelectrolyte and conductimetric titration revealed the cationic demand of 258 $\mu\text{eq. g/g}$ and the carboxyl group content of 54 $\mu\text{mol COOH/g}$, respectively, for the current enzymatic CNF. This suggests that amount of electrostatic repulsion between the CNFs is sufficient to be well dispersed within the PA 6 matrix, which is further corroborated by improvement in tensile properties [35]. Nevertheless, shorter chained polyamides such as PA 6 possess higher frequency of amide groups resulting in hydrophilicity and thus, leading to stronger interactions with CNF.

Capillary rheological properties are important to optimize the processing conditions and to know the rheological behavior of the nanocomposites with respect to the addition of CNF content. A rheogram representing variation of dynamic viscosity (μ) versus shear rate ($\dot{\gamma}_T$) can be obtained without having to use a sophisticated rheometer. We used an MFI type device to measure the melt flow indices of the samples with 5–6 different masses. By using different sets of masses, we were able to vary the shear stress. Subsequently, applying simple rheological equations, we traced a rheogram for the samples at 230 °C (Figure 4). The MFI values for the samples can be found in the Supplementary Materials. By studying the flow behavior through a capillary, relevant processing shear rates were characterized to confirm the process-ability of these nanocomposites. In addition, capillary rheological characterization by applied pressure closely resembles injection molding process [36]. All the samples displayed similar shear thinning behavior. PA 6/CNF nanocomposites behave as pseudoplastic fluids (non-Newtonian behavior) confirmed by decreasing viscosity with increasing shear rates. Moreover, pseudoplastic behavior is enhanced by the addition of CNF. For the nanocomposite samples, the viscosities increased with increase in CNF content with the highest viscosity seen for the 25 wt % formulation. At lower formulations (5 wt %), the CNF for the most part was like free particles and the nanocomposite melt had higher mobility. At higher formulations (15 and 25 wt %), the CNF disturbs the normal flow of nanocomposite melts and hinders the mobility causing high shear stresses, which is attributed to the hydrodynamic effect [37]. There was only a slight increase in viscosity for the nanocomposites samples when compared to neat PA 6, maybe due to the processing method employed and the aspect ratio of the CNF. This suggests the CNF was well dispersed and the presence of a percolating network [38]. Furthermore, rheological behavior is beneficial for process optimization and adjust processing conditions to improve the productivity.

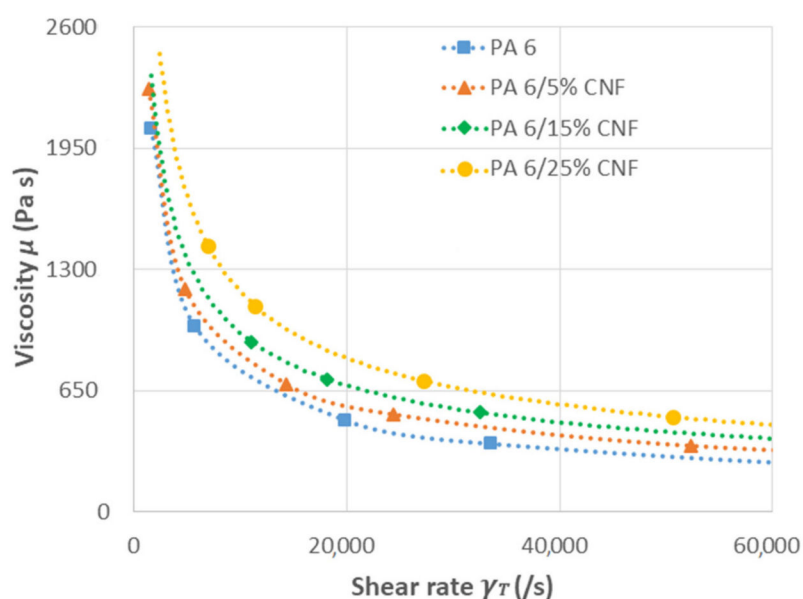


Figure 4. Rheological behavior of neat PA 6 and PA 6/CNF nanocomposites.

Further, water uptake study was carried out gravimetrically over a 24-h period. Mass measurements were noted periodically at 0 h, 0.5 h, 1 h, 3 h, 6 h, 12 h, 18 h and 24 h to determine the water absorption and associate it with the mechanical performance of the nanocomposite samples. In our case, two main interactions can be conjectured. The interaction between the water molecules and the amide groups of the PA 6. Then, the interaction of water molecules with the hydrophilic CNF. With the former dominating the absorption process in nanocomposite samples as the water uptake for nanocomposite samples decreased as function of CNF content but remained lower than the neat PA 6 (Figure 5). This is due to the strong hydrogen bonds between CNF and PA 6 along with the CNF–CNF interaction which are competing with water [39]. To study the influence of moisture on the mechanical properties, tensile samples were moisture conditioned for 48 h in a climatic chamber at 23 °C and relative humidity 50% prior to testing. From the Table 1, all the conditioned samples (48 h CC) showed reduced tensile modulus and strength. The reduction of modulus in the presence of moisture is common to most polyamides due to the plasticizing effect of water molecules on polyamides [40]. T_g for moisture conditioned PA 6 can decrease to room temperature and below, as water molecules interfere with hydrogen bonds between the polymer chain increasing the chain mobility. The reduced T_g causes a strong reduction of the amorphous modulus in the presence of moisture leading to decrease in the semicrystalline polymer [41]. Additionally, the reduction of modulus of matrix results in the modulus reduction of the nanocomposites. With increased mobility due to moisture conditioning, the yield stress also decreases and the deformation at break increases. Hence, moisture is a key factor affecting processing and final performance for PA 6/CNF nanocomposites.

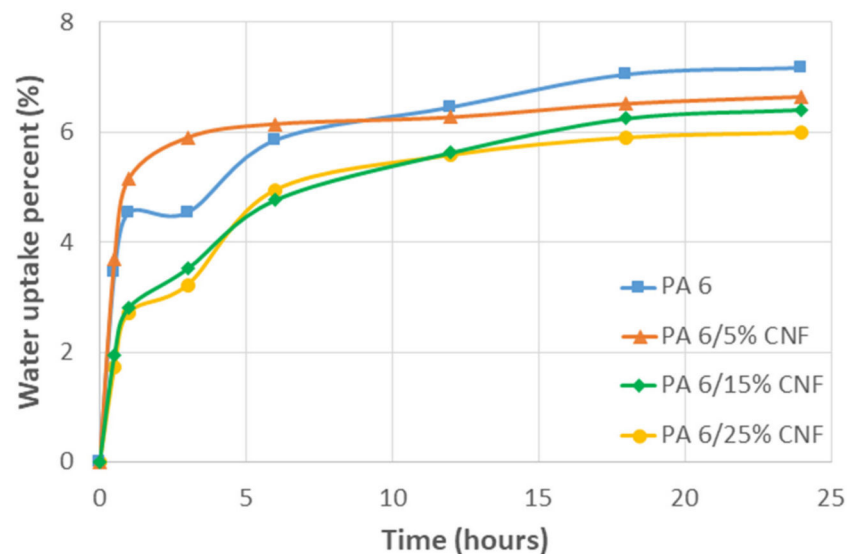


Figure 5. Water absorption percent versus time for neat PA 6 and PA 6/CNF nanocomposites at room temperature.

Fick's law was used to calculate diffusion coefficient D at lower times of immersion, i.e., when $M_t/M_\infty = 0.5$. The diffusion coefficient for all the samples is summarized in Table 2. It was observed that diffusion coefficient decreased as the amount of CNF increased with 25 wt % formulation showing the least D value. The lower D values can be related to the lower mobility of PA 6 chains inhibited by CNF reinforcement. Nevertheless, hydrogen bonding between the fibers and the PA 6 matrix can also have a negative effect on the diffusion of water through the composite samples [42]. The M_∞ values for nanocomposite samples were reached quicker when compared to neat PA 6 due to lower diffusion coefficients of the samples and the values remained below that of neat PA 6.

Table 2. Diffusion coefficient at 23 °C for PA 6/CNF nanocomposites.

CNF Content (wt %)	M_{∞} (%)	$D \times 10^{-9}$ (m ² s ⁻¹)
Neat PA 6	7.2	6.5
5	6.8	3.2
15	6.6	0.6
25	6.1	0.5

Thermogravimetric analysis (TGA) was conducted to determine the thermal behavior of nanocomposites and compare it with the neat samples. Thermograms indicating TGA curves and DTG curves for all the samples are shown in Figure 6. TGA plot revealed the region of degradation (Figure 6a) and moreover, elucidated the temperature range for processing the nanocomposites. The initial mass loss within the temperature range of 60–110 °C is attributed to the evaporation of water from the samples. This loss of water is important because water acts as an auto accelerator in the degradation process [27]. For temperatures above 300 °C, degradation of cellulosic materials kicks off giving away combustible volatiles such as methanol, acetic acid acetaldehyde and propenal. These volatiles components increase the rate of decomposition in the nanocomposites [43]. For the nanocomposites, the thermal stability decreased mildly with an increase in CNF content. The CNF char residue for the samples lied between the range of 2–4%. From the first derivative of TG (Figure 6b), the DTG thermal bands were obtained at 460 °C for neat PA 6. In our case, a maximum temperature of 230 °C was used during the processing of nanocomposites, thus avoiding excessive thermal degradation of CNF.

The TGA was performed for the enzymatic CNF gel (1.5 wt % consistency) by heating the sample in an aluminum pan from 30 to 230 °C at a heating rate of 50 °C/min. At 4 min 230 °C was reached and the CNF was checked for thermal degradation at isothermal conditions for 15 min. The TGA curve for CNF at isothermal conditions (230 °C) is shown in Figure 6c. The initial drop in the TGA curve is due to the loss of water from the CNF gel. The remaining pure CNF does not experience any thermal degradation at the processing temperature. This indicates that the thermal stability of the CNF was not compromised at a processing temperature of 230 °C for this time.

DSC analysis was conducted to recognize the effect of CNF content on the melting behavior and crystallinity of PA 6 matrix. Single, well defined endothermic peaks were obtained for all samples and the DSC thermogram for the heating cycle is shown in Figure 7. The values of glass transition temperature (T_g), melting temperature (T_m) and corresponding enthalpies (ΔH) are summarized in Table 3, according to Equations (11) and (12) in the experimental section.

Table 3. Thermal properties of neat PA 6 and PA 6/CNF nanocomposites.

CNF Content (wt %)	T_g (°C)	T_m (°C)	$\Delta H_{polymer}$ (J/g)	χ_c (%)
Neat PA 6	51.6	221.96	72.1	31.4
5	53.5	221.32	60.49	26.3
15	54.7	220.91	59.81	26.0
25	55.4	220.69	57.12	24.8

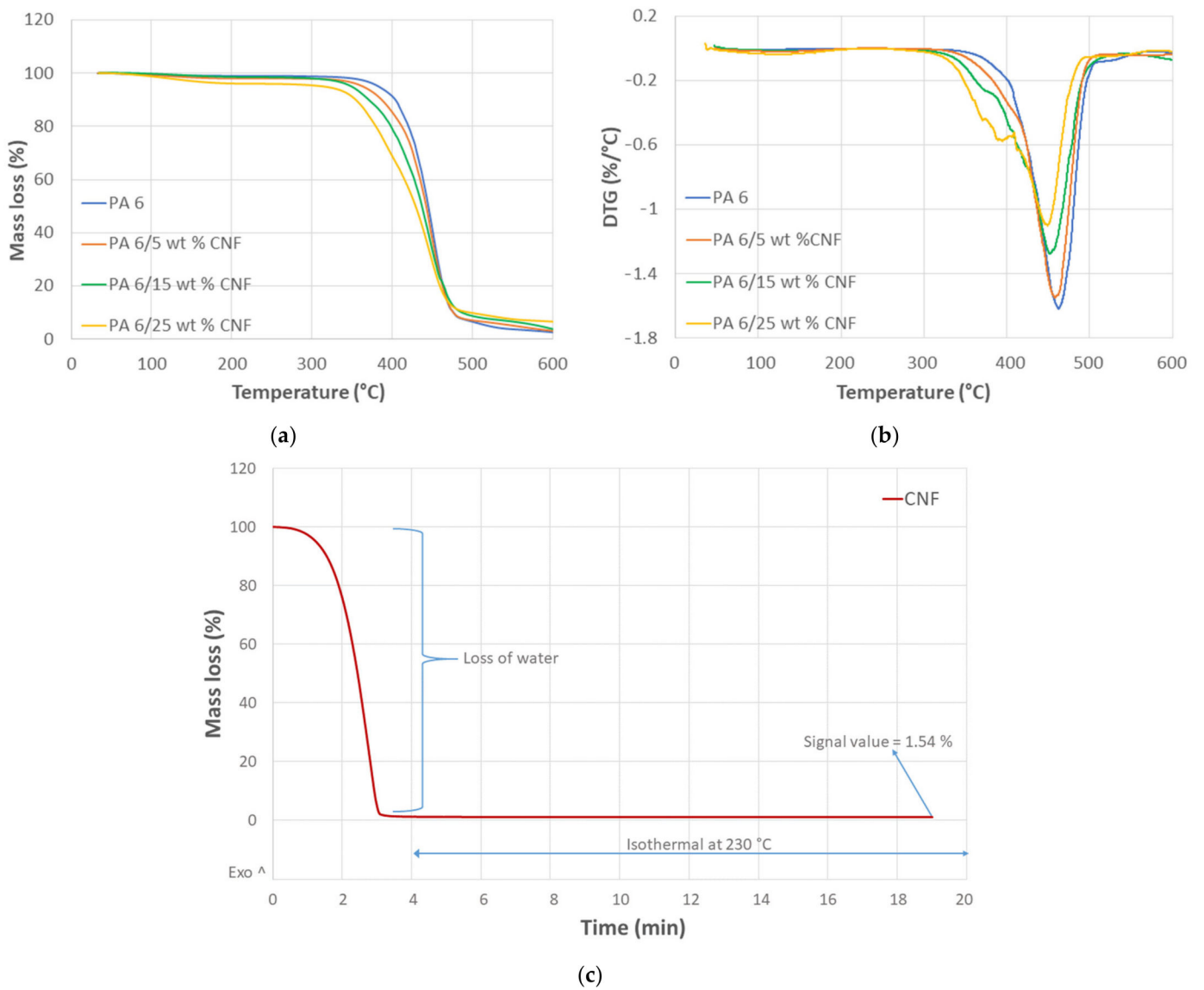


Figure 6. Thermograms, (a) TGA, (b) DTG for neat PA 6 and PA 6/CNF nanocomposites and (c) TGA of CNF gel at isothermal conditions at 230 °C.

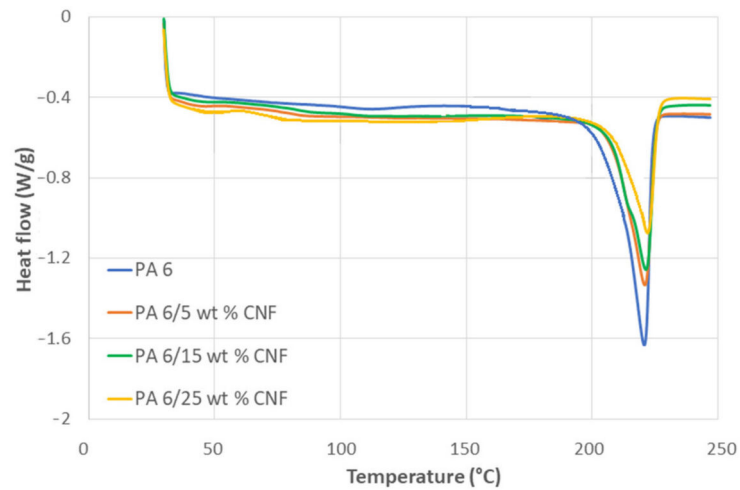


Figure 7. DSC thermogram, heating cycle for neat PA 6 and PA 6/CNF nanocomposites.

The DSC measurements indicate that the glass transition for the nanocomposite samples occurred at a slightly higher temperature when compared to neat PA 6. Additionally, the glass transition temperature increased with addition of CNF content. This was attributed to the strong interactions between polar amide groups of PA 6 and hydroxyl groups of CNF, thus reducing the segmental mobility of the nanocomposite structure [44]. The steady increase in T_g also indicated that the CNF was well dispersed in the PA 6 matrix [45]. The melting point of the neat PA 6 from the endothermic melting peak was detected at 221.96 °C, which can be associated to the α -form crystals of PA 6 [46]. There was no significant influence on the melting point of the nanocomposite samples as the changes in T_m was minuscule. The T_m for all samples were between 220 and 222 °C. The degree of crystallinity of the nanocomposite samples reduced with the addition of CNF. The crystallinity of PA 6 was 31.4%, while the crystallinity for the 25 wt % formulation was 24.8%. Identical decrease in crystallinity was observed for PA 6 nanocomposites containing microcrystalline cellulose and nanoclay [47,48]. The decrease in the crystallinity for nanocomposite samples is attributed to the vast surface on nanofillers, and the effect on the mobility of chains of polymer matrix. In some previous study, CNF acted as nucleating sites for crystallization [49]. The nucleating effect significantly contributes to the formation of transcrystalline layers around nanofillers thus, resulting in increase in crystallinity [50]. Nevertheless, the addition of nanofillers constrains the mobility of polymer chains hindering the crystal growth [45]. Thereby, decreasing the degree of crystallinity was the prevailing factor in our case.

The morphology of 5 wt % and 25 wt % formulations samples were observed under electron microscope. The SEM micrographs of the fractured surfaces for the nanocomposite samples are shown in Figure 8. The distribution of CNF appeared to be homogenous within the in-plane layers of the fractured samples with very few voids and no agglomerations in Figure 8(i),(iv). The fractured surfaces of the nanocomposite samples were almost identical to all formulations. The CNF show good adhesion to the PA 6 matrix and the interface bonding regions are observed in Figure 8(ii),(v). The morphology of fractured surfaces was formed under tension. Hence, the polymer strands had a fiber like shape, which were broken at some point during tensile elongation and were surrounded by CNF (Figure 8(v)). No major pull-out of the fibers was observed, but some broken fibers were found, which indicated suitable interface between PA 6 and CNF. Due to the hydrophilic nature of CNF and PA 6, the CNF demonstrated to be a suitable reinforcement to the polymer without problems of agglomeration. Under elongation, the different moduli of CNF and PA 6 created different deformation modes and the different strains were generated by the same load, which created stress concentration points at the interface of PA 6 and CNF. As this unmatched strain reached a magnitude of the interfacial adhesion between PA 6 and CNF, a sliding deformation occurs [31]. This sliding deformation is observed in Figure 8(vi). Moreover, the reinforcing effect was estimated by the effective stress transfer through interfacial adhesion, which was corroborated by the improved mechanical properties of the PA 6/CNF nanocomposites. Additionally, from the SEM micrographs, it was observed that the CNF integrity was unharmed, signifying no serious thermal degradation had taken place.

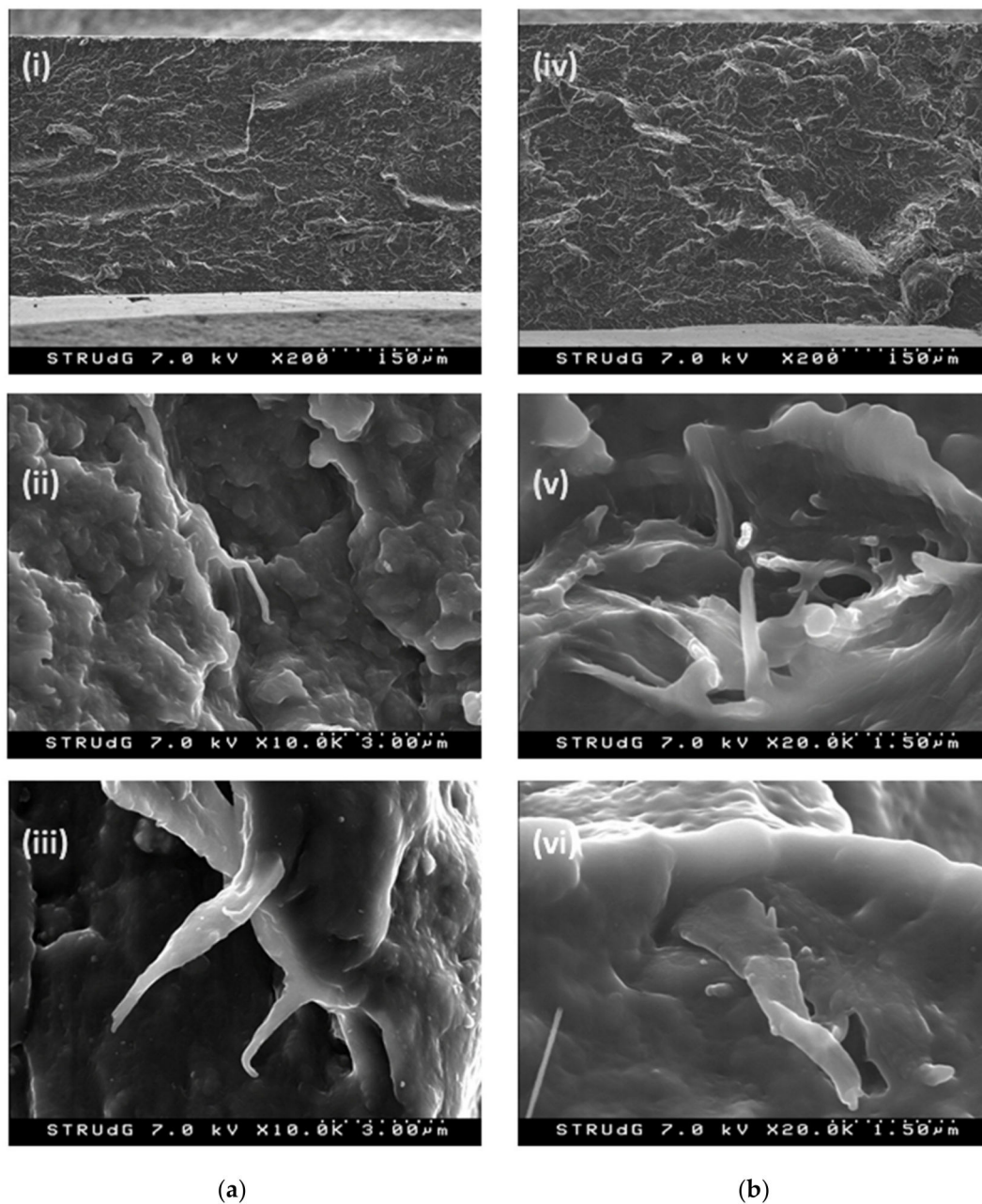


Figure 8. SEM micrographs of (a) 5 wt % and (b) 25 wt % PA/CNF nanocomposites.

4. Conclusions

PA 6 with its material properties has become a hot commodity in the automobile industry. There is tremendous emphasis on enhancing the mechanical properties using natural nanofillers. CNF with its high specific strength, aspect ratio and compatibility with PA 6 became a tangible ecofriendly and sustainable choice of reinforcement. To produce CNF reinforced polymer composites at an industrial level, successful incorporation of CNF within the polymer matrix is critical. This study corroborated that premixing and compounding via a thermokinetic mixer, PA 6/CNF nanocomposites with good dispersion could be obtained. Minimizing the exposure time of CNF to high processing temperatures was key in obtaining composites with the preserved integrity of CNF. Three different formulations: 5, 15 and 25 wt % formulations of PA 6/CNF nanocomposites were produced. The mechanical properties were improved with the addition of CNF, with 25 wt % formulation showing the highest tensile values, in Young's modulus and in tensile

strength. Water uptake study indicated that the water uptake reduced with the addition of CNF due to the hydrogen bonds between the PA 6 and CNF, which hindered the diffusion of water molecules. DSC analysis revealed that the degree of crystallinity reduced for the nanocomposites as the addition of CNF constrained the polymer chain hindering crystal growth. TGA expectedly implied that the thermal stability of nanocomposites reduced slightly for the nanocomposites. The capillary rheological study indicated that the dynamic viscosity increased with the addition of CNF. SEM micrographs showed homogenous interface morphology of fractured samples with hardly any fiber pull-out.

Further, producing samples with injection molding and optimizing processing methods will further increase the scalability of CNF/polymer composites on an industrial level. Ultimately, this study provides insightful prospects on sustainable materials and developing high performance nanocellulose reinforced polymer composites with high fiber weight fractions.

Supplementary Materials: The following are available online at <https://www.mdpi.com/article/10.3390/polym13091495/s1>, Table S1: melt flow indices (MFI) and melt volume flow rate (MVR) for neat PA 6 and PA 6/CNF nanocomposites at different masses.

Author Contributions: Conceptualization, P.K.S. and F.V.; methodology, P.K.S. and F.V.; validation, P.K.S. and F.V.; formal analysis, P.K.S.; investigation, P.K.S.; resources, P.K.S. and F.V.; data curation, P.K.S.; writing—original draft preparation, P.K.S.; writing—review and editing, P.K.S. and F.V.; visualization, P.K.S. and F.V.; supervision, F.V.; project administration, F.V.; funding acquisition, F.V. All authors have read and agreed to the published version of the manuscript.

Funding: This research was funded by the Wallenberg Wood Science Institute—KTH (KAW 2018.0451, Sweden) in Sweden, the by UdG grant (IFUdG 2017) in Spain, and by the Spanish Ministry of Science, Innovation and Universities (RTI 2018-102070-B-C22).

Institutional Review Board Statement: Not applicable.

Informed Consent Statement: Not applicable.

Data Availability Statement: The data presented in this study are available on request from the corresponding author.

Acknowledgments: The authors would like to thank the LEPAMAP group of the UdG for aiding in the use of laboratory equipment. The authors also want to thank Joan Pere López, Daniel Reyes Bautista and Albert Serra for helping to perform thermal analysis, SEM analysis and conductometric titration respectively. The Secretary of Chemical Engineering branch and the OITT of UdG are appreciated for their administrative support.

Conflicts of Interest: The authors declare no conflict of interest.

References

1. Annandarajah, C.; Langhorst, A.; Kiziltas, A.; Grewell, D.; Mielewski, D.; Montazami, R. Hybrid cellulose-glass fiber composites for automotive applications. *Materials* **2019**, *12*, 3189. [[CrossRef](#)]
2. Huber, T.; Müssig, J.; Curnow, O.; Pang, S.; Bickerton, S.; Staiger, M.P. A critical review of all-cellulose composites. *J. Mater. Sci.* **2012**, *47*, 1171–1186. [[CrossRef](#)]
3. Gholampour, A.; Ozbakkaloglu, T. A review of natural fiber composites: Properties, modification and processing techniques, characterization, applications. *J. Mater. Sci.* **2020**, *55*, 829–892. [[CrossRef](#)]
4. Corrêa, A.C.; de Moraes Teixeira, E.; Carmona, V.B.; Teodoro, K.B.R.; Ribeiro, C.; Mattoso, L.H.C.; Marconcini, J.M. Obtaining nanocomposites of polyamide 6 and cellulose whiskers via extrusion and injection molding. *Cellulose* **2014**, *21*, 311–322. [[CrossRef](#)]
5. Dufresne, A. Cellulose nanomaterials as green nanoreinforcements for polymer nanocomposites. *Philos. Trans. R. Soc. A Math. Phys. Eng. Sci.* **2018**, *376*. [[CrossRef](#)]
6. Boland, C.S.; De Kleine, R.; Keoleian, G.A.; Lee, E.C.; Kim, H.C.; Wallington, T.J. Life cycle impacts of natural fiber composites for automotive applications: Effects of renewable energy content and lightweighting. *J. Ind. Ecol.* **2016**, *20*, 179–189. [[CrossRef](#)]
7. Zimmermann, T.; Bordeanu, N.; Strub, E. Properties of nanofibrillated cellulose from different raw materials and its reinforcement potential. *Carbohydr. Polym.* **2010**, *79*, 1086–1093. [[CrossRef](#)]
8. Henriksson, M.; Henriksson, G.; Berglund, L.A.; Lindström, T. An environmentally friendly method for enzyme-assisted preparation of microfibrillated cellulose (MFC) nanofibers. *Eur. Polym. J.* **2007**, *43*, 3434–3441. [[CrossRef](#)]

9. Prakobna, K.; Berthold, F.; Medina, L.; Berglund, L.A. Mechanical performance and architecture of biocomposite honeycombs and foams from core-shell holocellulose nanofibers. *Compos. Part A Appl. Sci. Manuf.* **2016**, *88*, 116–122. [CrossRef]
10. Khalil, H.P.S.A.; Davoudpour, Y.; Islam, M.N.; Mustapha, A.; Sudesh, K.; Dungani, R.; Jawaid, M. Production and modification of nanofibrillated cellulose using various mechanical processes: A review. *Carbohydr. Polym.* **2014**, *99*, 649–665. [CrossRef] [PubMed]
11. Francisco, D.L.; Paiva, L.B.; Aldeia, W. Advances in polyamide nanocomposites: A review. *Polym. Compos.* **2019**, *40*, 851–870. [CrossRef]
12. Iwamoto, S.; Isogai, A.; Iwata, T. Structure and mechanical properties of wet-spun fibers made from natural cellulose nanofibers. *Biomacromolecules* **2011**, *12*, 831–836. [CrossRef] [PubMed]
13. Kong, I.; Tshai, K.Y.; Hoque, M.E. *Manufacturing of Natural Fibre-Reinforced Polymer Composites by Solvent Casting Method*; Springer: New York, NY, USA, 2015; pp. 331–349.
14. Lee, K.W.; Chung, J.W.; Kwak, S.-Y. Highly branched polycaprolactone/glycidol copolymeric green plasticizer by one-pot solvent-free polymerization. *ACS Sustain. Chem. Eng.* **2018**, *6*, 9006–9017. [CrossRef]
15. Wang, L.; Gardner, D.J.; Wang, J.; Yang, Y.; Tekinalp, H.L.; Tajvidi, M.; Li, K.; Zhao, X.; Neivandt, D.J.; Han, Y.; et al. Towards the scale-up production of cellulose nanocomposites using melt processing: A critical review on structure-processing-property relationships. *Compos. Part B Eng.* **2020**. [CrossRef]
16. Sridhara, P.K.; Vilaseca, F. Assessment of fiber orientation on the mechanical properties of PA6/cellulose composite. *Appl. Sci.* **2020**, *10*, 5565. [CrossRef]
17. Alonso-Montemayor, F.J.; Tarrés, Q.; Oliver-Ortega, H.; Espinach, F.X.; Narro-Céspedes, R.I.; Castañeda-Facio, A.O.; Delgado-Aguilar, M. Enhancing the mechanical performance of bleached hemp fibers reinforced polyamide 6 composites: A competitive alternative to commodity composites. *Polymers* **2020**, *12*, 1041. [CrossRef] [PubMed]
18. DUSATEC. Mixing Ultrahigh-Speed Thermokinetic Gelimat TM Technology. Available online: http://www.dusatec.net/images/Gelimat_brochure_final.pdf (accessed on 20 April 2021).
19. Gopakumar, T.G.; Page, D.J.Y.S. Compounding of nanocomposites by thermokinetic mixing. *J. Appl. Polym. Sci.* **2005**, *96*, 1557–1563. [CrossRef]
20. Park, B.; Balatinecz, J.J. A comparison of compounding processes for wood-fiber/thermoplastic composites. *Polym. Compos.* **1997**, *18*, 425–431. [CrossRef]
21. Lee, J.-A.; Yoon, M.-J.; Lee, E.-S.; Lim, D.-Y.; Kim, K.-Y. Preparation and characterization of cellulose nanofibers (CNFs) from microcrystalline cellulose (MCC) and CNF/polyamide 6 composites. *Macromol. Res.* **2014**, *22*, 738–745. [CrossRef]
22. Saito, T.; Isogai, A. TEMPO-mediated oxidation of native cellulose. The effect of oxidation conditions on chemical and crystal structures of the water-insoluble fractions. *Biomacromolecules* **2004**, *5*, 1983–1989. [CrossRef]
23. Shenoy, A.V.; Saini, D.R.; Nadkarni, V.M. Melt rheology of polymer blends from melt flow index. *Int. J. Polym. Mater. Polym. Biomater.* **1984**, *10*, 213–235. [CrossRef]
24. Guillot, P.; Colin, A. Determination of the flow curve of complex fluids using the Rabinowitsch-Mooney equation in sensorless microrheometer. *Microfluid. Nanofluidics* **2014**, *17*, 605–611. [CrossRef]
25. Wu, Q.; Liu, X.; Berglund, L.A. An unusual crystallization behavior in polyamide 6/montmorillonite nanocomposites. *Macromol. Rapid. Commun.* **2001**, *22*, 1438–1440. [CrossRef]
26. Millot, C.; Fillot, L.A.; Lame, O.; Sotta, P.; Seguela, R. Assessment of polyamide-6 crystallinity by DSC: Temperature dependence of the melting enthalpy. *J. Therm. Anal. Calorim.* **2015**, *122*, 307–314. [CrossRef]
27. Borsoi, C.; Zimmermann, M.V.G.; Zattera, A.J.; Santana, R.M.C.; Ferreira, C.A. Thermal degradation behavior of cellulose nanofibers and nanowhiskers. *J. Therm. Anal. Calorim.* **2016**, *126*, 1867–1878. [CrossRef]
28. Van De Velde, K.; Kiekens, P. Thermal degradation of flax: The determination of kinetic parameters with thermogravimetric analysis. *J. Appl. Polym. Sci.* **2002**, *83*, 2634–2643. [CrossRef]
29. Peng, Y.; Gardner, D.J.; Han, Y. Characterization of mechanical and morphological properties of cellulose reinforced polyamide 6 composites. *Cellulose* **2015**, *22*, 3199–3215. [CrossRef]
30. Faruk, O.; Bledzki, A.K.; Fink, H.P.; Sain, M. Progress report on natural fiber reinforced composites. *Macromol. Mater. Eng.* **2014**, *299*, 9–26. [CrossRef]
31. Nicharat, A.; Sapkota, J.; Weder, C.; Foster, E.J. Melt processing of polyamide 12 and cellulose nanocrystals nanocomposites. *J. Appl. Polym. Sci.* **2015**, *132*. [CrossRef]
32. Krishna, S.; Patel, C.M. Computational and experimental study of mechanical properties of Nylon 6 nanocomposites reinforced with nanomilled cellulose. *Mech. Mater.* **2020**, *143*. [CrossRef]
33. Lee, K.Y.; Aitomäki, Y.; Berglund, L.A.; Oksman, K.; Bismarck, A. On the use of nanocellulose as reinforcement in polymer matrix composites. *Compos. Sci. Technol.* **2014**, *105*, 15–27. [CrossRef]
34. Tarrés, Q.; Boufi, S.; Mutjé, P.; Delgado-Aguilar, M. Enzymatically hydrolyzed and TEMPO-oxidized cellulose nanofibers for the production of nanopapers: Morphological, optical, thermal and mechanical properties. *Cellulose* **2017**, *24*, 3943–3954. [CrossRef]
35. Wei, J.; Chen, Y.; Liu, H.; Du, C.; Yu, H.; Ru, J.; Zhou, Z. Effect of surface charge content in the TEMPO-oxidized cellulose nanofibers on morphologies and properties of poly(N-isopropylacrylamide)-based composite hydrogels. *Ind. Crops. Prod.* **2016**, *92*, 227–235. [CrossRef]
36. Dijkstra, D.J. Guidelines for rheological characterization of polyamide melts (IUPAC technical report). *Pure Appl. Chem.* **2009**, *81*, 339–349. [CrossRef]

37. Håkansson, K.M.O.; Fall, A.B.; Lundell, F.; Yu, S.; Krywka, C.; Roth, S.V.; Santoro, G.; Kvik, M.; Wittberg, L.P.; Wågberg, L.; et al. Hydrodynamic alignment and assembly of nanofibrils resulting in strong cellulose filaments. *Nat. Commun.* **2014**, *5*. [[CrossRef](#)]
38. Kiziltas, A.; Nazari, B.; Gardner, D.J.; Bousfield, D.W. Polyamide 6-cellulose composites: Effect of cellulose composition on melt rheology and crystallization behavior. *Polym. Eng. Sci.* **2014**, *54*, 739–746. [[CrossRef](#)]
39. Venkatraman, P.; Gohn, A.M.; Rhoades, A.M.; Foster, E.J. Developing high performance PA 11/cellulose nanocomposites for industrial-scale melt processing. *Compos. Part B Eng.* **2019**, *174*. [[CrossRef](#)]
40. Chaichanawong, J.; Thongchuea, C.; Areerat, S. Effect of moisture on the mechanical properties of glass fiber reinforced polyamide composites. *Adv. Powder. Technol.* **2016**, *27*, 898–902. [[CrossRef](#)]
41. Abacha, N.; Kubouchi, M.; Sakai, T. Diffusion behavior of water in polyamide 6 organoclay nanocomposites. *Express Polym. Lett.* **2009**, *3*, 245–255. [[CrossRef](#)]
42. Oliver-Ortega, H.; Méndez, J.A.; Espinach, F.X.; Tarrés, Q.; Ardanuy, M.; Mutjé, P. Impact strength and water uptake behaviors of fully bio-based PA11-SGW composites. *Polymers* **2018**, *10*, 717. [[CrossRef](#)] [[PubMed](#)]
43. Qua, E.H.; Hornsby, P.R. Preparation and characterisation of nanocellulose reinforced polyamide-6. *Plast. Rubber Compos.* **2011**, *40*, 300–306. [[CrossRef](#)]
44. Paci, M.; Filippi, S.; Magagnini, P. Nanostructure development in nylon 6-Cloisite®30B composites. Effects of the preparation conditions. *Eur. Polym. J.* **2010**, *46*, 838–853. [[CrossRef](#)]
45. Zhu, R.; Yadama, V.; Liu, H.; Lin, R.J.T.; Harper, D.P. Fabrication and characterization of Nylon 6/cellulose nanofibrils melt-spun nanocomposite filaments. *Compos. Part A Appl. Sci. Manuf.* **2017**, *97*, 111–119. [[CrossRef](#)]
46. Jin, J.; Rafiq, R.; Gill, Y.Q.; Song, M. Preparation and characterization of high performance of graphene/nylon nanocomposites. *Eur. Polym. J.* **2013**, *49*, 2617–2626. [[CrossRef](#)]
47. Kiziltas, A.; Gardner, D.J.; Han, Y.; Yang, H.S. Dynamic mechanical behavior and thermal properties of microcrystalline cellulose (MCC)-filled nylon 6 composites. *Thermochim. Acta* **2011**, *519*, 38–43. [[CrossRef](#)]
48. Goitisoló, I.; Eguiazábal, J.I.; Nazábal, J. Effects of reprocessing on the structure and properties of polyamide 6 nanocomposites. *Polym. Degrad. Stab.* **2008**, *93*, 1747–1752. [[CrossRef](#)]
49. Chavarria, F.; Paul, D.R. Comparison of nanocomposites based on nylon 6 and nylon 66. *Polymer* **2004**, *45*, 8501–8515. [[CrossRef](#)]
50. John, M.J.; Anandjiwala, R.; Oksman, K.; Mathew, A.P. Melt-spun polylactic acid fibers: Effect of cellulose nanowhiskers on processing and properties. *J. Appl. Polym. Sci.* **2013**, *127*, 274–281. [[CrossRef](#)]

A.3 Article III

Sridhara, P.K., Masso, F., Olsén, P. and Vilaseca, F., 2021. Strong Polyamide-6 Nanocomposites with Cellulose Nanofibers Mediated by Green Solvent Mixtures. *Nanomaterials*, 11(8), p.2127. DOI: 10.3390/nano11082127

Journal Impact Factor: 5.076 (2020), Journal Rank: JCR – Q1 (31/160 in Physics, Applied)



Article

Strong Polyamide-6 Nanocomposites with Cellulose Nanofibers Mediated by Green Solvent Mixtures

Pruthvi K. Sridhara ¹, Ferran Masso ², Peter Olsén ² and Fabiola Vilaseca ^{1,*}

¹ Advanced Biomaterials and Nanotechnology, Department of Chemical Engineering, University of Girona, 17003 Girona, Spain; pruthvi.sridhara@udg.edu

² Department of Fiber and Polymer Technology, KTH Royal Institute of Technology, 10044 Stockholm, Sweden; ferran.mass@gmail.com (F.M.); polsen@kth.se (P.O.)

* Correspondence: fabiola.vilaseca@udg.edu; Tel.: +34-667-292-597

Abstract: Cellulose nanofiber (CNF) as a bio-based reinforcement has attracted tremendous interests in engineering polymer composites. This study developed a sustainable approach to reinforce polyamide-6 or nylon-6 (PA6) with CNFs through solvent casting in formic acid/water mixtures. The methodology provides an energy-efficient pathway towards well-dispersed high-CNF content PA6 biocomposites. Nanocomposite formulations up to 50 wt.% of CNFs were prepared, and excellent improvements in the tensile properties were observed, with an increase in the elastic modulus from 1.5 to 4.2 GPa, and in the tensile strength from 46.3 to 124 MPa. The experimental tensile values were compared with the analytical values obtained by micromechanical models. Fractured surfaces were observed using scanning electron microscopy to examine the interface morphology. FTIR revealed strong hydrogen bonding at the interface, and the thermal parameters were determined using TGA and DSC, where the nanocomposites' crystallinity tended to reduce with the increase in the CNF content. In addition, nanocomposites showed good thermomechanical stability for all formulations. Overall, this work provides a facile fabrication pathway for high-CNF content nanocomposites of PA6 for high-performance and advanced material applications.

Keywords: cellulose nanofiber; polyamide-6; solvent casting; mechanical properties



Citation: Sridhara, P.K.; Masso, F.; Olsén, P.; Vilaseca, F. Strong Polyamide-6 Nanocomposites with Cellulose Nanofibers Mediated by Green Solvent Mixtures.

Nanomaterials **2021**, *11*, 2127.
<https://doi.org/10.3390/nano11082127>

Academic Editor:
Massimiliano Perduca

Received: 3 August 2021
Accepted: 18 August 2021
Published: 20 August 2021

Publisher's Note: MDPI stays neutral with regard to jurisdictional claims in published maps and institutional affiliations.



Copyright: © 2021 by the authors. Licensee MDPI, Basel, Switzerland. This article is an open access article distributed under the terms and conditions of the Creative Commons Attribution (CC BY) license (<https://creativecommons.org/licenses/by/4.0/>).

1. Introduction

Plant-based reinforcement is attractive for enhancing the mechanical properties of polymers in the context of biodegradable and sustainable materials [1]. The reinforcing effect of plant-based fibers originates from the highly crystalline cellulose hierarchical structure. Cellulose is both of a renewable origin and biodegradable [2]. In the nanocellulose form, cellulose exhibits an extraordinary potential as a reinforcing element in composites due to its high aspect ratio and high specific strength combined with its low density. It is also possible to chemically modify its surface to tailor the properties in applications such as foams, filter media films, adhesives, hierarchical materials, and electronic materials [3]. When well dispersed, nanocellulose exhibits a higher specific surface area, facilitating interface adhesion with the polymeric matrix which enables efficient stress transfer. Among the plant-based nanocelluloses, there are two major categories: cellulose nanocrystals (CNCs) and cellulose nanofibers (CNFs). Typically, CNCs are highly crystalline, needle-like structures, with a few hundred nanometers in length and a few nanometers in width [4]. On the other hand, CNFs are fibril-like structures that contain both crystalline and amorphous phases, with diameters in the order of tens of nanometers and lengths typically ranging from tens to hundreds of micrometers [5]. The linearity of cellulose polymer chains and their strong intermolecular bonds enables the formation of ordered crystalline structures, which impart exceptional mechanical properties to CNFs [6]. The extraction process of CNFs from natural fibers is an essential factor as the properties of CNFs depend mainly on the source of material and the method of extraction. CNFs are produced via mechanical

defibrillation, often facilitated by either chemical or enzymatic pretreatments to reduce the energy consumption of the process [7]. The inherent properties of CNFs make them an interesting sustainable choice of reinforcement for polymeric matrices intended for the automotive, construction, packaging, and energy sectors [8].

Polyamides as thermoplastic matrix materials with CNF reinforcement provide superior mechanical and thermal properties of composites. The most common type of polyamide is polyamide-6 (PA6, also called nylon-6). This polymorphic, biodegradable, and bio-compatible thermoplastic polymer is an attractive choice for its availability, higher mechanical properties, and compatibility with CNFs. Due to the hydrophilic nature of both PA6 and CNFs, good interface interactions are formed without the use of a compatibilizer or coupling reagents [9]. The compatibility of PA6 and CNFs results in an excellent dispersion, distribution, and interfacial adhesion. However, silane coupling agents can improve the adhesion between a polyamide matrix and CNFs [10].

Recent studies have shown increments in mechanical properties for composites of PA6 with cellulose pulp fibers and/or micro-fibrillated cellulose (MFC) through melt processing with the help of a high-speed thermo-kinetic mixer [11,12]. MFCs are more heterogeneous and larger in size than CNFs. As CNFs offer a larger specific surface area for the polymer to form strong and functional interface adhesion, the overall reinforcing potential of CNFs is greater than that of MFCs [13]. One of the drawbacks of melt processing PA6/cellulose composites is the high melting point of PA6 (~220 °C), which leads to the onset of thermal degradation of cellulose during processing. Techniques such as solvent casting circumvent thermal degradation, retaining the thermal stability of cellulose, and facilitate uniform CNF dispersion in the matrix [14]. The primary advantage of solvent casting is the ease of fabrication without specialized equipment that is essential for other techniques such as extrusion and injection molding processes. The cast film exhibits a homogenous thickness distribution and fiber dispersion [15]. Currently, the most commonly used solvent is dimethylformamide (DMF). DMF is aprotic by nature, has a high dielectric constant and low volatility, and provides a good dispersion of CNFs in PA6 matrices. However, DMF is a potent liver toxin and may cause abdominal problems and reduce sperm motility [16]. A green solvent alternative would be a significant leap forward. In this study, we used formic acid which is renewable and has a lower toxicity than DMF. Previous studies have reported formic acid as an excellent solvent for dissolving PA6. Formic acid dissolves PA6 at 30 °C with negligible degradation of the polymer, promoted by the weak acid characteristics [17,18]. CNFs have good dispersion in water [19]. Therefore, we considered a water/formic acid mixed system to both dissolve PA6 and disperse the CNFs. This study developed a green solvent casting system based on water and formic acid to produce high-CNF content PA6 nanocomposites. The nanocomposites were produced by diluting the CNF dispersion in water in formic acid containing 20 wt.% of dissolved PA6 corresponding to each formulation. The homogenous mixture was then dried to produce thin films for characterization.

2. Materials and Methods

2.1. Materials

An industrial grade of PA6 called Ultramid[®] B3S (density $\rho = 1.13 \text{ g/m}^3$) was commercially purchased from BASF SE (Ludwigshafen, Germany) in the form of pellets. This grade of PA6 is colorless, less viscous, and suitable for producing thin-walled technical parts. The pellets were powdered from Powder Plastics Europe SL (Valls, Spain) and then passed through a 1000-micron sieve to reduce the dissolving time of PA6 in formic acid (Sigma Aldrich 33015-1L-M, St. Louis, MO, USA). The grain size distribution of PA6 is shown in Table 1. Commercially available cellulose pulp provided by Nordic Paper Säffle AB (Säffle, Sweden) was used to derive the CNFs. This product was of a high cellulose content, with 87% of pure cellulose, 12 to 12.5% of hemicellulose, and less than 1% of lignin. CNFs were then used to reinforce the PA6 matrix.

Table 1. Grain size specification and distribution for PA6 powder.

Particle Size Specifications (Micron)	Composition (%)
>1000	0
>800	8.82
>500	33.86
>300	29.42
>100	19.79

2.2. Methods

2.2.1. Preparation of PA6-CNF Nanocomposite Films

The cellulose pulp was disintegrated into cellulose nanofibers (CNFs) by an enzymatic pretreatment described by Henriksson et al., 2007, using an endoglucanase enzyme, namely, Novozyme 476 (Novozymes AS, Bagsværd, Denmark) [20]. Enzymatic treatment provided a more specific, milder, and environmentally friendly method to increase the yield and expedite the disintegration of cellulose [21,22]. Firstly, the cellulose pulp fibers were beaten mechanically in a PFI mill (Hamjern, Hamar, Norway) at 1000 revolutions to increase the swelling in water and provide better accessibility of the enzyme to the cellulose. Further, enzymatic treatment was carried out by dispersing 3 wt.% pulp in 50 mM tris(hydroxymethyl)aminomethane/HCl buffer with pH 7 and 0.02 wt.% enzyme relative to the amount of pulp. The fibers were incubated for 2 h at 50 °C and later washed on a Büchner funnel. The fibers were kept for 30 min at 80 °C to cease the enzyme activity and later washed again. Then, the fibers were beaten in the PFI mill at 4000 revolutions. Following the enzyme pretreatment, 1.5 wt.% fiber suspension in water was prepared and subjected to homogenization (Laboratory Homogenizer 15M, Gaulin Corp., Boston, MA, USA) at a constant high pressure without heating. Initially, the suspension was at room temperature, but with an increasing number of passes, the temperature increased slightly, facilitating the homogenization of the CNFs [23]. The fibers were passed through the homogenizer six times until the suspension reached a consistent viscosity based on visual inspection to obtain a CNF gel with 1.5 wt.% consistency. Previous work in our group by Prakobna et al. determined that these CNFs have an average diameter ranging from 6 to 9 nm and lengths in the 0.7–2 µm range [24].

The Petri dish used for casting the PA6-CNF nanocomposites had an inner diameter of 8.8 cm. To produce thin films of thickness 0.1 mm, an approximate total weight of 0.8 g of the PA6-CNF mixture was required. The amount of PA6 powder required for each composition of cellulose was calculated using the density, mass, and volume relation. For obtaining 0.8 g of nanocomposite film, the weight specifications of CNF and PA6 are shown in Table 2.

Table 2. Weight specifications for casting PA6-CNF nanocomposites.

CNF Composition (wt.%)	CNF Dry Weight (g)	CNF Density (g/cm ³)	PA6 Dry Weight (g)	Composite Density (g/cm ³)
10	0.08	1.52 ± 0.03	0.72	1.159 ± 0.02
20	0.16		0.64	1.189 ± 0.02
30	0.24		0.56	1.220 ± 0.02
40	0.32		0.48	1.254 ± 0.03
50	0.4		0.4	1.289 ± 0.03

For every formulation, 20 wt.% of PA6 was dissolved completely in formic acid at 30 °C. The 1.5 wt.% CNF gel was then dispersed within formic acid to obtain a consistency of 0.75 wt.% CNF content in the solvent system. This pre-wetting of CNFs in the same solvent was conducted in order to further improve CNF/PA6 compatibility and their interfacial adhesion [15]. To ensure proper dispersion of CNFs, the solution was mixed with the help of an Ultraturrax (T 25, IKA, Königswinter, Germany) by stirring at a high speed of 7000 rpm for about 30 s. This solution was then left in an Ultrasonic bath (Exibel,

Clas Ohlson, Dalarna, Sweden) for 10 min to remove any possible bubbles. Finally, the CNF gel dispersed in formic acid and the dissolved PA6 in formic acid were mixed with the help of a stirrer for 2 h to ensure uniform mixing. This mixture was again left in the ultrasonic bath to remove any bubbles which might have been formed during mixing. The mixed solution was introduced onto the Petri dish carefully and placed in an oven (Memmert UM200, Büchenbach, Germany) at 50 °C for casting the PA6-CNF nanocomposite. When all the formic acid and water had evaporated, we placed the Petri dish containing the composite in a desiccator at ambient temperature to prevent deformation while cooling. The composite film was removed from the Petri dish with the help of a spatula and tweezers. Rectangular samples were cut using a hydraulic press (Stans & Press—TJT Teknik AB, Vilshult, Sweden) from the thin film for tensile and DMA characterizations. An example of the cast nanocomposite film (50 wt.%) is shown in Figure 1. The neat CNF film was produced by the filtration method. PA6 films were also prepared to be used as control samples.

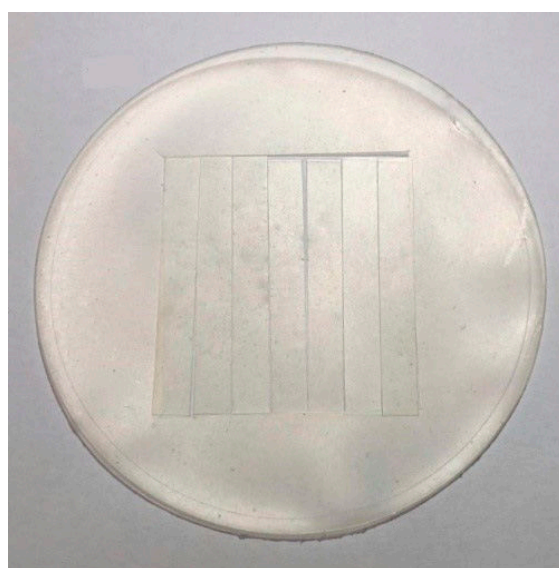


Figure 1. 50 wt.% PA6-CNF casted nanocomposite film.

2.2.2. Tensile Tests

Rectangular samples of dimensions ($l \times b$) 45 mm \times 6 mm were cut from the films to perform tensile tests. The thickness values of each nanocomposite sample were measured using a digital precision micrometer (Starrett, Athol, MA, USA). Prior to tensile testing, the rectangular samples were dried overnight in an oven at 50 °C and then conditioned at room temperature of 23 ± 2 °C and $50 \pm 5\%$ relative humidity (RH) for 48 h. The uniaxial tensile properties were measured on a Universal Testing Machine (Instron 5944, Norwood, MA, USA) where the extension was quantified with a high-precision camera. Tensile tests were performed with a 500 N load cell and strain rate of 0.1 min^{-1} . The measured tensile strength and modulus were averaged over at least five samples for statistical significance. For comparative assessment, the tensile strength of the nanocomposites was also estimated by a basic rule of mixtures (ROM) model:

$$\sigma_{NC} = \sigma_{CNF} V_{CNF} + \sigma_{PA6} (1 - V_{CNF}) \quad (1)$$

where σ_{NC} is the tensile strength of the nanocomposite, σ_{CNF} and σ_{PA6} are the experimental tensile strengths of CNFs and PA6, respectively, and V_{CNF} is the total volume fraction of CNFs. The value of σ_{NC} predicts the linear relationship between σ_{NC} and the CNF composition. An estimation of reinforcement efficiency for all the formulations of CNF content was resolved. All volume fractions were calculated assuming the densities of 1.13 g/m^3 for PA6 and 1.5 g/m^3 for CNFs.

The Cox–Krenchel micromechanical model was used to predict the tensile modulus. This model was developed based on the classical shear lag theory and is one of the most widely used models [1]. Assumptions used in this model are: (i) the fiber and matrix respond elastically, (ii) no axial loads on the fiber ends, and (iii) an ideal fiber matrix interface. The Cox–Krenchel model is defined as

$$E_{NC} = \eta_0 V_{CNF} E_{CNF} \left(1 - \frac{\tanh(ns)}{ns} \right) + (1 - V_{CNF}) E_{PA6} \quad (2)$$

where n is expressed by

$$n = \sqrt{2E_{PA6} / \left[E_{CNF} (1 + V_{PA6}) \ln \left(\frac{1}{V_{CNF}} \right) \right]} \quad (3)$$

In the above Equations (2) and (3), E_{NC} is the elastic modulus of the nanocomposite, E_{CNF} and E_{PA6} are the experimental moduli of CNFs and PA6, respectively, with the fiber orientation factor $\eta_0 = 3/8$ assuming an in-plane isotropic orientation of fibers in a random short fiber polymer composite, and s is the fiber aspect ratio where the weight average fiber length L can be used to calculate $s = L/D$, where D is the diameter of the fiber [25].

Similarly, elastic moduli were calculated assuming a random in-plane fiber orientation using the Tsai–Pagano model defined in Equation (4) [26].

$$E_{NC} = \left(\frac{3}{8} \right) E_L + \left(\frac{5}{8} \right) E_T \quad (4)$$

$$E_L = E_{CNF} V_{CNF} + E_{PA6} (1 - V_{CNF}) \quad (5)$$

$$E_T = \frac{E_{CNF} E_{PA6}}{E_{CNF} (1 - V_{CNF}) + E_{PA6} V_{CNF}} \quad (6)$$

where E_L and E_T are the longitudinal and the transverse modulus of the nanocomposite calculated longitudinally and transversely to the direction of the fiber assuming a unidirectional composite with cylindrical fibers. E_{NC} is the theoretical nanocomposite modulus for a random in-plane fiber orientation.

2.2.3. Scanning Electron Microscopy (SEM)

The morphology of samples fractured due to elongation during the tensile tests was observed under a scanning electron microscope (Hitachi S4800, Ibaraki, Japan) to characterize the interaction between CNFs and the PA6 matrix. The samples were observed at an accelerated voltage of 15.0 kV and a short working distance. The cross-sections of the fractured samples were coated with a thin layer (2–4 nm) of Pt:Pd with the help of a Cressington sputter prior to observation.

2.2.4. Fourier Transform Infrared Spectroscopy (FTIR)

The changes in the chemical structure and the binding configuration of the nanocomposite samples were analyzed by using Fourier transform infrared analysis. The FTIR spectrum of the films produced was obtained in transmission by performing the analysis in the IR frequency range of 500 to 4000 cm^{-1} using a Perkin Elmer Spectrum 100 spectrometer (PerkinElmer, Waltham, MA, USA).

2.2.5. Thermogravimetric Analysis (TGA)

The control samples and all the formulations of PA6-CNF nanocomposites were analyzed for thermal degradation using a TGA1 STAR^e System (Mettler Toledo, Greifensee, Switzerland) at the heating rate of 10 $^{\circ}\text{C}/\text{min}$. The tests were carried out by placing the sample in an open platinum pan within a nitrogen environment and heating it from 30 to 600 $^{\circ}\text{C}$.

2.2.6. Differential Scanning Calorimetry (DSC)

The thermal properties of the PA6 (powder and control film) and PA6-CNF nanocomposite films were measured using a DSC 1 STAR^e System (Mettler Toledo, Greifensee, Switzerland). The DSC was run three times for each sample. The samples were firstly heated from 30 to 260 °C and held at this temperature for 2 min followed by cooling of samples to 30 °C within a nitrogen environment. The heating and cooling rate was 10 °C/min. The degree of crystallinity of the polymer after processing was determined from the enthalpy corresponding to the melting endotherm of the first heating, according to Equations (7) and (8).

$$\Delta H_{polymer} = \Delta H_{sample} \cdot \left(\frac{1}{1 - \frac{w_{CNF}}{100}} \right) \quad (7)$$

$$\chi_c = \frac{\Delta H_{polymer}}{\Delta H_{100\%}} \cdot 100 \quad (8)$$

where ΔH_{sample} is the enthalpy of the melting endotherm of the sample from the first heating cycle, and $\Delta H_{polymer}$ is the melting enthalpy of the PA6 polymer in the sample. The degree of crystallinity (χ_c) considers the melting enthalpy for the 100% crystalline PA6, $\Delta H_{100\%} = 230$ J/g [27].

2.2.7. Dynamic Mechanical Analysis (DMA)

Rectangular samples of dimensions ($l \times b$) 15 mm \times 6 mm were cut from neat PA6 and PA6-CNF nanocomposite casted films to perform DMA in tensile mode. These samples were kept in the oven for 48 h at 55 °C prior to analysis. The analysis was performed using the instrument DMA Q800 (TA Instruments, New Castle, DE, USA) measuring from 30 °C and finishing at 160 °C, with a heating rate of 5 °C/min, preload of 1 N, a constant frequency of 1 Hz, and strain amplitude of 0.1%. The DMA tests were run three times for each formulation.

3. Results and Discussions

3.1. Morphology

The PA6 and CNF nanocomposite films produced via solvent casting had a good dispersion and distribution for all formulations, which was evident from the uniform translucency observed throughout the films. There were no visual signs of voids or agglomeration even for the high-CNF composition, thus confirming a good phase morphology. The films were generally flat and were easy to cut into rectangular samples for testing. The pure CNF film was obtained through the filtration process and had only small pores. As the sample thickness significantly affects the calculated mechanical properties, the thickness measurement was conducted with a digital precision micrometer. The mean thicknesses of all rectangular samples for each formulation used for tensile testing are shown in Table 3.

Table 3. Tensile properties for the control samples and PA6-CNF nanocomposites.

CNF Composition (wt.%)	Mean Thickness (μm)	Tensile Strength (MPa)	Elastic Modulus (GPa)	Strain at Break (%)
Neat PA6	96.2 \pm 8.4	46.3 \pm 2.35	1.52 \pm 0.08	12.6 \pm 0.42
10	111 \pm 7.3	54.1 \pm 2.87	1.85 \pm 0.05	11.1 \pm 1.72
20	108.6 \pm 1.9	67.3 \pm 1.60	2.30 \pm 0.08	10.1 \pm 1.69
30	116.8 \pm 6.3	78.4 \pm 0.35	3.48 \pm 0.47	9.2 \pm 0.49
40	91.3 \pm 3.0	110.5 \pm 7.80	4.10 \pm 0.26	7.8 \pm 1.17
50	99.8 \pm 2.9	123.9 \pm 6.12	4.20 \pm 0.27	7.3 \pm 0.50
CNF nanopaper	45.4 \pm 0.8	200.9 \pm 6.73	12.23 \pm 0.39	6.9 \pm 0.82

3.2. Tensile Tests

The tensile strengths and elastic moduli for all the formulations are summarized in Table 3. During tensile testing, there were no failures at the grips due to the clamping pressure. The tensile properties of the nanocomposites increased with the CNF content, corroborating that the CNFs were well dispersed within the PA6 matrix. Previous studies have demonstrated that carboxyl groups increase during enzymatic pretreatment [28]. These carboxyl groups play a vital role in the dispersion of CNFs within a matrix. The repulsion due to negative charges on the surface of the CNFs prevents fibril–fibril agglomeration, aiding in achieving a uniform distribution and consequently contributing to the mechanical properties of the nanocomposite films. The CNFs imparted intrinsic mechanical properties to the nanocomposites. Both the tensile strength and Young's modulus are appreciably higher, indicating good wetting and effective stress transfer at the PA6–CNF interface [29]. The uniform dispersion and distribution of CNFs provide a high surface area that increases the number of secondary interactions with the PA6 matrix [30]. The highest tensile stress at break and Young's modulus were observed for the 50 wt.% formulation nanocomposite with the values of 124 MPa and 4.2 GPa, respectively, corresponding to an improvement of 2.7 times when compared to the PA6 control sample. For the high-CNF content nanocomposites, casting/evaporation causes strong interactions between the CNFs, promoting strong percolating network formation through hydrogen bonding. The casting process ensures that the PA6 matrix penetrates this CNF network formation and enhances the mechanical properties. For such high-CNF content films, the improvement in tensile properties is dependent on the CNF network followed by successful penetration of the PA6 matrix and may not be attributed to the intrinsic stiffness of individual nanoparticles. For the neat CNF film, the maximum tensile strength of ~201 MPa and modulus of 12.23 GPa were obtained.

Previously, we prepared up to 25 wt.% CNF formulations with PA6 by melt compounding using a Gelimat thermo-kinetic mixer and observed good enhancement in mechanical properties [31]. Peng et al. obtained composite formulations up to 10 wt.% CNF content with PA6 via thermal compounding using a Brabender with minor improvements in the tensile properties [32]. Lee et al. prepared 40 wt.% CNF/PA6 by silane treatment and the calendaring process, achieving ~2.5 GPa and ~12.5 MPa for the tensile modulus and strength, respectively [33]. Joshi et al. obtained up to 50 wt.% of regenerated cellulose composite membranes with PA6 using the electrospinning method with tensile strength and modulus increments corresponding to ~12% and ~150%, respectively [34]. More relatively, Qua et al. used the solution casting technique to prepare PA6 and 5 wt.% flax and microcrystalline cellulose (MCC) nanofibers obtained from acid hydrolysis, and the composite's tensile strength was improved drastically, which is promising for our study [35]. Our study develops an energy-efficient approach towards solvent casting by adopting simple green solvent mixtures to fabricate PA6 nanocomposites using CNFs derived enzymatically, which is a more environmentally friendly way to extract CNFs when compared to other processes such as acid hydrolysis and TEMPO oxidation. In addition, tensile mechanical improvements of about 176% (for modulus) and 168% (for strength), when compared to neat PA6, were achieved for the 50 wt.% formulation without using any dispersion or coupling agents.

The strain at break decreased with an increase in the CNF composition. The CNFs provide larger surface areas for the PA6 matrix to form strong interfacial adhesion, enabling the effective stress transfer and imparting stiffness to the composite [36]. Our previous work with PA6 and cellulosic material biocomposites produced via melt processing showed a considerable drop in strain levels for 25 wt.% cellulose pulp [12,31]. Similarly, in this study, strain at break decreased with the increase in the CNF content. This behavior is inherent to a well-dispersed CNF network where the CNF behavior is retained in the corresponding CNF-polymer matrix nanocomposites [37]. CNFs hinder the nanocomposites' elongation due to stiffening caused by the reinforcing effect. Nevertheless, despite the higher CNF

contents, an elongation of ~7% was measured for the 50 wt.% formulation. Figure 2 shows the stress–strain plots and the deformation behavior during elongation for all the samples.

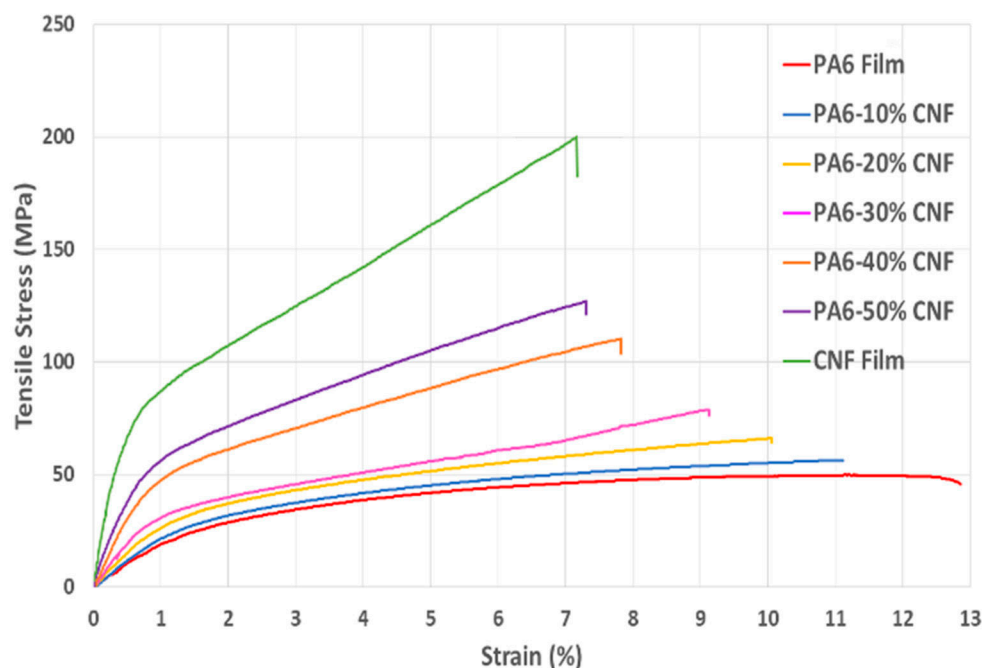


Figure 2. Stress vs. strain curves for control samples and PA6-CNF nanocomposites.

As an approximate assessment of nanocomposites' tensile strength (σ_{NC}), we used the basic rule of mixtures model (ROM). ROM assumes that σ_{NC} depends on the strength of the CNF nanopaper (σ_{CNF}) and neat PA6 (σ_{PA6}), scaled with the corresponding fiber volume fractions. The prediction from Equation (1) shows the nanocomposites' lower bound tensile strength as the tensile strength of a single CNF is assumed to be underutilized. Experimental values ranging from 103 to 232 MPa for the cellulose nanopaper were recorded in the previous literature [38,39]. The difference in tensile strength is due to the nanofiber and nanofiber networks [40]. Based on the ROM model, the experimental values of the tensile strength match reasonably well with the predicted values for all the CNF composition formulations (Figure 3A). Overall, for high-fiber volume fraction nanocomposites, the predicted values should be considered purely theoretical since the nanocellulose might not exist as a dense nanopaper network but as a 3D percolated network of CNFs [1].

Figure 3B shows the experimental elastic moduli for nanocomposites with moduli calculated from the Cox–Krenchel equations, Equations (2) and (3), and the Tsai–Pagano equations, Equations (4)–(6). The Tsai–Pagano model overestimates the elastic moduli of the nanocomposites except for two formulations (30 wt.% and 40 wt.%), suggesting that the stiffness of the cellulose nanofiber network was controlling the moduli of the nanocomposites. The Cox–Krenchel model considers the aspect ratio of CNFs and is a good method to approximate the effect on the nanocomposites' elastic modulus. As the aspect ratio of nanofibers decreases, the fiber ends act more effectively as stress and strain fields in the PA6 matrix due to the discontinuity [41]. The experimental values are similar to the estimated values for low-CNF composition nanocomposites (5 wt.% and 10 wt.%), whereas they are higher than the theoretical values with CNF compositions of 20 wt.%, 30 wt.%, and 50 wt.%. This suggests there was good impregnation of the PA6 matrix within the CNF network.

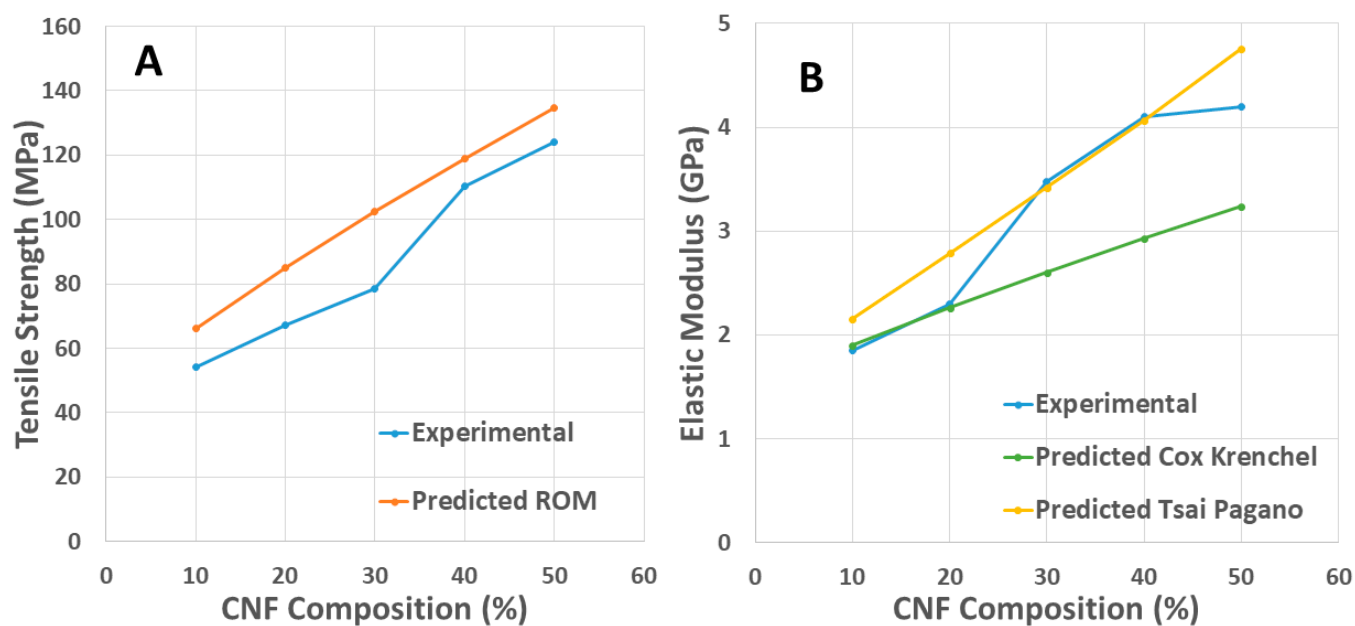


Figure 3. Experimental and theoretically predicted tensile strength (A) and modulus (B) values for PA6-CNF nanocomposites.

3.3. SEM Analysis

The morphology of the fractured tensile cross-sections of the 20 wt.% and 50 wt.% CNF nanocomposites and neat CNF nanopaper was analyzed with a scanning electron microscope. Figure 4 shows the SEM micrographs of the fractured surfaces at three different magnification levels. The distribution of CNFs appears to be homogenous within the in-plane layers at the nanoscale, with very few voids and no agglomerations for the nanocomposite films (Figure 4A,D). Typically, nanocomposites' fractured surfaces had a brittle fracture with deformation occurring in different planes. Under tensile load, the different moduli of PA6 and CNFs lead to different modes of deformation, generating different strains which create stress concentration points at the CNF-PA6 interface. When this unmatched strain surpasses the magnitude of interfacial adhesion, a sliding deformation occurs [31]. The resulting surface morphology due to this sliding deformation is seen in Figure 4B,E. As the CNF content increased, the surface morphology of the nanocomposites transitioned to be partially identical to that of the pure CNF nanopaper (Figure 4G). The fractured surfaces for the nanocomposites were formed due to elongation; hence, the PA6 strands have a fiber-like shape which have been fractured at some point under tension. These PA6 strands are adjoined by CNFs, indicating good adhesion, and the strands should not be confused for agglomerated fibers (Figure 4C,E). The dispersion of fibers can be observed from Figure 4B,C,E,F with strands of PA6 surrounded by tiny fibrils of CNFs. For the CNF nanopaper, the hydroxyl groups on the CNFs result in hydrogen bonding between individual CNFs, hence creating a 3D percolated network, as seen in Figure 4H,I.

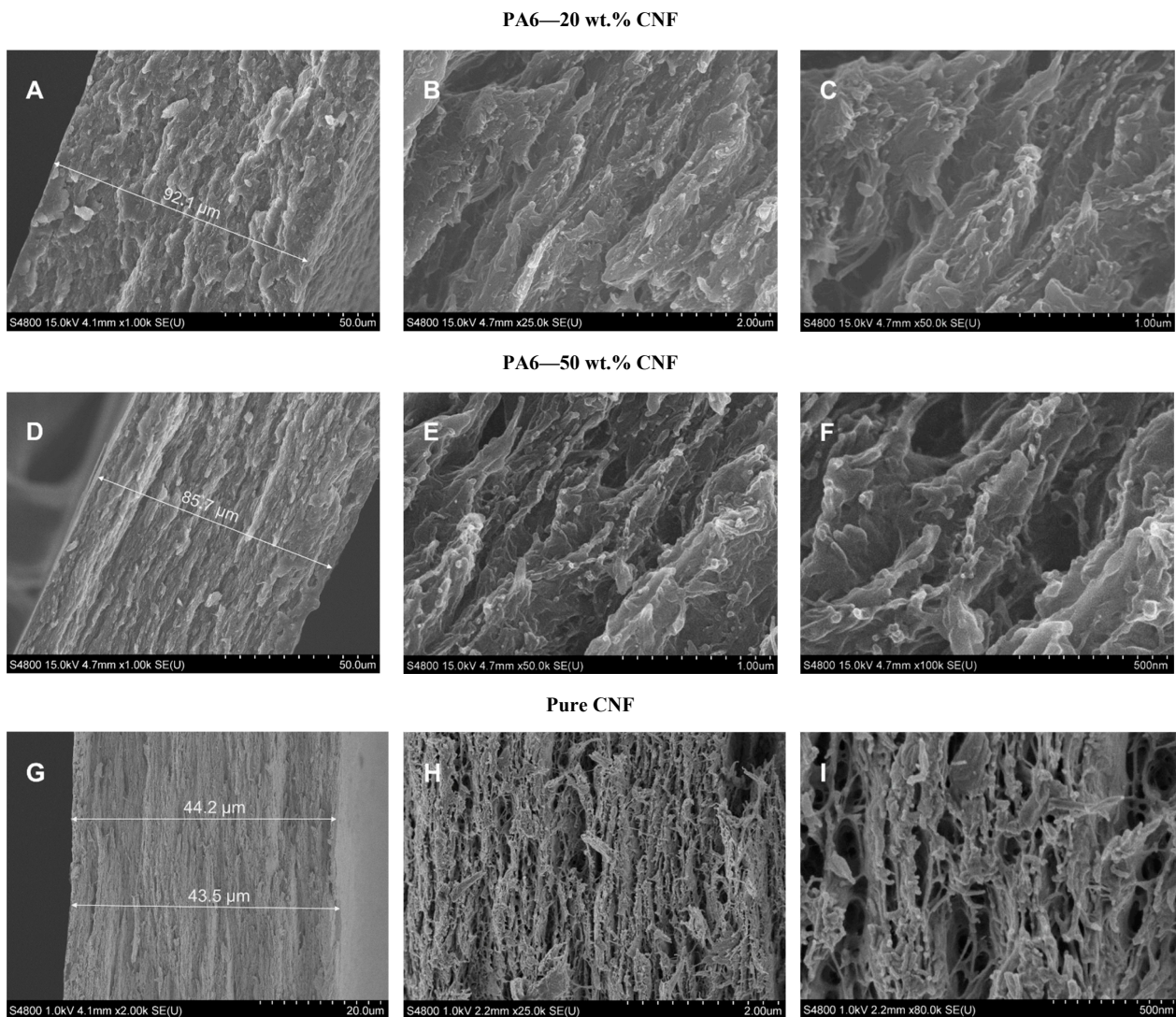


Figure 4. SEM micrographs for 20 wt.% (A–C), 50 wt.% (D–F) PA6-CNF nanocomposites, and CNF nanopaper (G–I).

3.4. FTIR Analysis

FTIR was used to confirm the hydrogen bonding behavior and crystallinity in the neat samples and PA6-CNF nanocomposites [42]. The FTIR spectra for the neat samples and 40 wt.% and 50 wt.% nanocomposite formulations are shown in Figure 5. The pure PA6 film had absorptions at 3323 cm^{-1} (hydrogen-bonded N-H stretching vibration), 3038 cm^{-1} (N-H in-plane bending), 2930 cm^{-1} (stretching vibration CH₂), 1634 cm^{-1} (stretching vibration C=O), 1537 cm^{-1} (stretching vibration C-N and CO-N-H bend), 1463 cm^{-1} (CH₂ in-plane bending), 966 cm^{-1} (stretching vibration C-CO), and 693 cm^{-1} (out-of-plane bending N-H) [43]. The PA6 polymer can effortlessly undergo a phase transition from the γ to the α form because of external inducement or modifications in the processing parameters as there are minor differences in energy between the α and γ forms. Hence, the structure and crystalline morphology are important to the PA6 properties [44]. The IR spectra below 1500 cm^{-1} are sensitive to the polymorph structure and are used as a spectroscopic marker to identify the presence of contrasting crystalline forms in the sample [45]. The sharp increase in marker bands (Figure 5B) correlates with the α form at 693 cm^{-1} , 920 cm^{-1} , 1200 cm^{-1} , and 1418 cm^{-1} in relation to the marker bands at 1172 cm^{-1} . The crystalline α -phase PA6 has a planar zig-zag structure and is thermodynamically more stable, while the γ phase has a helix structure and is metastable [34]. Since the CH₂ group is not ideally packed, hydrogen bonds are more efficient in the α form. Contrastingly, in the γ form,

hydrogen bonding is dominated by the ideal packing of methylene blocks [46]. Interactions lead to the formation of new hydrogen bonds with the amide groups of PA6 and the OH groups of cellulose. The intensity of the marker peaks after 1030 cm^{-1} , at lower-CNF composition nanocomposites, signifies the C-O stretching. The verge at 1722 cm^{-1} correlates with a C=O stretching vibration resulting from a small degree of esterification of the cellulose OH groups [47]. The affinity of CNFs and PA6 reorients the original hydrogen bond in the PA6 polymer chain. The reorientation of the hydrogen bonds is more evident for nanocomposites with a higher CNF content.

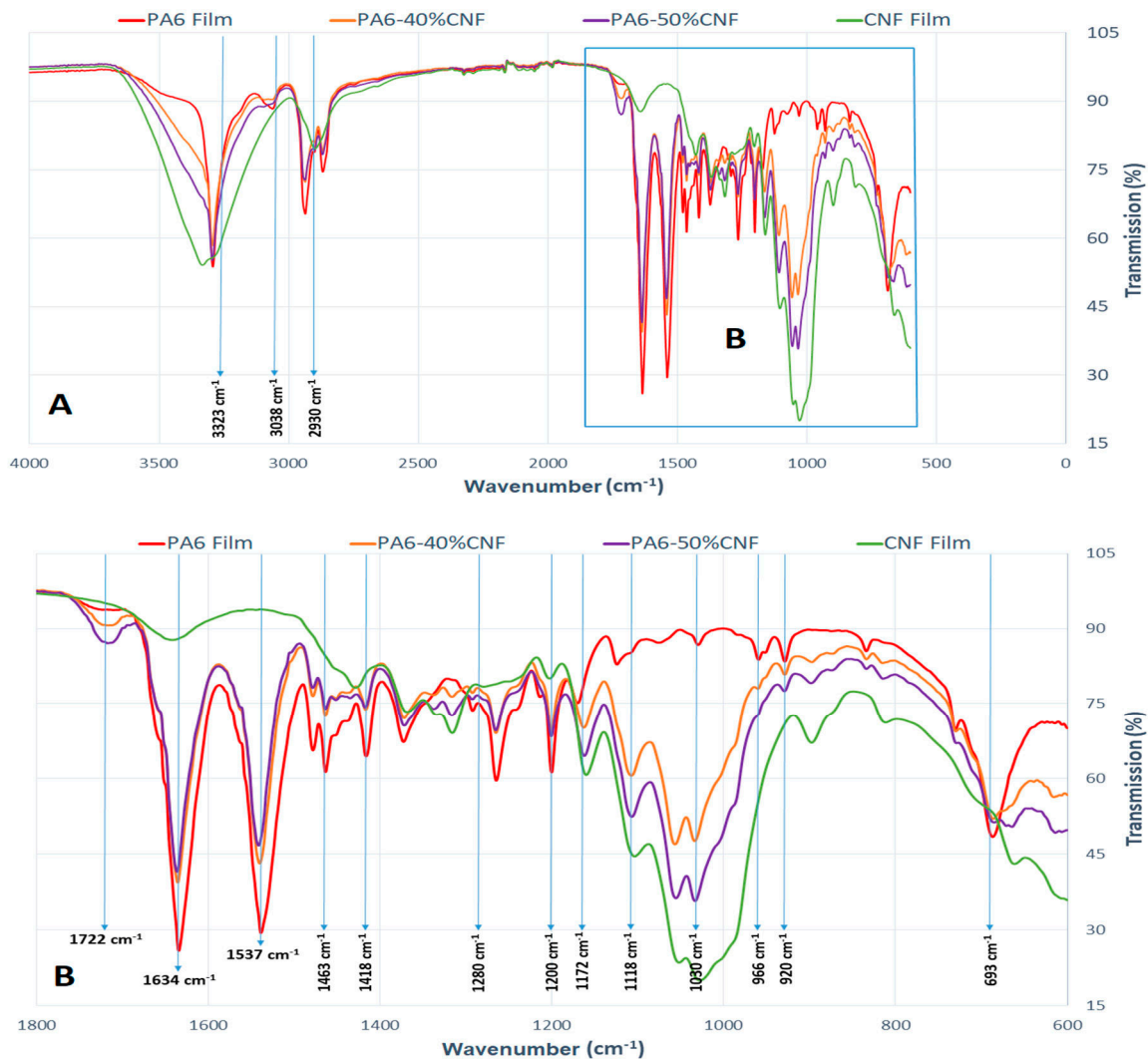


Figure 5. (A) FTIR spectra and (B) enlarged portion of the FTIR spectra at a lower wavelength for PA6 film, CNF film, and 40% and 50% formulation nanocomposite films.

3.5. TGA Analysis

Figure 6 shows the thermogravimetric (TGA) and the first derivative thermogravimetric (DTG) curves for the control samples and PA6-CNF nanocomposites. For the control samples, single-stage thermal decomposition bands with a distinct maximum weight loss peak were observed. However, for the nanocomposite films, the thermal bands seemed to have two-stage decomposition with two peaks indicating maximum weight loss. The two-stage thermal decomposition is clearly observed in Figure 6B for the 30 wt.% and 40 wt.% formulations. Degradation initiation of PA6 occurs at $\sim 405\text{ }^{\circ}\text{C}$, while for the nanocomposites, it starts at $\sim 290\text{ }^{\circ}\text{C}$ (Figure 6A). During thermal degradation of CNFs above $290\text{ }^{\circ}\text{C}$, cellulose decomposes, releasing combustible volatiles such as acetaldehyde,

propenal, methanol, and acetic acid. These volatile products accelerate the decomposition rate in the samples [34,48]. The degradation bands for the PA6-CNF nanocomposites were between the control samples' degradation bands (Figure 6B). From the DTG curves, maximum degradation temperatures of ~ 440 °C and ~ 350 °C were observed for the PA6 and CNF films, respectively. Overall, the presence of the CNF content in the nanocomposites reduces the thermal stability of the nanocomposites.

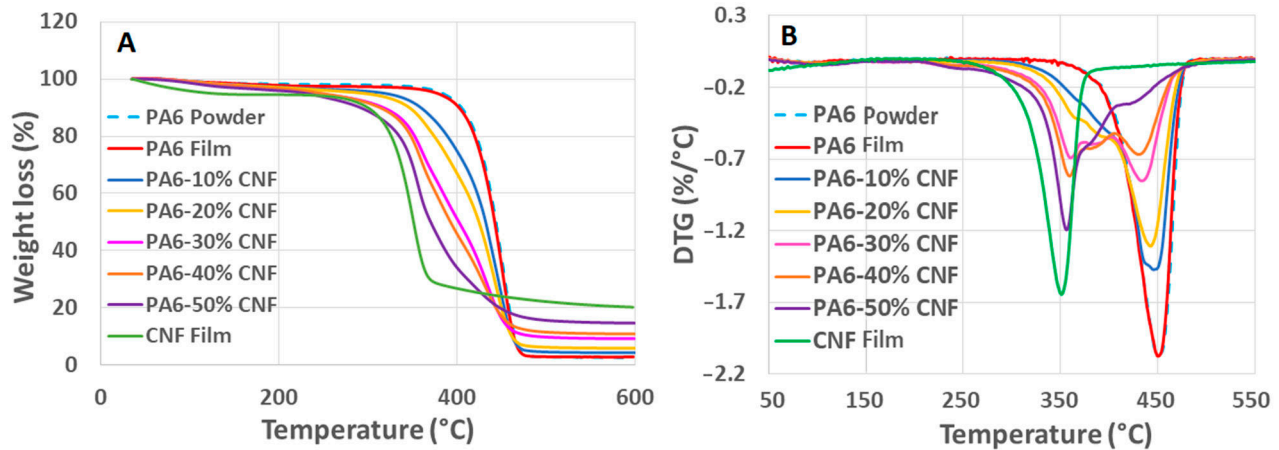


Figure 6. (A) TGA curves and (B) DTG curves for PA6, CNF, and PA6-CNF nanocomposite films.

3.6. DSC Analysis

The polymer's melting and crystallization behavior in the PA6 powder, PA6 film, and PA6-CNF nanocomposite films was analyzed with DSC. The glass transition temperature (T_g), melting temperature (T_m), crystallization temperature (T_c), and the degree of crystallinity (χ_c) of the PA6 polymer for all formulations are summarized in Table 4.

Table 4. Thermal parameters and degree of crystallinity for the PA6 polymer in the plain matrix and in the PA6-CNF nanocomposites.

CNF Composition (wt.%)	T_g (°C)	T_m (°C)	T_c (°C)	ΔH_{Sample} (J/s)	χ_c (%)
PA6 powder	43.4	223.2	193.7	120.4	52.3
0	44.2	223.2	194.0	114.9	49.9
10	48.4	220.3	190.3	101.6	49.1
20	50.2	218.7	189.3	81.4	44.2
30	51.0	217.2	188.0	68.3	42.4
40	53.6	217.0	187.2	54.9	39.8
50	50.9	213.8	182.5	43.7	38.0

The DSC thermograms corresponding to the first heating and cooling cycles appear in Figure 7. There was no morphological change in the crystal structure of the polymer between the PA6 powder and the PA6 film (Figure 7A) since the T_m was similar in both cases (~ 223 °C), which corresponded to the α -form and γ -form PA6 crystals [49]. A tendency for decreased T_m with the increase in the CNF content was observed because of a reduction in the crystalline order. The crystallinity of the PA6 pellets was slightly greater than that of the PA6 casted film. This change in crystallinity suggests that formic acid evaporation results in the formation of a metastable crystalline structure [50]. With the addition of CNFs, the T_g for the nanocomposites occurred at a moderately higher temperature compared to the control PA6 film. This increase in T_g is a result of the good dispersion of CNFs within the PA6 matrix and the strong interfacial adhesion [51,52]. As the CNF content increased, the crystallinity of nanocomposites reduced. Strong interactions between the polar amide groups of PA6 and the hydroxyl groups of CNFs resulted in

constrained segmental mobility of the PA6 chain [53]. This restricted conformational freedom for the PA6 polymer and reduced the crystallinity of the nanocomposites.

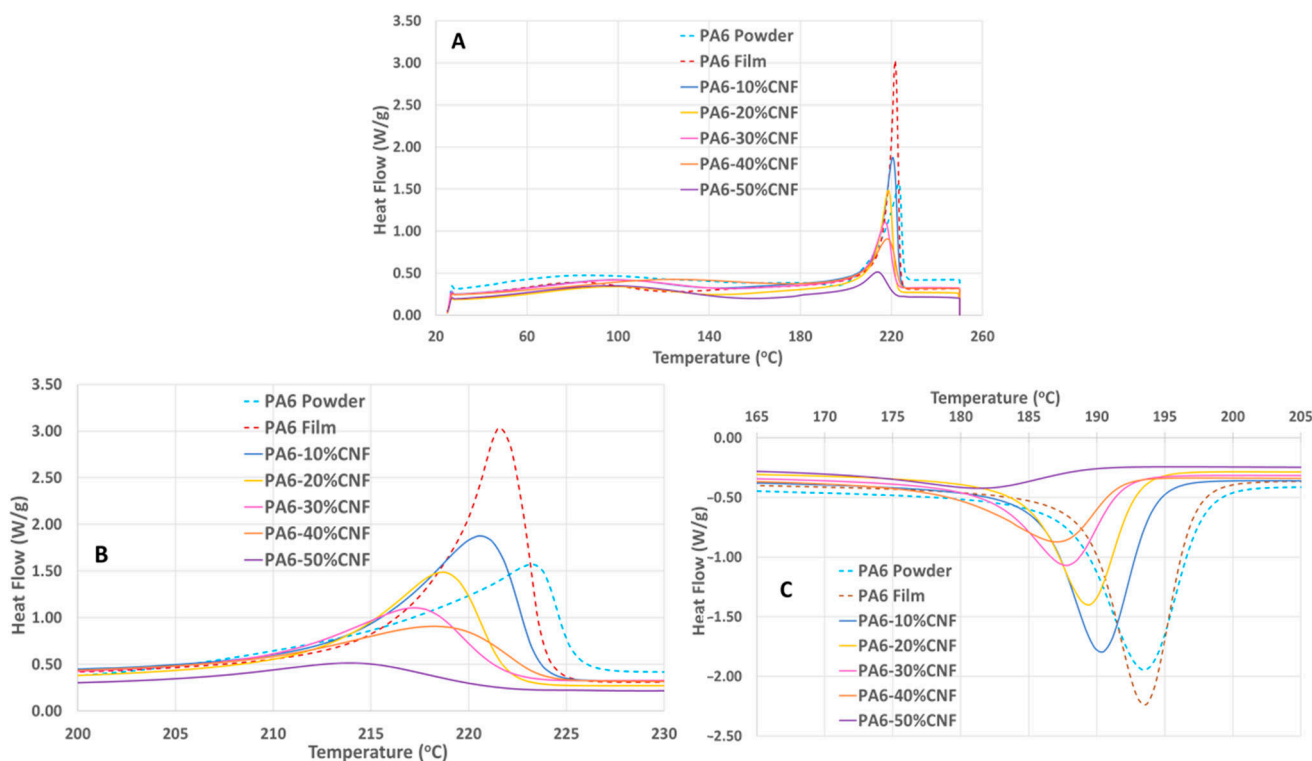


Figure 7. DSC thermograms: (A) heating cycle, (B) melting region, and (C) cooling region, all at a rate of 10 °C/min, for PA6 powder, PA6 film, and PA6-CNF nanocomposite films.

On cooling, a distinct crystallization exothermic peak (Figure 7B) for neat PA6 at ~194 °C relates to the α -form crystal [54]. T_c 's tendency to decrease as the CNF content increased means that crystallization of PA6 begins later in the nanocomposites when compared to neat PA6. Cellulosic materials at lower concentrations usually serve as nucleating agents that increase the crystallization rate in PA6 [55,56]. However, at high weight fractions of CNFs, the crystallization rate is retarded, reducing the degree of crystallinity, as observed in our nanocomposites. Overall, in our case, it can be stated that the mobility of PA6 chains is restricted by the addition of CNFs, thus reducing the crystallinity.

3.7. DMA Tests

Dynamic mechanical analysis was used for characterizing the viscoelastic behavior of neat PA6 and PA6-CNF nanocomposites by a sinusoidal deformation in tensile mode. Due to the polymer's viscoelastic nature, the stress and strain for such materials will represent a damping factor (δ). The reliance of the storage modulus (E') and $\tan \delta$ at temperatures between 30 and 150 °C for neat PA6 and the nanocomposite formulations is shown in Figure 8. From Figure 8A, the nanocomposite samples show good thermomechanical stability with an increase in the CNF composition. The improved thermomechanical properties of the nanocomposites indicate the presence of good interfacial bonding between the CNFs and the PA6 matrix [57]. With the increase in temperature, PA6 showed a drastic decrease in the storage modulus. The CNFs had a remarkable effect on the nanocomposites' viscoelastic behavior, with an increase in the storage modulus throughout the range of temperatures with the addition of CNFs. The presence of nanofibers reduces the elongation and promotes stiffness, aiding the stress transfer through the nanocomposites [58]. The increase in the storage modulus for the higher-CNF content nanocomposites suggests the presence of percolated network structures of cellulose in the PA6 matrix, constraining the

long-range motion of polymer chains and resulting in a pseudo-solid behavior [30]. The presence of nanofibers reduces the elongation and promotes stiffness, aiding the stress transfer through the nanocomposites [58]. Since the storage modulus serves as an accurate measure of molecular rigidity, it shows that the nanocomposites become more rigid with the addition of CNFs [59].

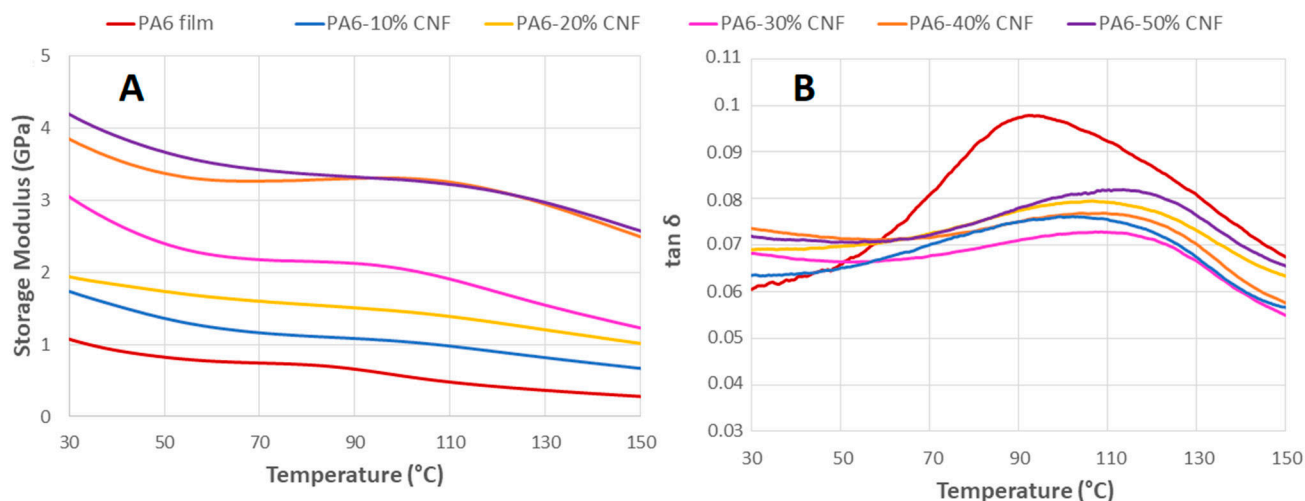


Figure 8. DMA results: (A) storage modulus (E'), and (B) $\tan \delta$ for neat PA6 and the PA6-CNF nanocomposite films.

Additionally, the $\tan \delta$ intensity for the nanocomposites after the glassy state decreased, as seen in Figure 8B. Traversing from low to high temperatures, the $\tan \delta$ peak for neat PA6 is about ~ 94 °C (Figure 8B). The values of $\tan \delta$ are related to the glass transition temperature (T_g) and are higher than the values obtained from the DSC analysis. This shift in the T_g is attributed to DMA being more sensitive than DSC as larger specimens are used [60]. Nevertheless, the T_g from the $\tan \delta$ peaks and the DSC results depict similar trends of an increase in the T_g with the addition of CNFs. The reinforcement factor (F_R), defined as the ratio of storage moduli of nanocomposites and control samples, is shown in Table 5 along with the DMA values obtained at the specific temperatures. Expectedly, F_R increases as the CNF composition increases, indicating improved stiffness and corroborating the reinforcement effect.

Table 5. Summary of storage modulus, damping factor, and reinforcement factor (F_R) for neat PA6 and the nanocomposite films at specific temperatures.

CNF Composition (wt.%)	E' at 50 °C (GPa)	E' at 80 °C (GPa)	E' at 120 °C (GPa)	$\tan \delta$ Peaks (°C)	F_R at 50 °C
0	0.82	0.71	0.44	94	-
10	1.35	1.12	0.89	102	1.6
20	1.72	1.55	1.29	108	2.1
30	2.38	2.15	1.71	110	2.9
40	3.36	3.27	3.09	112	4.1
50	3.68	3.36	3.10	117	4.5

4. Conclusions

Nanocomposite films of PA6, reinforced with a high content of CNFs, were successfully prepared with the solvent casting method using a green solvent mixture of formic acid and water. The CNFs obtained from enzymatic hydrolysis, followed by homogenization, endowed an excellent reinforcement effect, providing a good dispersion, and enabled an excellent stress transfer through the strong interface adhesion between the PA6 and CNFs. The tensile test results demonstrate the excellent reinforcement effect, where the tensile properties for the nanocomposites increased with an increase in the CNF composition. The maximum values of the tensile strength (~ 124 MPa) and modulus (~ 4.2 GPa) were

obtained with the 50 wt.% CNF formulation. The nanocomposite films were uniform, indicating a good dispersion of CNFs in the PA6 matrix, and no agglomeration was seen in the SEM micrographs. FTIR analysis revealed the molecular interactions between the CNFs and PA6 through hydrogen bonds with the OH groups of cellulose. The TGA results illustrate that with the increase in the CNF composition, the nanocomposites' thermal stability slightly decreased. DSC revealed small increases in the glass transition, followed by a gradual decrease in crystallinity with the increase in the CNF content as a result of the constrained mobility of PA6 chains upon the addition of CNFs. Maximum crystallinity (~49%) was obtained for the 10 wt.% formulation. The nanocomposites had superior thermomechanical stability with the increase in the CNF composition. This study presents an environmentally friendly method in the interest of high-performance and high-cellulose content bio-nanocomposites.

Author Contributions: Conceptualization, P.O. and F.V.; formal analysis, P.K.S. and F.V.; funding acquisition, F.V.; investigation, P.K.S., F.M. and P.O.; methodology, P.K.S., F.M. and P.O.; project administration, F.V.; resources, F.V.; software, P.K.S. and F.M.; supervision, F.V.; validation, P.O. and F.V.; writing—original draft, P.K.S.; writing—review and editing, P.O. and F.V. All authors have read and agreed to the published version of the manuscript.

Funding: This research was funded by the Biocomposites Program within the Knut and Alice Wallenberg Foundation (Sweden), a UdG grant (IFUdG 2017), Spain, and a three-month research grant from KTH (C2019-1106), Sweden. Support from the Spanish Ministry of Science, Innovation and Universities (RTI 2018-102070-B-C22) is also acknowledged.

Institutional Review Board Statement: Not applicable.

Informed Consent Statement: Not applicable.

Data Availability Statement: The data presented in this study are available on request from the corresponding author.

Acknowledgments: The authors want to thank the technical support as well as the use of the laboratories of the Wallenberg Wood Science Center (Stockholm, Sweden) and the RISE Institute (Stockholm, Sweden) for this study. The authors would also like to express appreciation to BASF GmbH for kindly providing the materials for this research.

Conflicts of Interest: The authors declare no conflict of interest.

References

1. Lee, K.Y.; Aitomäki, Y.; Berglund, L.A.; Oksman, K.; Bismarck, A. On the use of nanocellulose as reinforcement in polymer matrix composites. *Compos. Sci. Technol.* **2014**, *105*, 15–27. [[CrossRef](#)]
2. Kargarzadeh, H.; Huang, J.; Lin, N.; Ahmad, I.; Mariano, M.; Dufresne, A.; Thomas, S.; Gałęski, A. Recent developments in nanocellulose-based biodegradable polymers, thermoplastic polymers, and porous nanocomposites. *Prog. Polym. Sci.* **2018**, *87*, 197–227. [[CrossRef](#)]
3. Eichhorn, S.J.; Dufresne, A.; Aranguren, M.; Marcovich, N.E.; Capadona, J.R.; Rowan, S.J.; Weder, C.; Thielemans, W.; Roman, M.; Renneckar, S.; et al. Review: Current International Research into Cellulose Nanofibres and Nanocomposites. *J. Mater. Sci.* **2010**, *45*, 1–33. [[CrossRef](#)]
4. Dufresne, A. Cellulose nanomaterial reinforced polymer nanocomposites. *Curr. Opin. Colloid Interface Sci.* **2017**, *29*, 1–8. [[CrossRef](#)]
5. Moon, R.J.; Schueneman, G.T.; Simonsen, J. Overview of Cellulose Nanomaterials, Their Capabilities and Applications. *JOM* **2016**, *68*, 2383–2394. [[CrossRef](#)]
6. Börjesson, M.; Westman, G. *Crystalline Nanocellulose—Preparation, Modification, and Properties*; Börjesson, M., Westman, G., Eds.; IntechOpen: London, UK, 2015; pp. 159–191.
7. de Assis, C.A.; Houtman, C.; Phillips, R.; Bilek, E.M.; Rojas, O.J.; Pal, L.; Peresin, M.S.; Jameel, H.; Gonzalez, R. Conversion economics of forest biomaterials: Risk and financial analysis of CNC manufacturing. *Biofuels Bioprod. Biorefin.* **2017**, *11*, 682–700. [[CrossRef](#)]
8. Kiziltas, A.; Erbas Kiziltas, E.; Boran, S.; Gardner, D.J. Micro- and nanocellulose composites for automotive applications. In Proceedings of the SPE Automotive Composites Conference and Exhibition, Novi, MI, USA, 11–13 September 2013; pp. 11–13.
9. Francisco, D.L.; Paiva, L.B.; Aldeia, W. Advances in polyamide nanocomposites: A review. *Polym. Compos.* **2019**, *40*, 851–870. [[CrossRef](#)]
10. Shokoohi, S.; Arefazar, A.; Khosrokhavar, R. Silane coupling agents in polymer-based reinforced composites: A review. *J. Reinf. Plast. Compos.* **2008**, *27*, 473–485. [[CrossRef](#)]

11. Alonso-Montemayor, F.J.; Tarrés, Q.; Oliver-Ortega, H.; Espinach, F.X.; Narro-Céspedes, R.I.; Castañeda-Facio, A.O.; Delgado-Aguilar, M. Enhancing the Mechanical Performance of Bleached Hemp Fibers Reinforced Polyamide 6 Composites: A Competitive Alternative to Commodity Composites. *Polymers* **2020**, *12*, 1041. [[CrossRef](#)]
12. Sridhara, P.K.; Vilaseca, F. Assessment of Fiber Orientation on the Mechanical Properties of PA6/Cellulose Composite. *Appl. Sci.* **2020**, *10*, 5565. [[CrossRef](#)]
13. Lo Re, G.; Sessini, V. Wet feeding approach for cellulosic materials/PCL Biocomposites. In *Biomass Extrusion and Reaction Technologies: Principles to Practices and Future Potential*; ACS Publications: Washington, DC, USA, 2018; pp. 209–226; ISBN 19475918.
14. Dufresne, A. Cellulose nanomaterials as green nanoreinforcements for polymer nanocomposites. *Philos. Trans. R. Soc. Math. Phys. Eng. Sci.* **2018**, *376*, 20170040. [[CrossRef](#)]
15. Kong, I.; Tshai, K.Y.; Hoque, M.E. Manufacturing of natural fibre-reinforced polymer composites by solvent casting method. In *Manufacturing of Natural Fibre Reinforced Polymer Composites*; Springer: Berlin/Heidelberg, Germany, 2015; pp. 331–349.
16. Chang, H.-Y.; Shih, T.-S.; Guo, Y.L.; Tsai, C.-Y.; Hsu, P.-C. Sperm function in workers exposed to N,N-dimethylformamide in the synthetic leather industry. *Fertil. Steril.* **2004**, *81*, 1589–1594. [[CrossRef](#)]
17. Nirmala, R.; Panth, H.R.; Yi, C.; Nam, K.T.; Park, S.-J.; Kim, H.Y.; Navamathavan, R. Effect of solvents on high aspect ratio polyamide-6 nanofibers via electrospinning. *Macromol. Res.* **2010**, *18*, 759–765. [[CrossRef](#)]
18. Hocker, S.; Rhudy, A.K.; Ginsburg, G.; Kranbuehl, D.E. Polyamide hydrolysis accelerated by small weak organic acids. *Polymer* **2014**, *55*, 5057–5064. [[CrossRef](#)]
19. Sucharitpong, T.; Lam, N.T.; Sukyai, P. Production of Nylon-6/Cellulose Nanocrystal Composite Films Using Solvent Dissolution. *Sugar Tech* **2020**, *22*, 328–339. [[CrossRef](#)]
20. Henriksson, M.; Henriksson, G.; Berglund, L.A.; Lindström, T. An environmentally friendly method for enzyme-assisted preparation of microfibrillated cellulose (MFC) nanofibers. *Eur. Polym. J.* **2007**, *43*, 3434–3441. [[CrossRef](#)]
21. Tarrés, Q.; Boufi, S.; Mutjé, P.; Delgado-Aguilar, M. Enzymatically hydrolyzed and TEMPO-oxidized cellulose nanofibers for the production of nanopapers: Morphological, optical, thermal and mechanical properties. *Cellulose* **2017**, *24*, 3943–3954. [[CrossRef](#)]
22. Wang, J.; Liu, X.; Jin, T.; He, H.; Liu, L. Preparation of nanocellulose and its potential in reinforced composites: A review. *J. Biomater. Sci. Polym. Ed.* **2019**, *30*, 919–946. [[CrossRef](#)]
23. Herrick, F.W. Process for Preparing Microfibrillated Cellulose. U.S. Patent 4,481,077, 6 November 1984.
24. Prakobna, K.; Berthold, F.; Medina, L.; Berglund, L.A. Mechanical performance and architecture of biocomposite honeycombs and foams from core-shell holocellulose nanofibers. *Compos. Appl. Sci. Manuf.* **2016**, *88*, 116–122. [[CrossRef](#)]
25. Krenchel, H. Fibre reinforcement. In *Theoretical and Practical Investigations of the Elasticity and Strength of Fibre-Reinforced Materials*; Akademisk Forlag: Copenhagen, Denmark, 1964; pp. 157–159.
26. Agarwal, B.D.; Broutman, L.J.; Chandrashekhara, K. *Analysis and Performance of Fiber Composites*; John Wiley & Sons: Hoboken, NJ, USA, 2017; ISBN 1119389984.
27. Millot, C.; Fillot, L.A.; Lame, O.; Sotta, P.; Seguela, R. Assessment of polyamide-6 crystallinity by DSC: Temperature dependence of the melting enthalpy. *J. Therm. Anal. Calorim.* **2015**, *122*, 307–314. [[CrossRef](#)]
28. Nie, S.; Zhang, K.; Lin, X.; Zhang, C.; Yan, D.; Liang, H.; Wang, S. Enzymatic pretreatment for the improvement of dispersion and film properties of cellulose nanofibrils. *Carbohydr. Polym.* **2018**, *181*, 1136–1142. [[CrossRef](#)]
29. Krishna, S.; Patel, C.M. Computational and experimental study of mechanical properties of Nylon 6 nanocomposites reinforced with nanomilled cellulose. *Mech. Mater.* **2020**, *143*, 103318. [[CrossRef](#)]
30. Aydemir, D.; Kiziltas, A.; Erbas Kiziltas, E.; Gardner, D.J.; Gunduz, G. Heat treated wood-nylon 6 composites. *Compos. Eng.* **2015**, *68*, 414–423. [[CrossRef](#)]
31. Sridhara, P.K.; Vilaseca, F. High Performance PA 6/Cellulose Nanocomposites in the Interest of Industrial Scale Melt Processing. *Polymers* **2021**, *13*, 1495. [[CrossRef](#)]
32. Peng, Y.; Gardner, D.J.; Han, Y. Characterization of mechanical and morphological properties of cellulose reinforced polyamide 6 composites. *Cellulose* **2015**, *22*, 3199–3215. [[CrossRef](#)]
33. Lee, J.A.; Yoon, M.J.; Lee, E.S.; Lim, D.Y.; Kim, K.Y. Preparation and characterization of cellulose nanofibers (CNFs) from microcrystalline cellulose (MCC) and CNF/polyamide 6 composites. *Macromol. Res.* **2014**, *22*, 738–745. [[CrossRef](#)]
34. Joshi, M.K.; Tiwari, A.P.; Maharjan, B.; Won, K.S.; Kim, H.J.; Park, C.H.; Kim, C.S. Cellulose reinforced nylon-6 nanofibrous membrane: Fabrication strategies, physicochemical characterizations, wicking properties and biomimetic mineralization. *Carbohydr. Polym.* **2016**, *147*, 104–113. [[CrossRef](#)]
35. Qua, E.H.; Hornsby, P.R. Preparation and characterisation of nanocellulose reinforced polyamide-6. *Plast. Rubber Compos.* **2011**, *40*, 300–306. [[CrossRef](#)]
36. Faruk, O.; Bledzki, A.K.; Fink, H.P.; Sain, M. Progress report on natural fiber reinforced composites. *Macromol. Mater. Eng.* **2014**, *299*, 9–26. [[CrossRef](#)]
37. Ansari, F.; Skrifvars, M.; Berglund, L. Nanostructured biocomposites based on unsaturated polyester resin and a cellulose nanofiber network. *Compos. Sci. Technol.* **2015**, *117*, 298–306. [[CrossRef](#)]
38. Lee, K.-Y.; Tammel, T.; Schultzer, K.; Kiiskinen, H.; Samela, J.; Bismarck, A. High performance cellulose nanocomposites: Comparing the reinforcing ability of bacterial cellulose and nanofibrillated cellulose. *ACS Appl. Mater. Interfaces* **2012**, *4*, 4078–4086. [[CrossRef](#)]

39. Sehaqui, H.; Liu, A.; Zhou, Q.; Berglund, L.A. Fast preparation procedure for large, flat cellulose and cellulose/inorganic nanopaper structures. *Biomacromolecules* **2010**, *11*, 2195–2198. [[CrossRef](#)]
40. Henriksson, M.; Berglund, L.A.; Isaksson, P.; Lindstrom, T.; Nishino, T. Cellulose nanopaper structures of high toughness. *Biomacromolecules* **2008**, *9*, 1579–1585. [[CrossRef](#)]
41. Facca, A.G.; Kortschot, M.T.; Yan, N. Predicting the elastic modulus of natural fibre reinforced thermoplastics. *Compos. Appl. Sci. Manuf.* **2006**, *37*, 1660–1671. [[CrossRef](#)]
42. Li, G.; Meng, H.; Hu, J. Healable thermoset polymer composite embedded with stimuli-responsive fibres. *J. R. Soc. Interface* **2012**, *9*, 3279–3287. [[CrossRef](#)] [[PubMed](#)]
43. Zhang, H.; Li, S.; Branford White, C.J.; Ning, X.; Nie, H.; Zhu, L. Studies on electrospun nylon-6/chitosan complex nanofiber interactions. *Electrochim. Acta* **2009**, *54*, 5739–5745. [[CrossRef](#)]
44. Ma, Y.; Zhou, T.; Su, G.; Li, Y.; Zhang, A. Understanding the crystallization behavior of polyamide 6/polyamide 66 alloys from the perspective of hydrogen bonds: Projection moving-window 2D correlation FTIR spectroscopy and the enthalpy. *RSC Adv.* **2016**, *6*, 87405–87415. [[CrossRef](#)]
45. Quarti, C.; Milani, A.; Civalleri, B.; Orlando, R.; Castiglioni, C. Ab initio calculation of the crystalline structure and IR spectrum of polymers: Nylon 6 polymorphs. *J. Phys. Chem.* **2012**, *116*, 8299–8311. [[CrossRef](#)]
46. Galimberti, D.; Quarti, C.; Milani, A. Polymorphism of even nylons revisited through periodic quantum chemical calculations. *Polymer* **2015**, *67*, 167–173. [[CrossRef](#)]
47. van der Berg, O.; Capadona, J.R.; Weder, C. Preparation of homogeneous dispersions of tunicate cellulose whiskers in organic solvents. *Biomacromolecules* **2007**, *8*, 1353–1357. [[CrossRef](#)] [[PubMed](#)]
48. Wang, N.; Ding, E.; Cheng, R. Thermal degradation behaviors of spherical cellulose nanocrystals with sulfate groups. *Polymer* **2007**, *48*, 3486–3493. [[CrossRef](#)]
49. Jin, J.; Rafiq, R.; Gill, Y.Q.; Song, M. Preparation and characterization of high performance of graphene/nylon nanocomposites. *Eur. Polym. J.* **2013**, *49*, 2617–2626. [[CrossRef](#)]
50. Penel-Pierron, L.; Depecker, C.; Séguéla, R.; Lefebvre, J.-M. Structural and mechanical behavior of nylon 6 films part I. Identification and stability of the crystalline phases. *J. Polym. Sci. Polym. Phys.* **2001**, *39*, 484–495. [[CrossRef](#)]
51. Sunday, D.F.; Green, D.L. Thermal and Rheological Behavior of Polymer Grafted Nanoparticles. *Macromolecules* **2015**, *48*, 8651–8659. [[CrossRef](#)]
52. Karsli, N.G.; Aytac, A. Tensile and thermomechanical properties of short carbon fiber reinforced polyamide 6 composites. *Compos. Eng.* **2013**, *51*, 270–275. [[CrossRef](#)]
53. Paci, M.; Filippi, S.; Magagnini, P. Nanostructure development in nylon 6-Cloisite[®] 30B composites. Effects of the preparation conditions. *Eur. Polym. J.* **2010**, *46*, 838–853. [[CrossRef](#)]
54. Zhu, R.; Yadama, V.; Liu, H.; Lin, R.J.T.; Harper, D.P. Fabrication and characterization of Nylon 6/cellulose nanofibrils melt-spun nanocomposite filaments. *Compos. Appl. Sci. Manuf.* **2017**, *97*, 111–119. [[CrossRef](#)]
55. Kiziltas, A.; Nazari, B.; Gardner, D.J.; Bousfield, D.W. Polyamide 6—Cellulose Composites: Effect of Cellulose Composition on Melt Rheology and Crystallization Behavior. *Polym. Eng. Sci.* **2014**, *54*, 739–746. [[CrossRef](#)]
56. Chavarria, F.; Paul, D.R. Comparison of nanocomposites based on nylon 6 and nylon 66. *Polymer* **2004**, *45*, 8501–8515. [[CrossRef](#)]
57. Rezaee Niaraki, P.; Krause, A. Correlation between physical bonding and mechanical properties of wood–plastic composites: Part 2: Effect of thermodynamic factors on interfacial bonding at wood–polymer interface. *J. Adhes. Sci. Technol.* **2020**, *34*, 756–768. [[CrossRef](#)]
58. López-Suevos, F.; Eyholzer, C.; Bordeanu, N.; Richter, K. DMA analysis and wood bonding of PVAc latex reinforced with cellulose nanofibrils. *Cellulose* **2010**, *17*, 387–398. [[CrossRef](#)]
59. Shumigin, D.; Tarasova, E.; Krumme, A.; Meier, P. Rheological and Mechanical Properties of Poly (lactic) Acid/Cellulose and LDPE/Cellulose Composites. *Polym. Compos.* **2011**, *17*, 32–37. [[CrossRef](#)]
60. Saba, N.; Safwan, A.; Sanyang, M.L.; Mohammad, F.; Pervaiz, M.; Jawaid, M.; Allothman, O.Y.; Sain, M. Thermal and dynamic mechanical properties of cellulose nanofibers reinforced epoxy composites. *Int. J. Biol. Macromol.* **2017**, *102*, 822–828. [[CrossRef](#)] [[PubMed](#)]